In vivo assessment of a novel dual cell cancer therapy using conventional and novel cell tracking methods

Katherine Louise Ordidge

A thesis submitted to UCL for the degree of Doctor of Philosophy

Declaration

I, Katherine Louise Ordidge, confirm that the work presented in this thesis is my own. Where information has been derived from other sources, I confirm that this has been indicated in the thesis.

Abstract

Adoptive immunotherapy for cancer is a rapidly expanding field. Along with new techniques and technologies for cell engineering comes a pressing clinical need to discover the location of these cells after injection and to quantify the number of cells in a particular location. The use of agents to enhance tissue contrast is crucial to improve the ability of imaging techniques to distinguish cells from background signal, in order to track cells *in vivo*.

Human donor T cells were transduced to express a tumour antigen specific T cell receptor. Transduced T cells were labeled with novel and conventional radiolabels for *in vivo* tracking using a combined single photon emission computed tomography and computed tomography (SPECT/CT) scanner.

Transduced T cells were used in combination with TRAIL-expressing MSCs to produce a novel dual cell anti-cancer therapy in an *in vivo* lung metastases cancer model.

The data in this thesis demonstrates that a novel tri-functional probe designed for long-term cell tracking, whilst resulting in superior cell labeling and retained activity over time compared with conventional methods, causes significant cell toxicity.

It also demonstrates, for the first time, that a tumour antigen specific T cell therapy can be effective against lung metastases, leading to a significant reduction in tumour burden. These engineered T cells combined with MSC TRAIL also significantly reduce metastatic tumour burden, although there was no significant benefit to using the dual cell therapy.

Acknowledgements

I would like to thank the Medical Research Council for funding my PhD through UCL's Doctoral Training Programme in Medical and Biomedical Imaging.

Secondly, I would like to thank my primary supervisor, Dr. Sam Janes, for his unwavering support and encouragement over the course of the past four years, both professionally and personally.

I am grateful to second supervisor, Prof. Mark Lythgoe, for teaching me about overcoming obstacles in research and successful collaboration. Also, to my tertiary supervisor, Dr Adam Badar, who has always been ready to help me and buy me a coffee.

I would like to thank my Immunology Department collaborator, Dr. Emma Morris, who has been an important mentor and unofficial supervisor.

This project would not have been possible without the kindness, patience and daily assistance of two wonderful post-doctoral researchers, Dr Tammy Kalber and Dr Maryam Ahmadi.

As always, my family (on both sides of the English channel) has been a constant source of support. I would particularly like to thank my sister, Dr. Gemma Ordidge, for all her PhD advice, my father, Prof. Roger Ordidge, for inspiring me to pursue a career in imaging, and my mother-in-law, Mme Nicole Allain, for her encouragement and support.

Lastly and most importantly, I would like to thank my husband, Dr. Baptiste Allain, to whom I dedicate this thesis.

Table of Contents

List of Figures

List of Equations

List of Tables

List of Abbreviations

αMEM	Minimum essential media, alpha modifications
APAF1	Apoptotic protease activating factor 1
APC	Antigen presenting cell
ATP	Adenosine triphosphate
BLI	Bioluminescence imaging
CD3	Cluster of differentiation 3
CD4	Cluster of differentiation 4
CD8	Cluster of differentiation 8
cFLIP	Cellular FLICE-like inhibitory protein
CLG	CLGGLLTMV, derived from LMP2 antigen, HLA-A2-restricted fluorescent pentamer
Cr^{51}	Chromium-51
CT	Computed tomography
DAPI	4',6-diamidino-2-phenylindole
DcR1/2	Decoy receptor 1/2
DISC	Death-inducing signaling complex
DMEM	Dulbecco's modified eagle medium
DMSO	Dimethyl sulfoxide
DR4/5	Death receptor 4/5
DTNB	5,5'-dithiobis-(2-nitrobenzoic acid)
EBNA	Epstein-Barr virus nuclear antigen
EBV	Epstein-Barr virus

ELISA	Enzyme-linked immunosorbent assay
FADD	Fas-associated protein with death domain
FBS	Fetal bovine serum
FLI	Fluorescence imaging
FLICE	FADD-like interleukin-1-beta converting enzyme
GFP	Green fluorescent protein
GVHD	Graft-versus-host disease
H&E	Hematoxylin and eosin stain
HLA-A2	Human leucocyte antigen-A2
HMPAO	Hexamethylpropyleneamine oxime
hNET	Human norepinephrine transporter
hNIS	Human sodium iodide symporter
HPLC	High-performance liquid chromatography
HSC	Haemopoietic stem cells
HSV1-tk	Herpes simplex virus type 1 thymidine kinase reporter gene
HSV1-TK	Herpes simplex virus type 1 thymidine kinase
IAP	Inhibitors of apoptosis
I-DM	Iodide-dansyl maleimide
IDO	Indoleamine 2,3-dioxygenase
IFN-γ	Interferon-γ
IL-2	Interleukin 2
IL-4	Interleukin 4
IMDM	Iscove's modified Dulbecco's medium

I-RM	Iodide-rhodamine maleimide
LMP1/2	Latent membrane protein ½
MART-1	Melanoma antigen recognized by T cells 1
MHC	Major histocompatibility complex
MRI	Magnetic resonance imaging
MRP1	Multidrug resistance-associated protein 1 export pump
MSC	Mesenchymal stem cell
NOD/SCID	Non-obese diabetic/severe combined immunodeficiency mice
NLV	NLVPMVATV, derived from cytomegalovirus structural protein pp65 antigen, HLA-A2-restricted fluorescent pentamer
NSCLC	Non-small cell lung cancer
NSG	NOD/SCID gamma mice
OPG	Osteoprotegerin
PBMCs	Peripheral blood mononuclear cells
PBS	Phosphate buffered saline
PET	Positron emission tomography
PFA	Paraformaldehyde
PI	Propidium Iodide
ROI	Region of interest
RPMI	Roswell Park Memorial Institute medium
SMAC	Second mitochondria-derived activator of caspases
SPECT	Single photon emission computed tomography
SPIO	Superparamagnetic iron oxide nanoparticles

T2	Transverse relaxation time (exponential decay of signal due to spin-spin interactions)
T2*	Transverse relaxation time in tissues (includes dephasing caused by magnetic field inhomogeneities and susceptibility effects)
TAA	Tumour associated antigen
TCR	T cell receptor
Th1	T helper 1 cell
Th2	T helper 2 cell
Th17	T helper 17 cell
TNB	2-nitro-5-thiobenzoic acid
TNFα	Tumour necrosis factor alpha
TRAIL	TNF-related apoptosis-inducing ligand
Treg	Regulatory T cell
WT1	Wilm's tumour 1 antigen

1. Introduction

1.1. Background

Cell therapies for cancer are an attractive form of personalised medicine that can avoid the systemic side effects of conventional radiotherapy and chemotherapy. Adoptive immunotherapy has shown promise as a cancer therapy, as it harnesses the specificity of lymphocytes to kill cancer cells. In addition, TNF-related apoptosis-inducing ligand (TRAIL) expressing mesenchymal stem cells (MSCs), have previously been shown to home to and incorporate within lung metastases, leading to reduction or in some cases, elimination of lung metastases. A combination of these two cell therapy approaches may result in far superior cancer cell death than that observed using a single therapy alone.

1.2. Lung Cancer

Lung cancer is the second commonest form of cancer in the United Kingdom, representing 13.7% of all cancer diagnoses in men and 11.2% in women. [1] The majority of cases can be attributed to tobacco smoking, although other risk factors such as passive smoking, exposure to indoor radon gas, exposure to industrial or chemical carcinogens and air pollution are also recognized. Whilst the incidence of lung cancer in developed countries is declining in males and reaching a plateau in females due to a decline in smoking rates, the incidence is increasing in developing countries, reflecting increased smoking prevalence. [2] The incidence of lung cancer due to non-smoking causes is also increasing in females in developing countries, due to household air pollution from heating and cooking fires.

The histological subtype of lung cancer is normally used to determine treatment, and distinguishes small cell lung cancer from non-small cell lung cancer. Small cell lung cancer accounts for a minority of lung cancers and is more aggressive, producing early metastasis. Non-small cell carcinoma has several subtypes, of which adenocarcinoma and squamous cell carcinoma are the most prevalent. Histological diagnosis is usually made using a tissue specimen collected during a bronchoscopic procedure or with percutaneous needle biopsy.

Tumour staging is assessed using CT imaging, using the tumour, nodes, metastases (TNM) classification. Along with an assessment of the patient's fitness, the TNM stage is used to determine operability of the tumour. Generally, patients with stage I or II tumours, with N0 or N1 (no regional lymph node involvement or involvement of ipsilateral peribronchial, hilar or pulmonary nodes) are considered to be operable and have a reasonable chance of cure by surgery alone. Unfortunately, since the majority of patients present late, in the advanced stages of disease, survival rates remain extremely low, because early stage surgical resection offers the only hope of complete cure.

Combination chemotherapy containing one platinum-based agent, for example cisplatin, with third-generation cytotoxic agents such as gemcitabine, has traditionally been the first-line treatment for both small cell and non-small cell lung cancer and provides a modest survival benefit. Unfortunately, the majority of patients treated with platinum-based agents will relapse as resistance to these develops over time. The use of platinum-based chemotherapy is also associated with severe side effects, particularly nephrotoxicity, nausea and vomiting, neurotoxicity and ototoxicity.

An important breakthrough in the last 10 years was the approval of targeted chemotherapy agents for specific histological subtypes of lung cancer, for example, the antifolate agent pemetrexed for adenocarcinoma and large-cell carcinoma. [3] In a phase III trial following patients with advanced non-small cell carcinoma (stage IIIB or IV disease), pemetrexed treatment resulted in significantly improved overall survival of 13.4 months versus 10.6 months with placebo and best supportive care. [4] However, even with these new treatment options, the 5-year survival rate is less than 10% of patients with stage III or IV disease. [1]

Recently, research into genomic subsets of adenocarcinoma has identified specific driver mutations that can provide differential sensitivities to chemotherapy agents, leading to a more personalized approach to treatment. Mutations of the tyrosine kinase domain of the epidermal growth factor receptor can be treated with tyrosine kinase inhibitors, such as gefitinib and erlotinib, leading to a clinical response in approximately 20% of patients. [5] Significantly,

these agents also produced much less toxicity than conventional chemotherapy regimens.

Mutations involving fusion between the echinoderm microtubule-associated protein-like 4 gene and the anaplastic lymphoma kinase (ALK) gene, have also been identified in non-small cell lung cancer. [6] These mutations can be targeted with anaplastic lymphoma kinase inhibitors, such as crizotinib. However, this fusion gene was only detected in 6.7% of non-small cell lung cancers, representing a small minority of lung cancer cases. [7] The small percentage of patients whose cancer is positive for ALK experience a dramatic increase in survival with crizotinib therapy (12 month survival of 70% versus 44% in crizotininb naïve patients). [8]

Unfortunately these advances have not yet resulted in a significant survival benefit to patients because the response to these chemotherapy agents remains transient. Median five-year survival rates for UK patients are currently 7.8% for men and 9.3% for women, and survival rates have not changed significantly since the 1970s. [1]

In an attempt to diagnose more lung cancers at an early stage, several trials have explored screening programmes for current or ex-smokers using chest radiographs or low dose spiral computed tomography (CT). The largest of these, the National Lung Screening Trial, enrolled 53,454 subjects randomized to three annual screenings using chest radiographs or low dose spiral CT, and found a mortality reduction of 20% with low dose CT. [9] However, there is currently no lung cancer screening programme in place in the UK. [10]

In the future, cancer genotyping and personalized chemotherapy with targeted agents may increase survival rates, and genotyping could be used to identify biomarkers of resistance or response, and adapt chemotherapy regimens. [11]

1.3. Immunotherapy for cancers

Immune cells are known to play an important role in the control and development of malignancy, as evidenced by the increased incidence of malignancy in immunocompromised individuals, and an accumulation of immune cells at sites of malignancy. The immune system can be harnessed to treat cancer via four different methods: cytokine therapies, antibody therapies, vaccines and cell-based therapies.

Cytokine-based therapies aim to stimulate the immune system to mount a response against tumour cells. The cytokine interleukin-2 (IL-2) activates adaptive immune cells and has been used as an intravenous bolus to treat malignant melanoma and renal cell carcinoma, with complete regression of disease in 7% of patients. [12] However, these are the only solid tumours known to respond to cytokine therapy, and despite over 20 years of experience in these agents, there is currently no cytokine therapy approved to treat lung cancer.

Monoclonal antibodies are also used to stimulate a host immune response, and in addition have been developed to block certain cancer cell signaling pathways, or to act as a vehicle to deliver other therapies. In the past 10 years, many monoclonal antibodies targeting known tumour ligands or receptors have been approved for clinical use. An example is rituximab, a monoclonal antibody against CD20, which is used to treat non-Hodgkin's lymphoma. Ipilimumab, a monocloncal antibody against CTLA-4, a receptor expressed on the surface of helper T cells that inhibits T cell function, has recently been combined with conventional first-line chemotherapy agents to treat non-small cell lung cancer with a small increase in progression-free survival (5.7 months compared with 4.6 months with the control regimen). [13] However, monoclonal antibody therapy for lung cancers has not yet delivered the dramatic increase in survival rates that can be seen in other cancers.

For the treatment of non-small cell lung cancer, there have been several recent trials evaluating allogeneic cancer vaccines, with the aim of stimulating a humoral immune response against a tumour antigen. Target antigens include mucin-1, [14] epidermal growth factor [15] and the melanoma antigen encoding gene A3, [16] and patients treated with these vaccines in phase II/III trails have

experienced a modest survival benefit (for example, 6 months progression free survival of 43.2% with the vaccine TG4010 targeting mucin 1, compared with 35.1% for chemotherapy alone). [17]

Lastly, cell-based immunotherapy consists of administering immune cells to the patient that have anti-tumour effects. The most potent tumour killing immune cells are cytotoxic T cells, which have the ability to specifically lyse tumour cells.

1.4. T cells

T cells are lymphocytes that play a crucial role in adaptive cell-mediated immunity. They are known as T cells since they mature in the thymus, although they originate from lymphoid progenitors derived from bone marrow haemopoietic stem cells (HSCs). Chemoattractive molecules secreted by the thymus during fetal development attract the circulating T cell precursors, which then populate the thymus. [18] In the cortex of the thymus, developing T cells (thymocytes) proliferate and interact with cortical epithelial cells. Each T cell undergoes random gene rearrangement to form a unique T cell receptor, so that within the millions of T cells generated, there are some cells with T cell receptors specific for potential microbial antigens. This process is known as the generation of diversity. [19]

In the cortex, positive selection occurs, where thymocytes are presented with self-antigens; major histocompatibility complex (MHC) class I or II molecules. Those that can weakly bind self-MHC molecules are selected, whilst those that cannot recognize MHC undergo apoptosis. [20, 21] (Figure 1.1)

The thymocytes then migrate into the medulla where they undergo negative selection. [22] Here dendritic cells or macrophages express self-antigens on MHC molecules. If a T cell binds to self-antigen it undergoes apoptosis, so that the remaining T cells have central tolerance and will not react to self-antigen and cause autoimmune disease.

Less than 5% of thymocytes survive the process of selection. [23] Those that survive can recognize foreign, non-self antigen displayed by self-MHC

molecules only. These migrate to peripheral lymphoid tissues, such as the spleen and lymph nodes, where they complete their maturation.

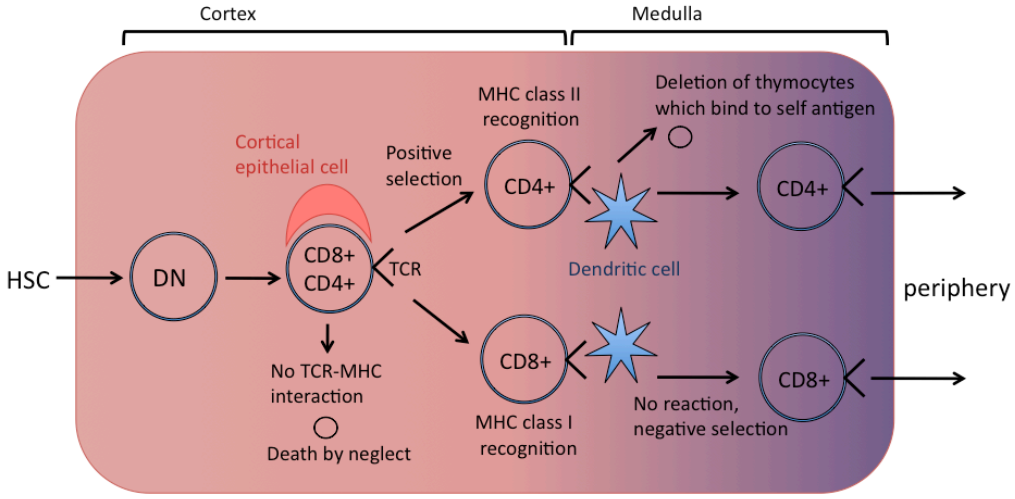

Figure 1.1: T cell development in the thymus. HSC migrate to the thymus and begin development in the cortex. Thymocytes begin as double negative (DN) for CD4 and CD8 molecules. After successful TCR gene rearrangement they become double positive, expressing both CD4 and CD8, and move into the cortico-medullary junction. Positive selection occurs when double positive T cells bind to cortical epithelial cells expressing MHC class I or II, and self-antigen, with enough affinity to get a survival signal. Surviving T cells move into the medulla, where they undergo negative selection. T cells that bind to dendritic cells expressing MHC class I or II, and self-antigen, undergo apoptosis. Surviving T cells express either CD4 or CD8 and recognize foreign antigen only if they are displayed on MHC class I or II molecules.

1.4.1. The T cell receptor (TCR)

The TCR is located within the cell membrane and consists of two different protein chains, an alpha and a beta chain, each of which contain a constant region and a variable region. The TCR forms a complex with CD3, so that the variable regions face outwards and the constant regions are closer to the cell membrane (Figure 1.2). [24]

Assembly of the TCR occurs in the endoplasmic reticulum, where the α and β chains bind to CD3 molecules. [25] This complex then passes through the Golgi apparatus, before joining the cell membrane.

Cell mediated, or adaptive immunity, is a result of the action of T cells interacting with antigen associated with MHC class I or II molecules, through their TCR. This is in contrast to innate immunity, which is a non-specific response involving complement, acute phase proteins and cytokines, as well as cells such as phagocytes, natural killer cells, mast cells and basophils.

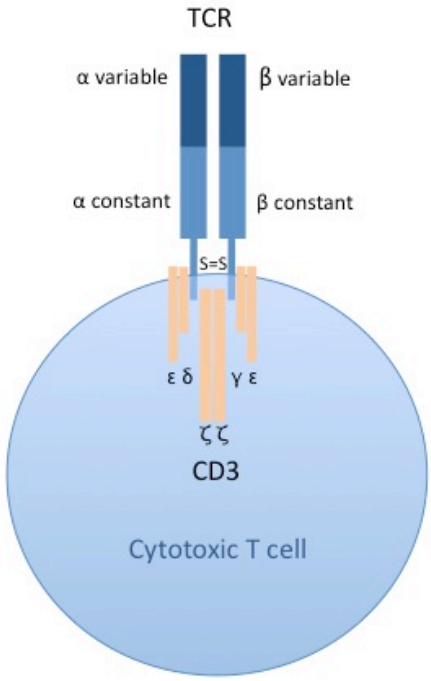

Figure 1.2: Diagram showing the structure of the T cell receptor, which is made up of α and β chains, each with a variable and constant region. CD3 anchors the TCR to the cell membrane.

1.4.2. Helper T cells/ CD4+ T cells

Helper T cells play an important role in the activation of other T cells by releasing cytokines, such as interleukin-2 (IL-2). They can be differentiated from other T cells by their expression of cluster of differentiation 4 (CD4) molecules. Helper T cells display a specific TCR that recognizes and binds a particular antigen, displayed by major histocompatibility complex (MHC) class II molecules on the surface of antigen presenting cells (APCs). CD4 also binds to MHC class II molecules to create this link.

In order to activate naïve T helper cells, another interaction must also occur between CD28 on the T cell and co-stimulatory molecules CD80 and CD86, expressed by APCs. This helps the T cell distinguish between foreign antigens and host antigens, as CD80 and CD86 are only displayed by APCs, thus reducing the risk of auto-immunity. To date, four distinct populations of helper T cells have been identified, and the fate of a naïve helper T cell is determined by the pattern of signals it receives during activation with antigen. [26] T helper 1 (Th1) cells mediate immune responses against intracellular pathogens, especially mycobacterium, and secrete interferon-γ (IFNγ), lymphotoxin α and IL-2, leading to activation of macrophages and CD4/CD8 cell memory formation. [27] T helper 2 (Th2) cells secrete many different interleukins, including interleukin-4 (IL-4) and destroy extracellular parasites, such as helminths. [28] T helper 17 (Th17) cells also produce various interleukins and mediate immune responses against extracellular bacteria and fungi. [29] Regulatory T cells (Treg) control the immune response and have an important role in immune self-tolerance. [30]

1.4.3. Cytotoxic T cells/ CD8+ T cells

Cytotoxic T cells are capable of killing infected or damaged cells, for example virally infected cells. Similar to helper T cells they also express a specific TCR, however, this recognizes antigen presented by MHC class I molecules. [31] Cytotoxic T cells also display cluster of differentiation 8 (CD8), that binds to MHC class I during T cell activation, to stabilize the interaction between the TCR and antigen.

The function of MHC class I molecules is to display short peptide sequences formed by the breakdown of cellular proteins by the proteosome system. [32] In order for this to occur, these peptides must be translocated across the endoplasmic reticulum, and combined with MHC class I and β_2 microglobulin. After assembly, this complex passes through the Golgi apparatus for secretion to the cell surface. [33]

This antigen display allows cytotoxic T cells to recognize foreign cells, or those with cellular changes caused by viral infection, since MHC class I molecules are present on all nucleated cells in the body, as well as on specialized antigen presenting cells (APCs). The function of APCs, such as dendritic cells, is to internalize exogenous antigen by endocytosis or phagocytosis, then present the antigen, with co-stimulatory molecules CD80 or CD86, to activate both helper and cytotoxic T cells.

Cytotoxic T cells are also thought to provide some protection against malignancy, by recognizing antigenic differences caused by altered proteins in mutated cells. [33, 34]

1.4.4. Cytotoxic T cell killing

Cytotoxic T cells can kill target cells by several different pathways. Once TCR-antigen recognition occurs, the cytotoxic T cell can release perforin, which punches holes through the cell membrane of the target cell, and granzymes, enzymes that cleave peptide bonds in proteins (Figure 1.3). This activates the caspase cascade and initiates apoptosis. Alternatively, activated cytotoxic T cells express Fas ligand that can bind to Fas expressed on the target cell. This recruits Fas-associated death domain (FADD) and procaspases 8 and 10 to form a death-inducing signaling complex (DISC). This also activates the caspase cascade, leading to apoptosis. [35]

Finally, cytotoxic T cells can kill target cells indirectly, by the secretion of cytokines such as tumour necrosis factor α (TNFα) and IFNγ, during interaction of the TCR with the MHC class I/antigen complex. Secreted TNFα causes apoptosis in surrounding target cells through the caspase cascade by binding to

its receptor on the target cell. IFNγ increases target cell death through the Fas pathway, by increasing transcription of MHC class I and Fas. [33]

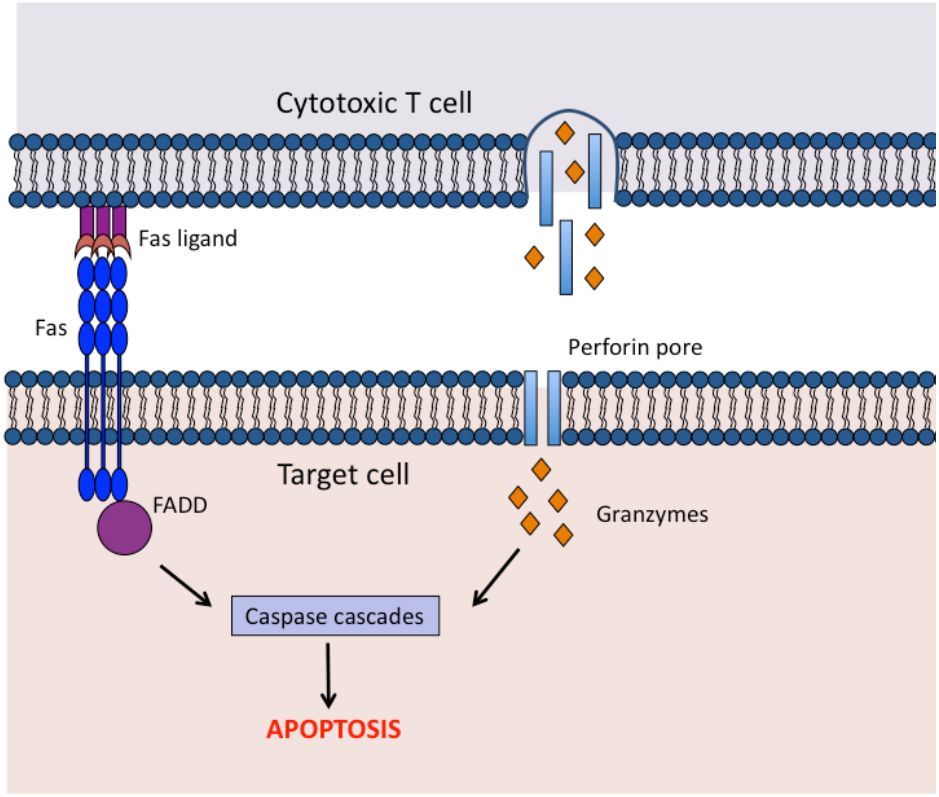

Figure 1.3: Mechanisms of apoptosis induced by cytotoxic T cells. Cytotoxic T cells can trigger apoptosis by secreting perforin and granzymes, activating the caspase cascades, or via the binding of Fas ligand to Fas, which also activates the caspase cascades.

1.5. Adoptive Immunotherapy for Cancer

1.5.1. Tumour Antigens

Malignant cells can express fragments of new or mutated intracellular proteins on their cell membrane, that can act as antigens to the immune system (Figure 1.5). TCRs can specifically recognize these peptide sequences, resulting in T cell activation and cell-mediated killing. Therefore, if tumour antigens bind to TCRs on cytotoxic T cells, the tumour cell is destroyed specifically. [36] Unfortunately, most cancers fail to trigger a response from cytotoxic T cells. This may be due to several different reasons; for example, the mutation will be immunologically silent if the antigen fails to bind with high affinity to MHC class I or II molecules on the tumour cell, and hence cannot be presented to T cells. [37] Another possibility is that tumour cells express antigens that are poorly immunogenic and fail to trigger a T cell response, so the tumour is allowed to evolve unchecked. Evidence suggests that tumour growth could be linked to selection of these cells, which fail to initiate an immune response. [38]

Finally, many of the known tumour antigens are also expressed in normal tissues (tumour associated antigens or TAA), such as the Wilm's tumour 1 antigen (WT1), expressed in leukaemias and some solid tumours. [39] T cells with high avidity for these antigens are removed by central or peripheral tolerance to reduce the risk of autoimmunity. As a result, T cells fail to provide protection against a tumour displaying these antigens. In these cases, using engineered T cells with high avidity for the TAA could result in damage to normal tissues. Therefore, T cell immunotherapy must provide high affinity T cell receptors recognising the correct MHC-peptide complex for adequate tumour control.

Figure 1.5: Tumour antigens targets for adoptive immunotherapy. 1. Viral mutations can cause the expression of new antigens (Dawson 2012 [40]). 2. Other mutations can confer a new antigenic determinant that can also be recognized (Sharkey 2004 [41], Robbins 1996 [42]). 3. Lastly, amplification or overexpression of genes can produce a target antigen for immunotherapy (Sierra 2011 [43]).

1.5.2. Adoptive T Cell Therapy

Adoptive T cell therapy is a form of personalised medicine, involving the transfusion of lymphocytes into a patient for the treatment of cancer or chronic infection. For tumour therapy, the aim is to generate tumour antigen specific cytotoxic T cells. [44] Early attempts of adoptive immunotherapy using tumour-infiltrating lymphocytes from tumour biopsies in melanoma patients resulted in a clinical benefit in 8 out of 10 patients treated. [45] In this study, lymphocytes from melanoma tumour biopsies were cultured *ex vivo*, with selection of tumour specific cells using antigen stimulation, followed by clonal expansion of cytotoxic T cell subsets that could cause lysis of target cancer cells, and transfusion of these cells in divided doses. Following this study, it was quickly discovered that lymphoablative chemotherapy before the transfer of lymphocytes could improve the clinical response. [46-48] However, this approach was very labour and time intensive, requiring the testing and expansion of multiple T cell populations, and a significant number of patients failed to respond to the therapy.

To solve this problem, high affinity tumour antigen-specific TCRs were identified by measuring *in vitro* activity and the genes for these TCR were isolated and transduced into peripheral blood lymphocytes, resulting in efficient lysis of target cells *in vitro*. [49, 50] This approach allowed quicker generation of a large number of lymphocytes with specific anti-tumour activity, without the need to clonally expand and test a large number of tumour-infiltrating lymphocytes. However, data from clinical studies was less favourable, with just 2 patients out of 13 showing complete regression of their metastatic melanoma, and the rest having no response. [51] This was thought to be a result of the level of expression of the TCR transgene, which decreased over time, possibly due to the mispairing of the introduced α-chains and β-chains with endogenous chains. It has been shown that expression levels of the introduced TCR α–chains and β-chains modulate antigen recognition, with higher expression leading to better T cell response against antigen. [52]

An advantage to this cell engineering approach is that both CD8+ and CD4+ T cells can be transduced, resulting in antigen-specific cytotoxic T cells as well as helper T cells. This may be important for the complete elimination of tumour and

the establishment of memory for long-term maintenance. [53] Recently, efforts have focused on engineering T cells expressing a TCR with stable high expression and high affinity for tumour antigens. [54]

T cell receptor gene transfer methods have also been used to insert TCRs with high affinity for tumour-associated antigens. For example, Xue et al. have shown that Wilm's Tumour 1 (WT1) engineered TCRs in human T cells can eliminate human leukaemia cells expressing WT1, in NOD/SCID mice. [55] The TCR gene was later modified using codon optimization to improve synthesis, and a cysteine bond in the constant domains to prevent mispairing between endogenous and introduced chains. The resulting WT1-TCR had improved expression and was 5-fold more active against leukaemia cells in a Chromium-51 cytotoxicity assay. Further testing using the optimized WT1-TCR to engineer a patient's T cells to target autologous leukaemia cells in a NOD/SCID model resulted in a significant improvement of survival rates. [56] This study provided the rationale to proceed into phase I/II clinical trials at the Royal Free Hospital for adult patients with acute myeloid leukaemia and chronic myeloid leukaemia.

1.5.3. The Epstein-Barr Virus

The Epstein-Barr virus (EBV) is a gamma herpesvirus, which commonly causes a mild viral illness in childhood. If an individual is infected as an adolescent or young adult it causes infectious mononucleosis, commonly known as glandular fever. The virus primarily infects nasopharyngeal stratified squamous epithelial cells and B cells, where it establishes latency. In fact, more than 90% of adults have latent EBV infection and this is linked to certain cancers, such as Burkitt's lymphoma, Hodgkin's lymphoma and nasopharyngeal carcinoma. [57]

EBV-positive cells can express latency in different patterns, corresponding to the expression of certain viral proteins. In immunocompetent hosts, the latency III proteins EBV nuclear antigen (EBNA) 3A, 3B and 3C are immunodominant and EBV specific T cells control the latency. [58] In contrast, EBV-positive Hodgkin's lymphoma and nasopharyngeal carcinomas express the latency II antigens EBNA 1 and the latent membrane proteins (LMP) 1 and 2. [59, 60]

Latent membrane protein 2 (LMP2) is a transmembrane protein that can be utilized as a tumour antigen for adoptive immunotherapy. However, producing effective latency II antigen-specific T cells is difficult due to the weak immunogenicity of these antigens. Therefore, a cell engineering approach is needed to overcome this problem.

Allogeneic donor cytotoxic T cells specific for EBV latency proteins have been used to combat lymphoproliferative disease resulting from reactivation of EBV, following bone marrow transplantation, for over 10 years. [59] Following the success of this treatment, donor EBV-specific cytotoxic T cells were used clinically in pilot studies for patients with EBV positive Hodgkin's lymphoma. [60] In this study, cytotoxic T cells were not specific to the LMP2 antigen, and most patients (5/6) had disease progression after treatment.

In another pilot study, patients with EBV-related nasopharyngeal carcinoma were transfused with autologous EBV-specific cytotoxic T cells that had been isolated and expanded *ex vivo*. [61] Out of the ten patients in the study, 2 had a partial response and 4 had stable disease, while 4 patients experienced disease progression. There were 4 patients who had LMP2 specific T cell responses, 3 of which had a clinical benefit; leading the authors to hypothesise that increasing the number of T cells specific for LMP1 and LMP2 could enhance antitumour response. Therefore, adoptive immunotherapy without selection of LMP2-specific EBV-TCR T cells has failed to deliver significant clinical benefit.

In an attempt to overcome this problem, dendritic cells and EBV-lymphoblastoid cell lines have been transduced to express the LMP2 antigen using an adenovirus. These were then used to stimulate and expand LMP2 specific T cells from patients *ex vivo*, which were transfused into the patient to provide a treatment for relapsed Hodgkin's lymphoma. This resulted in 4 complete clinical responses and 1 partial response out of 6 patients with relapsed disease refractory to standard chemotherapy treatment. [62, 63]

To further improve LMP2 targeting, a modified EBV-TCR has been developed that can be inserted using a retrovirus into peripheral blood lymphocytes. [64] This approach allows genetic transfer of TCRs with a high specificity to LMP2 into a large proportion of proliferating T cells, rather than relying on the

expansion of a small subset of the population with TCRs that express reactivity to LMP2. The engineered TCR contains murine constant regions to enhance TCR association with CD3 molecules on the cell membrane, a self-cleaving 2A sequence for equimolar expression of both alpha and beta chains, and has been codon optimized to improve gene translation. The resulting human leukocyte antigen-A2 (HLA-A2) restricted EBV-TCR is dominant and suppresses the surface expression of endogenous TCR.

In this thesis, I have used the direct retroviral gene transfer technique to transduce human donor peripheral blood lymphocytes to express the HLA-A2 restricted LMP2 specific EBV-TCR described above. Instead of targeting leukaemia cells, these engineered T cells will be used to target lung metastases. The lung cancer cell line will be transduced to express the LMP2 antigen, to provide an antigen target for the EBV-TCR T cells.

1.5.4. Adoptive T cell immunotherapy for lung cancer

Adoptive immunotherapy for lung cancer was first described in 1987 by Kradin et al., who used tumour-infiltrating lymphocytes that were expanded *ex vivo* with IL-2 to target adenocarcinoma of the lung. [65] The next studies to look at adoptive immunotherapy to treat lung cancer were not published until 1995. In a randomized controlled clinical study spanning 7 years, Kimura et al. used injections of lymphokine-activated killer cells and recombinant IL-2 to target lung cancer as an adjuvant treatment to chemotherapy, radiotherapy or surgery, showing a significant improvement in survival rates in patients with adenocarcinoma but no difference in survival in those with squamous cell carcinoma. [66]

Simultaneously, Ratto et al. were investigating the use of infusions of tumour-infiltrating lymphocytes and recombinant IL-2 for non-small cell lung cancer (NSCLC), first in a pilot study, [67] then in a larger randomized controlled trial showing a significant difference in survival rates. [68] Unfortunately, a further phase II clinical trial looking at survival rates using this therapy in patients with advanced (stage III) NSCLC showed no benefit to patients with adoptive immunotherapy. [69] Most recently, the authors have published another phase I/II clinical trial using transfused autologous PBMC and recombinant IL-2,

combined with chemotherapy, as a neo-adjuvant treatment for patients with surgically resectable stage III NSCLC. [70] This study showed no immediate survival benefit to the neo-adjuvant therapy, but an increased 5-year survival rate.

However, apart from these studies there has been little development in the field of adoptive immunotherapy for lung cancer, and no attempts of adoptive immunotherapy with T cells targeting tumour associated antigens. [71] In fact, most recently, Babiak et al. have started searching for tumour associated antigen candidates for an adoptive T cell therapy. [72] Therefore, adoptive immunotherapy with T cells having a high expression of high affinity tumour antigen specific TCRs is an important impending development in the field of lung cancer research.

1.5.5. Disadvantages of adoptive T cell immunotherapy

Despite the potential of adoptive immunotherapy to treat cancer without the systemic effects of radiotherapy and chemotherapy, there can be adverse effects associated with T cell transfusion. For example, adoptive immunotherapy against melanoma has resulted in cases of vitiligo, where transferred cytotoxic T cells have also attacked melanocytes. This side effect has occurred using both tumour-infiltrating lymphocytes [73] and genetically engineered T cells specific for the melanoma antigen recognized by T cells 1 (MART-1) TCR. [74] Similar 'on-target' side effects have also been noted using a TCR specific for carcinoembryonic antigen, expressed by colorectal carcinomas, where physiological expression of this antigen in the colon lead to inflammatory colitis after T cell transfer. [75] Therefore, careful selection of the tumour antigen target is needed.

Viral antigens caused by malignant transformation, or mutated proteins caused by the genomic instability of cancer cells provide good targets to avoid damage to normal tissues. [76] The inclusion of a suicide gene into engineered T cells, such as inducible caspase-9, so that they can be destroyed in the event of serious side effects, provides extra safety and control over the therapy. [77]

More concerning is the possibility of tumour escape variants arising during adoptive immunotherapy, which would cause failure of the treatment. Genomic instability and a heterogeneous cancer cell population within tumours might favour the natural selection of tumour cells that do not express the antigen of interest during adoptive immunotherapy. [78] It is well known that antigen expression in tumours can change over time. For example, melanoma tumours have been shown to lose the tumour antigen MART-1, and become more heterogeneous, as the disease progresses. [79] This antigen loss could lead to failure of adoptive immunotherapy in advanced disease.

Work by Restifo et al. has also shown that tumours can lose MHC class I molecules. In their study 4 out of 13 patients who had undergone adoptive immunotherapy for melanoma had lost MHC class I molecules from tumour cells after their treatment. [80] This was found to be due to a loss of β_2-microglobulin expression, meaning that tumour antigens could not be processed in the endoplasmic reticulum for display on the cell surface membrane, giving the resulting tumour an immunoresistant phenotype.

These studies may explain the resistance of some tumours to adoptive immunotherapy, although much further work is required in this area. At the moment the reasons why some patients respond to immunotherapy while others do not are poorly understood. It is possible that other complementary cell therapies may be required to optimize the anti-tumour response.

1.6. Stem Cells

A stem cell has an unlimited capacity for self-renewal, and as well as dividing to renew itself it can also give rise to more differentiated progenitor cells. Stem cells are broadly divided into adult and embryonic stem cells. Adult stem cells are thought to be more cell lineage restricted than pluripotent embryonic stem cells. Adult stem cells can be found in stem cell niches present in many different tissues within the body, and are thought to play a role in tissue regeneration and repair after injury. Of these niches, bone marrow derived stem cells are the easiest to access, and can be aspirated with a simple bone marrow biopsy. These stem cells are a mixture of mesenchymal stem cells and haematopoietic stem cells. Mesenchymal stem cells can be isolated from other cell types due to their ability to adhere to tissue culture plastic. This thesis is concerned with adult mesenchymal stem cells only.

1.7. Mesenchymal Stem Cell (MSC) Therapy

1.7.1. MSCs

Mesenchymal stem cells (MSCs) are present in adult human bone marrow and are described as stem cells due to their ability to proliferate over many generations and their potential to differentiate into multiple cell lineages, such as bone, cartilage, tendon and fat. [81] They can be readily removed from the body, isolated, and expanded.

Whilst MSCs are predominantly present in the bone marrow, they are also found in large amounts in fat. They can be activated in response to specific chemical signals such as interleukins or growth factors from damaged areas, which can also cause recruitment of MSCs from the bone marrow. [82]

This property of MSCs means they are able to home to, and incorporate themselves into areas of inflammation within the body that have increased expression of immunogenic markers. [83] Similarly, injected mesenchymal stem cells are also able to home to and incorporate into tumours. [84] In fact, MSCs labelled with superparamagnetic iron oxide nanoparticles (SPIOs) have been shown to migrate to and incorporate into lung metastases in a murine model

within 1 hour of i.v. administration, with a further increase at 24 hours, using magnetic resonance imaging (MRI). [85] However, in this paper immunostaining of the lungs for DiI labelled MSCs within the lung metastases was not convincing, with only 2 DiI labelled cells observed in a single lung metastasis and this DiI signal did not match the iron containing cells located with Prussian blue staining. Macrophage staining on these sections suggests that a number of the iron containing cells in the lung metastases are in fact macrophages, so this differentiation is crucial to the interpretation of their data. To further characterise the iron-containing cells, it would have been useful to use anti-TRAIL immunostaining to demonstrate definitively that the iron containing cells were not macrophages but were instead MSC TRAIL that had lost their DiI label over time. Anti-TRAIL staining would have been a convincing argument that these iron-containing cells were MSC that had homed to the metastases.

The tumour homing potential of MSCs has been demonstrated with intra-peritoneal, intra-venous and subcutaneous injection, although in these cases a proportion of the injected cells will also end up in the liver, lungs, kidneys and spleen. [86] Stem cells have been imaged trafficking to tumours using bioluminescence imaging [87], magnetic resonance imaging (MRI) [88], and positron emission tomography (PET) [89]. This tumour homing mechanism means that MSCs can be used as vectors for the delivery of anti-tumour treatments. In addition, MSCs are immunoprivileged, lacking MHC II and co-stimulatory molecules CD80, CD86 and CD40. [90] This property means that allogenic cells could be used without the risk of immune rejection, and without the need for an HLA matched donor.

1.7.2. Tumour necrosis factor-related apoptosis-inducing ligand (TRAIL)

The aim of cancer therapies is to cause apoptosis (programmed cell death) within a population of tumour cells, whilst limiting or avoiding apoptosis in surrounding healthy cells. Chemotherapy and radiotherapy cause DNA damage that results in apoptosis via the intrinsic apoptotic pathway (Figure 1.4). This is mediated by the tumour suppressor gene p53, which activates bax and bak, causing the release of cytochrome c from mitochondria. This forms an apoptosome with ATP, procaspase 9 and apoptotic protease activating factor 1 (APAF 1) that activates

caspase 9, causing activation of effector caspases such as caspase 3. Unfortunately, during carcinogenesis more than half of tumours acquire mutations of p53. [91, 92] This results in the development of resistance to activation of the intrinsic apoptotic pathway and hence, resistance to chemotherapy agents and radiotherapy. [91]

Death ligands can induce apoptosis independently of p53 via the extrinsic apoptotic pathway. Tumor necrosis factor–related apoptosis-inducing ligand (TRAIL), is a type 2 transmembrane protein [93, 94] that has been shown to cause selective apoptosis of tumor cells, through the extrinsic apoptosis pathway. [95] On binding of the ligand to the TRAIL receptor, the receptor is oligomerized and Fas associated protein with death domain (FADD), and caspase 8 are recruited, to form a death inducing signaling complex (DISC). This results in the activation of caspase 3 and cell apoptosis (Figure 1.4). Activation of the death inducing signaling complex can be inhibited by FLICE-like inhibitory protein (cFLIP), which prevents activation of caspase 8.

There are five known receptors for TRAIL. Apoptosis is triggered after TRAIL binds as a homotrimer to death receptors 4 or 5 (DR4 or DR5). [96, 97] These receptors have a cytosolic death domain, however, there are other receptors than can bind TRAIL without leading to apoptosis (Figure 1.5). Decoy receptor 1 (DcR1) lacks a cytosolic death domain and is attached to the cell membrane by a glycophospholipid anchor, whereas decoy receptor 2 (DcR2) has a cytosolic domain that is shorter and unable to trigger apoptosis. [98] Osteoprotegerin (OPG) is a secreted receptor that inhibits osteoclastogenesis and increases bone density. [99] It can bind to TRAIL with a weaker affinity than DR5, and is capable of blocking TRAIL-induced apoptosis. [100] However, its role as a decoy receptor is not fully established.

The sensitivity of cancer cells to TRAIL and selective apoptosis of cancer cells over normal cells has been shown in several *in vitro* and *in vivo* studies. [101, 102] TRAIL is therefore an attractive therapy for cancer patients, due to its ability to kill cancer cells selectively, whilst sparing normal tissue, and without the unpleasant systemic side effects of chemotherapy or radiotherapy, such as nausea and vomiting, and immunosuppression.

1.7.3. MSCs Expressing TRAIL

The use of MSCs as a vehicle to deliver TRAIL to tumours harnesses the ability of MSCs to home to and incorporate into tumours, and also overcomes a major problem in the systemic delivery of TRAIL; the short *in vivo* half-life of recombinant TRAIL and TRAIL monoclonal antibodies. [103]

MSCs can be transduced to express TRAIL using a lentiviral vector, and treatment of subcutaneous tumours in a murine model using these cells has resulted in significantly reduced tumour growth compared to controls. [104] Using these cells in a pulmonary metastases model resulted in complete clearance of metastatic disease in 38% of mice after 5 doses of MSC TRAIL, given at 7 day intervals. [104]

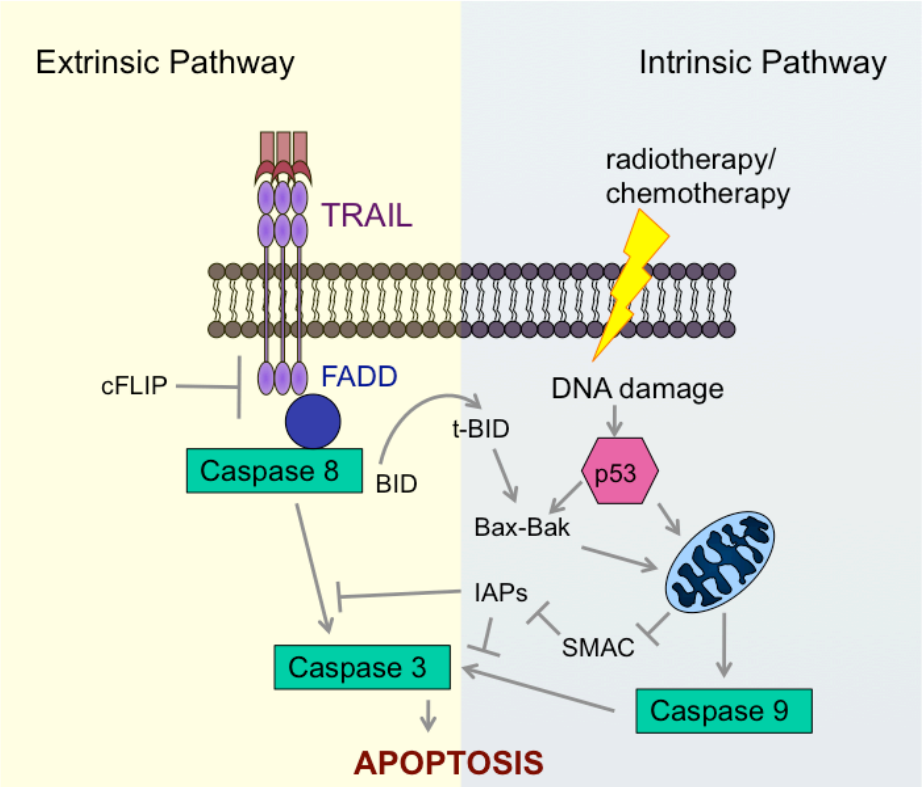

Figure 1.4: Traditional cancer therapies act via the intrinsic apoptotic pathway, causing DNA damage, activation of pro-apoptotic Bax and Bak and the release of cytochrome c from mitochondria. This in turn activates caspase 9, which cleaves procaspase-3 into caspase 3. Caspase 3 initiates apoptosis by cleaving intracellular proteins resulting in morphological and biochemical changes to the cell. The extrinsic apoptotic pathway is activated by the binding of a death ligand to a receptor (in this case TRAIL), causing receptor oligomerization and recruitment of Fas associated protein with death domain (FADD) and caspase 8. This cleaves and activates caspase 3, as well as cleaving and activating t-BID, which can bind to Bax and Bak, resulting in mitochondrial membrane permeabilization and cytochrome c release. Along with apoptotic protease-activating factor 1 (APAF1) and caspase 9, cytochrome c combines with ATP to form an apoptosome that cleaves and activates caspase 9, which then cleaves caspase 3, resulting in apoptosis. The two pathways are interlinked and regulated by inhibitors (headless arrows) such as inhibitors of apoptosis (IAPs) and cellular FLICE-like inhibitory protein (cFLIP), as well as activators such as SMAC that deactivates IAPs, preventing them from inhibiting apoptosis.

Figure 1.5: TRAIL receptors- only DR4 and DR5 have active cytoplasmic death domains. Decoy receptor DcR1 lacks an intracellular region, while DcR2 has a shortened and inactive cytosolic region. TRAIL can also bind to Osteoprotegerin (OPG), a soluble decoy receptor, at low affinity. Figure adapted from Kimberley et al. "Following a TRAIL: Update on a ligand and its five receptors". [99]

1.8. A combined EBV-TCR T cell and MSC TRAIL therapy

1.8.1. Advantages of a dual cell therapy

While the field of adoptive immunotherapy with tumour antigen specific T cells for lung cancer has not yet been developed, it is likely that this therapy alone will not be sufficient to clear the entire tumour and associated metastases, particularly if there are large masses. This has been seen in multiple studies using tumour antigen specific TCR T cells in Hodgkin's disease [63] and malignant melanoma. [51]

In addition, the chimeric LMP2 specific EBV-TCR T cells have not yet been tested in mouse models of cancer. Although their effectiveness *in vivo* is unknown, *in vitro* assays have shown greater than 80% target specific killing at T cell to tumour cell ratios of 5:1 and above, and around 40% at cell ratios of 1:1. [64] A comparison between this study and the work carried out by Loebinger et al. looking at target cell killing with MSC TRAIL is difficult due to the different methods used for cell killing assays, however, using MSC TRAIL at ratios of 1:1 with tumour cells also results in approximately 40% tumour cell lysis. [104] A significant difference between these two cell therapies is that the EBV-TCR T cell lysis of tumour cells is much quicker, occurring after 4 hours of incubation, whereas the MSC TRAIL tumour cell killing assay is measured after 48 hours of incubation. However, it seems likely that these two cell therapy methods are

equally effective, except that MSC TRAIL takes longer to cause their tumour cell killing effect.

In this thesis I have used MSC TRAIL and EBV-TCR transduced T cells synergistically, as a dual cell therapy, targeting tumour cells expressing the LMP2 antigen in a murine model of pulmonary metastases. This approach to cell therapy has never been explored and could yield promising results, with the aim of improved tumour clearance to that produced by a single cell therapy.

In particular, the inflammatory cytokines released by both CD4+ and CD8+ T cells could aid homing and engraftment of MSCs at the tumour sites, making MSC TRAIL treatment for pulmonary metastases more effective than the 38% complete clearance rate previously reported by Loebinger et al. [104] This benefit would be in addition to the tumour reduction caused by LMP2 antigen specific EBV-TCR T cells.

1.8.2. The effect of MSCs on T cell function

It is important to consider the effects of MSCs on T cell function, as MSCs are known to have immunosuppressive effects. For example, MSCs have been used successfully as immunomodulators in graft versus host disease (GVHD) in phase II clinical trials. [105] However, it is important to note that this early success with MSC immunomodulation was not repeated in larger phase III clinical trials, where there was no significant difference between MSC and placebo. [106]

In particular, MSCs have been shown to inhibit T cell responses to stimuli, resulting in reduced proliferation, [107] and response to their cognate peptide. [108] The mechanisms underlying this inhibition remain unclear, but are thought to involve both soluble factors secreted by the MSCs and mechanisms needing cell contact. One example of soluble factors affecting T cell function is indoleamine 2,3-dioxygenase (IDO), secreted by MSCs in response to interferon-gamma released in T-cell activation, which catalyses the conversion of tryptophan to kynurenine, suppressing allogeneic T cell responses. In this pathway, IDO catalyses oxidative cleavage of the 2,3 double bond in the indole ring of tryptophan to form N-formyl-kynurenine, which is then catalysed further into various metabolites, determined by downstream enzymes. Both *in vitro* and

in vivo studies have demonstrated that overexpression of IDO results in immunosuppression and reduced antigen-specific T cell responses. [109] Co-culture experiments with MSCs and mixed lymphocytes resulted in IDO secretion, with depletion of tryptophan and production of kynurenine, and reduced proliferation of lymphocytes. [110] Proliferation could be restored with the addition of tryptophan into the cell culture media, confirming IDO-mediated tryptophan metabolism as the cause of reduced proliferation.

In another study, MSCs were shown to selectively and irreversibly inhibit proliferation of T cells by down-regulating cyclin D2 expression. T cells were shown to arrest at the early G1 phase of the cell cycle, although this did not interfere with T-cell activation, and the suppressive effect on function was transient. [111]

Whilst it is clear that MSCs suppress T cell proliferation by a number of different pathways, studies examining the effect of MSCs of cytotoxic T cell function are more controversial. One study shows inhibition by MSCs of the formation of cytotoxic T cells, but no actual inhibition of cytotoxic T cell function. [112] Another study reports inhibition of proliferation, cytotoxicity and IFN-γ production in naïve, antigen-reactive and memory T cells, by MSCs in a dose-dependant fashion. [108] This effect was shown to be cell-contact dependent by control experiments using a transwell system where the numbers of pentamer positive CD8 T cells were not changed after exposure to MSC secreted soluble factors. The authors suggest that the MSCs may be physically hindering the T cells from contact with antigen, which could be seen to argue against their hypothesis of MSC inhibition, pointing instead to experimental flaws as they failed to control for increased cell numbers in their Chromium-51 cytotoxicity assay inhibiting T cell lysis.

The EBV-TCR transduced CD4 and CD8 T cells used in these experiments were cultured separately from MSCs to avoid any inhibitory effects on T cell activation or expansion. Therefore, this system may avoid the inhibitory effects of MSCs altogether, especially since MSCs have not been shown to inhibit cytotoxic T cell function *in vivo*.

1.9. Cell Labeling and Tracking

Along with rapidly developing advances in cell therapy for cancer, there is a pressing need to trace the cells *in vivo* as they home to tumours. There are many techniques available for cell labeling and tracking, none of which fulfill all of the ideal requirements needed for this purpose.

An ideal cell-labeling agent should be biocompatible and nontoxic, and should not change or damage the structure and functionality of the cell. [113] This is especially important for cell therapies, where the cell must retain its capability to provide an effect against the tumour. It is also desirable that the agent can be imaged with a high sensitivity and specificity, and that it provides a good contrast between background signal and contrast agent enhanced signal. Ideally, imaging the labeling agent will provide precise anatomical location of the cells and could be used to monitor signal, and hence, the efficacy of cell therapy, over a long period of time.

Cell labeling techniques can be divided into direct and indirect methods of labeling. [114] Direct labeling involves using labels that can be phagocytosed or transported into the cell, [115] or attached to the cell membrane, and subsequent injection of labelled cells. The disadvantages of direct labelling are that the label can elute out of the cell, or be diluted in daughter cells as the cell divides and that dead cells cannot be distinguished from live cells and other cells that have taken up the label by phagocytosis of labeled dead cells, for example, macrophages. [116]

Indirect labelling uses a reporter gene introduced into cells, which is translated into enzymes, receptors, symporters or proteins. [117] These cells can express the label over their entire lifetime, and this is also passed on to daughter cells, allowing the possibility of tracking expanding populations of cells, for example T cells during immunotherapy. [118] Since these proteins are transcribed only in live cells, live cells can be distinguished without background signal from dead cells.

1.10. Indirect Cell Labeling Methods

1.10.1. Magnetic Resonance Imaging (MRI)

MRI offers distinct advantages over the nuclear imaging modalities in terms of the achievable spatial resolution, and over both CT and nuclear imaging as it uses non-ionising radiation, although its sensitivity is limited. (Table 1-1) For MR imaging, cells have been transfected to express biotin on their cell surface membranes. This can be labelled with intravenously administered streptavidin iron oxide nanoparticles. [119] Alternatively, an adenoviral vector can be used to deliver ferritin transgenes to cells of interest, causing the cells to accumulate iron and become paramagnetic. [120] Both of these labelling methods result in shortened T2 and T2* and hence signal hypointensities in images, which can be difficult to localise and quantify. To overcome this problem, a reporter gene encoding lysine-rich protein has been developed, which provides MR contrast by the selective saturation on the resonant frequency of lysine (chemical-exchange saturation transfer). [121]

1.10.2. Optical Imaging

Bioluminescence imaging most commonly uses the luciferase enzyme, which catalyses the oxidation of the substrate luciferin, a reaction producing a photon of light that can be measured with a highly sensitive, charge-coupled device camera. (Chemical reaction Equation 1-1)[122] Luciferase can be transduced into cells using a lentiviral vector, after which the cell can be tracked for prolonged periods of time with multiple injections of substrate, with no background signal.

$$\text{Luciferase} + \text{Luciferin} + \text{ATP} \rightarrow \text{Luciferyl-AMP} + PP_i$$
$$\text{Luciferase.luciferin-AMP} + O_2 \rightarrow \text{Luciferase} + \text{AMP} + CO_2 + \text{Oxyluciferin} + \text{light}$$

where :

ATP = adenosine triphosphate

AMP = adenosine monophosphate

PP_i = pyrophosphate

O_2 = oxygen

CO_2 = carbon dioxide

Equation 1-1: Reaction sequence of firefly luciferase catalyzing the substrate luciferin to produce yellow-green light (λ_{max} = 560nm). [123, 124]

An advantage of bioluminescent cell tracking is the absence of ionizing radiation. However, this also results in limited tissue penetration as the signal is reduced 10-fold every centimeter of tissue depth, so that the maximum penetration depth is just 2 cm in tissue. The scattering of light in tissue also results in poor spatial resolution, which is dependent on, and is roughly equal to the signal depth, for example a signal depth of 3 mm results in a maximum achievable resolution of 3 mm. [125] Despite this disadvantage, it is a very sensitive technique, able to image 10-100 cells subcutaneously, or 10^6 cells at 2cm depth. [126] In addition to firefly luciferase, there are 4 types of beetle luciferase with emission wavelengths ranging from green to orange, as well as renilla luciferase from the sea pansy and gaussia luciferase from the marine copepod. [118]

There are numerous proteins available for fluorescent imaging that cover the entire spectrum of visible light, and these have been used for many years to study gene expression and promoters, to label proteins and study protein interactions, and as sensors to monitor the activity of enzymes. [127] However, the high background autofluorescence of tissue severely limits the sensitivity of fluorescence imaging in the visible spectrum. [128] This problem can be overcome with the use of filters for background subtraction, and by using infrared proteins, which minimize autofluorescence and have better tissue penetration. [129] Examples of far-red and infrared proteins that have been incorporated into cells using an adenovirus for *in vivo* fluorescence imaging are Neptune and Infrared protein. [130] However, optical imaging methods for cell tracking are limited to animal models because the maximum tissue penetration depth with infrared proteins is between 1 and 2 cm. [131]

1.10.3. SPECT Imaging

Single-photon emission computed tomography (SPECT) and positron emission tomography (PET), offer great advantages for cell tracking due to their high sensitivity, allowing radiolabels to be detected at picomolar or lower concentrations [114] and cells to be detected in the region of a few hundred cells, in a dedicated small animal PET scanner. [132]

The most important advantage of PET over SPECT imaging is its sensitivity. In PET imaging the radiotracers used decay by emitting a positron that is annihilated upon interaction with an electron, producing two gamma rays travelling at approximately 180 degrees apart, both with an energy of 511 keV. [133] The gamma rays are detected without the need for collimators, using coincidence-detection to accept or reject the photon. The lack of collimation improves sensitivity and results in an increased signal-to-noise ratio and improved temporal resolution. Another advantage of PET imaging is that the measured tissue activity can be quantified in Bq/mL tissue, after corrections for photon attenuation and scatter. [134]

However, spatial resolution in PET is limited by photon non-collinearity, resulting from the net momentum of the annihilated positron and electron leading to small deviations from 180 degrees and hence, image blurring. [135] Spatial resolution is also limited by the distance the positron travels through tissue before annihilation, which depends on the isotope used and the tissue type, for example, the spatial resolution lost is three times higher in lung than in soft tissue. [136]

An important advantage of SPECT imaging is that multiple radioisotopes can be used for simultaneous imaging using different energy windows, providing the isotopes decay with different energy levels. [137] Common examples of radionuclides used for SPECT imaging are Technetium-99m (140 keV, half-life 6.0 hours), Indium-111 (171 keV and 245 keV, half-life 2.8 days) or Iodine-125 (35 keV, half-life 59.4 days). These radionuclides can be attached to antibodies, receptor ligands and other molecules of interest, or used to label cells directly with the addition of a chelating agent. [129] Unfortunately, SPECT imaging is less sensitive than PET, due to the requirement for collimators to reject photons that are not within a small range of angles. The collimation also negatively impacts the spatial resolution, requiring that a balance be struck between sensitivity and resolution. [135] However, the design of pinhole collimators has improved the trade-off between sensitivity and spatial resolution, resulting in sub-millimetre image resolution for small animal SPECT scanners.

In contrast to PET, SPECT imaging has traditionally been regarded as non-quantitative, however, the implementation of software algorithms to correct for photon scatter and attenuation, and improvements in hardware, have resulted in improvements in the accuracy of quantification. [138]

In a high resolution, small-animal SPECT scanner, four pinhole collimators and four detectors, commonly consisting of Thallium-doped Sodium Iodide crystals, collect the incident gamma rays as they rotate on a gantry around the animal. [139] The resulting data is run through a filtered back-projection algorithm to reconstruct a 3D image. [140] Combining SPECT with CT imaging allows more accurate anatomical location of the SPECT signal, combining the strengths of CT (fast anatomical imaging) and SPECT (highly sensitive detection of radiotracer and the capability to do molecular imaging). [137]

Reporter genes have been used to track cells using SPECT and PET, such as the Herpes simplex virus thymidine kinase type 1 (HSV1-tk), which does not occur naturally in cells. Radiolabeled thymidine analogues are phosphorylated by the Herpes simplex virus thymidine kinase type 1 (HSV1-TK) enzyme, and trapped inside the cell, where they accumulate. Examples of the substrates used are uracil nucleoside derivatives such as 5-iodo-2′-fluoro-2′-deoxy-1-β-d-arabinofuranosyl-5-iodouracil (FIAU) labeled with Iodine-131, [141] and acycloguanosine derivatives such as 8-[Fluorine-18]-fluoropenciclovir ([^{18}F]FPCV). [142] Unfortunately, this reporter gene cannot be used in the brain because the substrates cannot pass the blood-brain barrier. It is also more difficult to quantify the expression of this reporter gene compared to others, as the signal produced by HSV1-TK is dependent on the amount of tracer metabolized by the enzyme, and not the concentration of the enzyme. Therefore, a kinetic study or tracer kinetic modelling is needed to accurately quantify expression. [143] In addition, there have also been immune responses in patients to the nonhuman HSV1-tk protein. [144]

Another common reporter gene is the human norepinephrine transporter (hNET), expressed by presynaptic terminals in the nervous system and responsible for the transport of norepinephrine into the nerve cell. Transduced cells can accumulate a norepinephrine analogue, metaiodobenzylguanidine, labeled with iodine-131

for SPECT imaging or an iodine-124 labeled version for PET imaging [145] As it is a human protein, there are little concerns about its immunogenicity, and its probe is already in routine clinical use with a proven safety record.

The human sodium/iodide symporter gene (hNIS) is responsible for active transport of sodium and iodide across the cell membrane and is highly expressed by the thyroid, with lower concentrations in other tissues, such as the salivary glands, stomach and thymus. The advantages to this system are that transfected cells can be imaged without the need to chemically engineer an analogue, simply using iodine-123 or iodine-131, and it is non-immunogenic to humans. [146] However, the iodine leaks out of cells except for those in the thyroid, which express thyroperoxidase for organification of the iodine, and iodine also cannot cross the blood-brain barrier.

These reporter gene imaging techniques have now been translated into clinical settings, with Jacobs et al. reporting the first use of HSV1-tk reporter gene imaging using PET in patients with glioblastoma. [147]

1.11. Direct Cell Labeling Methods

1.11.1. Conventional Cell Radiolabeling

Indium-111 has been used since 1976 [148] to radiolabel leukocytes for clinical applications, such as imaging infection, fever of unknown origin and osteomyelitis.

The most commonly used compound for leukocyte labeling is indium-111 oxine. Oxine chelates indium-111 ions, to form 3:1 complexes. The indium complex has a neutral charge and the oxine is lipophilic, so the complex diffuses into leucocytes. The complex has a low stability and dissociates, the indium-111 forming bonds with nuclear and cytoplasmic proteins that are stronger chelating agents in an exchange reaction, while the oxine diffuses out of cells. [149]

Tropolone is a chelating agent also used with indium-111. Similarly it is lipophilic and forms 3:1 complexes, however, unlike indium-111 oxine leukocyte

labeling, where cells must be removed from plasma, indium-111 tropolone has the advantage that cells can be labeled in plasma. [150]

However, despite the ease of use of indium-111 and its labeling efficiency of 50-80% within cells, its disadvantage is the high radiation dose given to labeled cells. This is primarily due to low energy Auger electrons emitted during radioactive decay, rather than external gamma radiation from extracellular label. [151] This high dose has lead researchers to search for a Technetium-99m complex (^{99m}Tc).

^{99m}Tc-hexamethylpropylene amineoxine (^{99m}Tc-HMPAO) labeling of leukocytes was first proposed in 1986. [152] This compound is also lipophilic, so crosses leukocyte cell membranes to label the cell, although its labeling efficiency is only 30-50%. [153] It also elutes out of cells after labeling, unlike indium-111, which is trapped inside the cell. An advantage of ^{99m}Tc-HMPAO is that it gives a lower total nuclear radiation dose to cells than ^{111}In (0.05 Gy/MBq rather than 1.4 Gy/MBq), [154] leading to increased leukocyte survival. It can also be produced less expensively by a bench-top eluting generator, and has a half-life of 6 hours. However, the short half-life and elution of the label out of cells, results in a rapidly decreasing signal and reduced specificity of the signal. [155]

Both methods of direct cell labeling have been extensively used in both clinical and preclinical studies, for example, indium-111 oxine has recently been used to image MSCs *in vivo* using SPECT/CT after their injection into the tibia of rats. [156]

1.11.2. Cell Labeling with Nanoparticles for MRI

Superparamagnetic iron oxide nanoparticles (SPIOs) have been used to label cells for in vivo tracking using MRI. [85, 157] These particles cause local inhomogeneities in the magnetic field, causing rapid dephasing of spins and a reduced tissue T2 and T2* relaxation time, leading to a reduced signal intensity in a T2 or T2*-weighted image. [158] However, this reduced signal can be hard to detect in tissues that already have low signal, for example, the lungs. [159]

1.11.3. Summary of Cell Tracking Methods

In conclusion, there is no perfect modality for cell tracking as each modality presents its own advantages and limitations (Table 1-1), and similarly no ideal method of cell labeling.

Indirect cell labeling methods are difficult and time-consuming, requiring the engineering of reporter genes and vectors for their delivery into cells. Other limitations with this technique arise from endogenous background signal and available tracers that are either expensive to make or do not have favorable kinetics or distribution. However, an advantage of these systems is that once the reporter has been incorporated into cells, they can be tracked repeatedly over time and cell expansion *in vivo* can be monitored.

Yaghoubi et al. first used a reporter gene to image a cell therapy in a patient in 2009, using the Herpes virus 1 thymidine kinase reporter for PET imaging of cytotoxic T cells. [160] However, it is likely that overcoming regulatory hurdles will be a significant challenge for reporter gene imaging in patients. [114]

Direct cell labeling methods are easier, quicker and very clinically translatable, but only allow short-term tracking (over 5-7 days with indium-111 oxine [161]), due to the elution of label from the cells and the short half life of the radioisotopes. Direct cell labeling using radiopharmaceuticals is an established technique for tracking leukocytes in the clinic, and has also recently been used to track defined cell populations such as neutrophils and eosinophils. [162] Direct cell labeling for tracking cell therapies in patients has been used for approximately a decade, after Blocklet et al. used indium-111 and technetium-99m to monitor antigen-loaded dendritic cells as a cancer vaccine. [163] MRI techniques for direct cell labeling have lagged behind the nuclear medicine modalities but are now being used in clinical studies, for example, dendritic cell labeling with SPIO for MRI tracking of a cell therapy against melanoma. [164] However, there is still an ongoing need for labeling agents that allow medium or long-term cell tracking and that do not elute quickly out of the cells of interest.

Modality	Advantages	Disadvantages
MRI	High spatial resolution	Sensitivity to tracers
	Non-ionising radiation	Quantification difficult
	Reporter genes can allow tracking of cells over time	Iron oxide nanoparticle based contrast agents reduce signal so tracking can be difficult
	High soft tissue contrast	Expensive
Bioluminescence	High SNR	Limited depth penetration
	Unlimited tracking over time	Low spatial resolution (depth dependant)
	Indicates cell survival	Limited clinical applicability
	Quantification possible	Cells must be transduced ex-vivo
Nuclear imaging	High sensitivity	Ionising radiation
	Quantification possible	Low spatial resolution
	Correlation with anatomy when combined with CT	Conventional cell labeling techniques can result in a high radiation dose to cells
	Reporter genes allow tracking of cells over time	

Table 1-1: Advantages and disadvantages of cell tracking methods

1.12. Cell Labeling Using Cell Surface Thiols

Thiols are found on the side chain of cysteine (an amino acid with an uncharged polar side chain- therefore, zero net charge at neutral pH). The side chain has a sulfhydrl group (-SH), which is an important component of the active site of many enzymes. Under oxidizing conditions the –SH groups of two cysteines can spontaneously form a dimer, cystine, which contains a covalent cross-link called a disulfide bond (-S-S-). [165] A disulfide linkage contributes to the stability of the three-dimensional shape of the protein molecule.

Oxidation and reduction of thiol proteins on the cell membrane is thought to be the predominant mechanism in cellular signal transduction pathways for reactive oxidants. [166] Cells are exposed to many different reactive oxidant species that can act as initiators or second messengers for thiol- based redox signaling, which is fundamental to a wide range of receptor-mediated pathways.

It has been shown that oxidation decreases cell surface membrane thiols and reduction increases cell surface membrane thiols, by reducing disulfide bridges

via thiol-disulfide exchange reactions. [167] Studies have shown that thiol groups are expressed by freshly isolated peripheral blood mononuclear cells in the range of 3-18 x 10^9 thiol groups per cell, measured using a 5,5′-dithiobis(2-nitrobenzoic acid) (DTNB) assay. [168, 169] In particular, freshly isolated lymphocytes from patients have been shown to express 4-15nmol thiol groups per 10 million cells, equating to 0.25-0.93 x 10^9 thiol groups per cell, measured using AlexaFluor®-maleimide fluorescent staining and flow cytometry analysis. [167]

Recently there has been increasing interest in using these thiol groups as a target for cell labeling. [167, 170, 171] Maleimide is a compound commonly used for this purpose, as its double bonds readily and selectively react with the disulfide bonds in cysteine molecules, forming a stable carbon-sulphur bond. Other conjugation groups that have also been used are bromobimanes [172] and iodoacetamides. [173]

The maleimide labeling strategy will be explored in this thesis using a novel tri-functional probe, consisting of a fluorescent molecule, the radioisotope Iodine-125 (^{125}I) and a maleimide group, developed by UCL's Radiochemistry Department (Dr Ran Yan, Dr Erik Arstad). The fluorescent reporter will allow quantification of cell labeling *in vitro* using flow cytometry, as well as showing the location of labeled cells in tumours *ex vivo* after tissue preparation for histology. The radioisotope reporter allows the cells to be tracked *in vivo* using SPECT imaging (Figure 1.6, Figure 1.7).

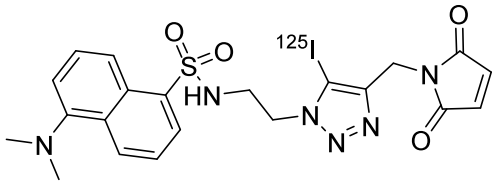

Figure 1.6: Chemical structure of the I^{125}-Dansyl maleimide probe

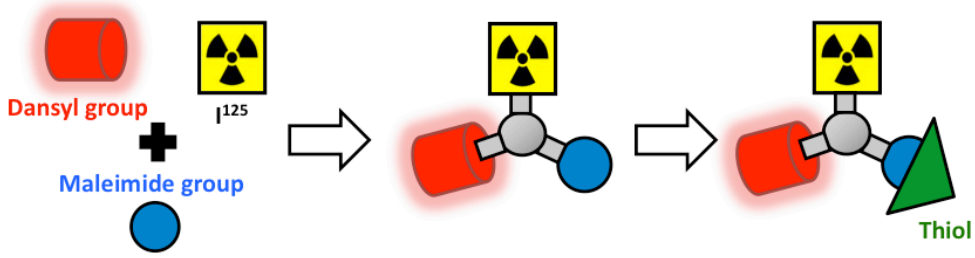

Figure 1.7: Schematic diagram of the structure of the I^{125}-Dansyl maleimide probe

This dual imaging potential allows two imaging modalities with different and distinct advantages to be combined, to look at labeled cells at a cellular and a macroscopic level. This multi-scale, dual imaging approach has previously been used to look at colorectal tumours using the carcinoembryonic antigen (CEA) specific antibody A5B7 as the binding group, with an ^{125}I reporter and a fluorescent rhodamine reporter. [174] However, maleimide labeling of a cell therapy with a tri-functional probe is a novel approach to tracking a cell therapy.

1.13. Summary

The concept of two engineered cell therapies working in tandem to target lung cancer is intriguing, and could result in better tumour clearance than that observed with a single cell therapy alone. This thesis combines tumour antigen specific T cells with MSC TRAIL to provide a completely novel approach in cell therapy. As discussed previously in the cell therapy sections, MSC TRAIL alone or tumour antigen specific T cells alone are not capable of consistently clearing tumours. This is likely due to several factors, including, but not limited to, antigen escape variants and the immunosuppressive tumour environment. It is possible that cytokines secreted by the T cells will aid MSC homing and engraftment, leading to improved tumour clearance, and that MSC TRAIL could kill residual tumour with antigen escape variants.

Furthermore, I will test novel and conventional direct cell labeling strategies to enable imaging of these therapies *in vivo*. The ability to track a cell therapy *in vivo* would answer many questions about the location and persistence of transfused cells. Indirect cell methods present many challenges, including the difficulty translating them from animal models into patients. Efforts to develop

reporter genes strategies and their optimization are ongoing at the Centre for Advanced Biomedical Imaging at UCL, and are outside the scope of this thesis. Therefore, a direct cell labeling method will be simpler, quicker and more clinically translatable.

Contributions arising from this thesis are as follows:

- The first *in vitro* and *in vivo* application of a dual cell therapy for cancer.
- The first *in vivo* studies using the chimeric LMP2-specific EBV-TCR.
- The first use of T cells with a tumour antigen specific TCR to target lung cancer *in vivo*.
- The first known application of bioluminescence imaging to track tumour antigen specific TCR T cells homing to lung metastases.
- Testing a novel tri-functional probe targeting cell surface thiol groups for labeling cell therapies.

1.14. Hypothesis

A combination therapy of EBV-TCR T cells and MSC TRAIL, when injected into mice bearing lung metastases, will result in better tumour clearance than in mice injected with a single cell therapy.

Tri-functional probes with a fluorescent reporter and a radioisotope reporter will enable imaging of these cells homing to lung metastases *in vivo*.

1.15. Aims

The aims of this work are as follows:

1. Transduce T cells to express the EBV-TCR and test their efficacy *in vitro*.
2. Explore conventional cell radiolabeling strategies and assess their suitability for T cell tracking.
3. Test the novel tri-functional probe for T cell tracking and compare to conventional cell radiolabeling strategies.
4. Combine EBV-TCR T cells and MSC TRAIL as a therapy for *in vivo* murine models of lung metastases, and image the cells homing to the lungs.

2. Materials and Methods

This chapter describes all the experimental procedures, reagents and equipment used to gather data for this thesis.

2.1. Cell culture

All sterile tissue culture media, sterile tissue culture grade trypsin/EDTA, tissue culture antibiotics and fetal bovine serum (FBS) were purchased from Invitrogen (Paisley, UK) unless otherwise stated. Sterile tissue culture flasks and plates were obtained from Nunc (Roskilde, Denmark). All the cell types used in experiments are described below. (Table 2-1)

Cell name	Cell type	Purpose
MDA-MB-231	Human breast adenocarcinoma cell line	Used *in vivo* as a model for lung metastases
Jurkat cells	Human acute T cell leukaemia cell line	Used in place of EBV-TCR T cells for preliminary experiments in cell labelling
Peripheral blood mononuclear cells (PBMCs)	Human donor lymphocytes (70-90%), monocytes and dendritic cells	Used to produce EBV-TCR T cells
MSC TRAIL	Human mesechymal stem cells expressing full length TRAIL	Used as a cancer cell therapy
Phoenix Ampho cells	Human kidney epithelial cell line	Highly transfectable cell line used to produce retrovirus for transductions
T2 cells	Human lymphoblastic cell line	MHC class II negative cell line used to present exogenous peptide to T cells during restimulation

Table 2-1: Summary of the different cell types used during experiments.

MDA-MB-231 cells were the cancer cells used for *in vitro* and *in vivo* studies, as these cells reliably form lung metastases in xenograft mouse models. Adenocarcinoma is the commonest form of non-small cell lung cancer, and these tumours tend to metastasize early throughout the lung, hence the choice of this tumour model. The cell membrane of MDA-MB-231 tumour cells have also been shown to be a potent chemoattractor for MSCs, relative to other cancer cell lines.

[175] MDA-MB-231 cells were cultured in Dulbecco's modified Eagle's medium (DMEM) with 4 mM L-glutamine, 50 units/mL penicillin and 50 μg/mL streptomycin and 10% (v/v) fetal bovine serum (FBS) and were incubated at 37°C in a humidified, 5% CO_2 atmosphere. They were passaged at 1:12 twice weekly, by washing twice with phosphate buffered saline (PBS), then using 3 mL trypsin EDTA to lift off adherent cells.

Jurkat leukaemia cells were obtained from the Institute of Child Health and were cultured in Roswell Park Memorial Institute 1640 media (RPMI) with 4 mM L-glutamine, 50 units/mL penicillin and 50 μg/mL streptomycin and 10% (v/v) fetal bovine serum (FBS) added, and were incubated at 37°C in a humidified, 5% CO_2 atmosphere. They were passaged at 1:10 twice weekly, by aspirating and discarding old media and replacing it with fresh media.

Human donor peripheral blood mononuclear cells (PBMCs) were obtained from the Royal Free Hospital Biobank, and cultured at the Immunology Department of the Royal Free Hospital, London. PBMCs were defrosted into RPMI media, with 4mM L-glutamine, 50 units/mL penicillin and 50 μg/mL streptomycin and 10% (v/v) fetal bovine serum (FBS) and were incubated at 37°C in a humidified, 5% CO_2 atmosphere. OKT3 CD3 antibody and interleukin-2 (IL-2) (Chiron) were added into the cell suspension at 30 ng/mL and 600 units/mL respectively, to stimulate expansion of T cells. After transduction, the media was aspirated every 2-4 days, and replaced with fresh RPMI media, with 200 units/mL IL-2 added.

Human mesenchymal stem cells (MSC) expressing full length TRAIL, were obtained from Krishna Kolluri and Dr Zhengqiang Yuan in the UCL Division of Medicine Lungs for Living Lab. These were cultured in triple layer flasks in Alpha Modified Eagle's Media (αMEM) with 16% FBS, 4mM L-glutamine, 50 units/mL penicillin and 50 μg/mL streptomycin added. Before use in experiments, they were washed twice with PBS and harvested using 10 mL trypsin-EDTA.

Phoenix Ampho cells were cultured in Iscove's Modified Dulbecco's Medium (IMDM) with 10% FBS, 4mM L-glutamine, 50 units/mL penicillin and 50 μg/mL streptomycin added. They were defrosted from stock vials at least one

week before use and were not used for more than two transductions. They were passaged twice weekly using trypsin-EDTA to lift off the adherent cells and replated at 1:5 to 1:8 ratios to keep cell confluence below 80%.

T2 cells were cultured in RPMI media as described above and were passaged twice weekly at a 1:10 to 1:12 ratio by aspirating old media and replacing it with fresh media.

2.2. T cell transductions

Retroviral transductions were performed to generate EBV-TCR T cells, using a plasmid supplied by Dr Shao-An Xue. (Figure 2.1) A new T cell transduction was usually performed before each experiment, using several donor PBMCs. Before starting the transductions, a large quantity of viral plasmid was produced using the standard QIAGEN Maxi Prep kit and protocol.

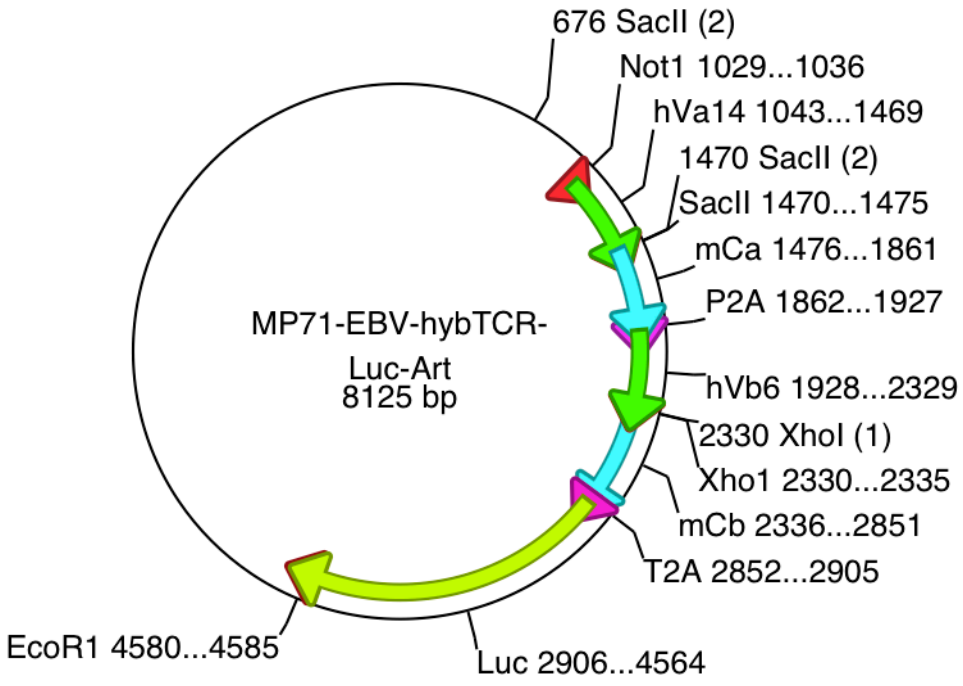

Figure 2.1: Plasmid used in transductions to create EBV-TCR T cells

To start, Phoenix Ampho packaging cells (Nolan lab, Stanford University, USA) were plated at 2 x 10^6 cells in a 10 cm Petri dish in 8 mL Iscove's Modified Dulbecco's Medium (IMDM) with 10% FBS, 4mM L-glutamine, 50 units/mL penicillin and 50 μg/mL streptomycin added.

The following day, these cells were transfected with plasmid so that they produce retrovirus containing the EBV-TCR plasmid. On the morning of the transfection day, PBMCs from the BioBank were activated after defrosting and plated in a 6 well plate at 1 million cells/ml of RPMI, 8 mL per well, with OKT3 30 ng/mL and IL-2 600 units/mL added. Transfection of the Ampho cells was carried out in the afternoon. Thirty minutes prior to transfection, the medium was removed and replaced with 5 mL fresh IMDM. A Fugene transfection mix was prepared; in one eppendorf 300 μl of Opti-MEM® medium (Invitrogen, Paisley, UK) was mixed with 10 μl Fugene HD (Promega, Southampton). In a second eppendorf, 1.5 μg pCl-amp and 2.6 μg DNA was mixed with 46.1 μl distilled water. The second solution was added to the first and the mixture was left at room temperature for 15-20 minutes. After 15-20 minutes the mixture was added drop wise to the Ampho cells, and the plates gently swirled, before being placed back in the incubator overnight.

The following day the media on the transfected Phoenix Ampho cells was replaced with 5 mL fresh RPMI, and a 24 well plate was coated with RectroNectin® (Takara Bio Incorporated, Japan) 750 μl of 30 μg/ml in each well. The plate was covered and left overnight in the refrigerator. RectroNectin® is a recombinant polypeptide containing functional domains capable of binding viruses and cell surface proteins, and is used to improve transduction efficiency.

On the transduction day, the RectroNectin® was removed from the plate and blocked with 2% bovine serum albumin (BSA) in PBS, 500 μL/well for 30 minutes at room temperature, after which the plate was washed twice with PBS. Activated PBMCs were plated in a 24 well plate at 1 million cells/mL of RPMI and additives, with 600 units/mL of IL-2 added. The viral supernatant from the Phoenix Ampho cells was carefully removed and spun at 1500 rpm for 5 minutes to remove cells and cell debris. One millilitre of viral supernatant was added to each well of T cells and the cells were incubated overnight at 37°C and 5% CO_2.

The next day, viral supernatant was carefully removed from the T cell wells and replaced with fresh RPMI with IL-2 100 units/mL added. Transduced T cells were used 2-3 days post-transduction.

2.3. Flow cytometry for measuring EBV-TCR expression

In a flow cytometer, cells in suspension are aspirated and sheath fluid is used to hydrodynamically focus the cells into a thin stream of liquid, one cell wide, so that each cell can be read individually. Laser light is focused onto the stream of cells, and there are detectors at the opposite side of the stream, and perpendicular to the laser source. Cells in the stream scatter the light source, and the forward and side scatter is used to look at properties of the cell, such as granularity and size. Different coloured lasers can be used to excite a range of fluorophores, so that several parameters can be measured at once. [176]

To determine transduction efficiency (expression level of introduced TCR), transduced T cells were stained with anti-CD4.APC-Cy7 (1:50) for T helper cells, anti-CD8.PE-Cy7 (1:50) for cytotoxic T cells, anti-murine cβ.APC (2:50) for the murine constant region of the β-chain, and CLG pentamer.PE (2:50) a pentamer specific for the EBV-TCR. The pentamer consists of 5 MHC-CLG peptide complexes, arranged in a circular configuration so that all the MHC molecules can interact with CD4 or CD8. Combining MHC molecules in this fashion has been shown to increase binding stability between the probe and the TCR, as T cells generally have a low binding affinity for their cognate peptide-MHC complex. [177] The MHC molecules are connected via a linker protein to 5 fluorescent PE molecules, producing both high avidity binding and bright staining of EBV-TCR positive T cells. All the fluorescent antibodies were purchased from Invitrogen^{TM} (Paisley, UK) and the CLG pentamer was purchased from ProImmune Ltd. (Oxford, UK).

In addition to routine quality control checks, a daily calibration was performed on the flow cytometer using latex beads before running any experiments. Before running the samples, appropriate single colour controls were used to calculate the compensation needed to correct for spectral overlap. These were an unstained control, anti-CD8.FITC (2:50), anti-CD8.PE (2:50), anti-CD8.PE-Cy7 (1:50),

anti-CD4.APC-Cy7 (1:50) and anti-CD4.APC (2:50). After washing with PBS and resuspending in FACS buffer, the cells were run on a BD™ LSR II flow cytometer using FACSDiva™ software. All flow cytometry data was analyzed using TreeStar FlowJo software.

2.4. T cell stimulation

Peptide stimulation is used to activate and expand the population of T cells that express the specific TCR of interest. Autologous donor PBMC cells and T2 cells were used to stimulate EBV-TCR transduced T cells. T2 cells suspended at 200,000 cells/40 μL in an eppendorf tube were loaded with CLG peptide at 100 μM concentration, and incubated for 2 hours at 37°C, 5% CO_2. 2 x 10^5 T2 cells and 2 x 10^6 feeder PBMCs were used per well, and these were irradiated for 14 and 7 minutes respectively (80 Gy and 50 Gy), to prevent cell proliferation. The irradiated cells were added to transduced T cells plated at 5 x 10^5 cells per well, and plated in a 24 well plate with 2 μL/mL IL-2 added. The cells were then left to incubate at 37°C and 5% CO_2, for the EBV-TCR transduced cells to expand. The percentage of cells expressing the EBV-TCR was monitored 4 days post-stimulation using flow cytometry as described above. Five to seven days post-stimulation, cells were used in chromium-51 and co-culture assays.

2.5. Tumour cell transduction

Phoenix ampho cells were also used to make virus for the transduction of MDA-MB-231 cells with LMP2 antigen. The viral construct also included green fluorescent protein (GFP) as a transduction marker. Transduction was carried out as described above, except that MDA-MB-231 cells replaced PBMCs, and were plated at a density of 100,000 cells per well, in 1 mL DMEM with 1 mL viral supernatant added to each well. Flow cytometry was performed to check the transduction efficiency of the cells, using green fluorescent protein (GFP) to measure LMP2 expression, and untransduced MDA-MB-231 cells as a control.

2.6. Chromium release assay for EBV-TCR transduced T cells

This assay is used to assess TCR-antigen mediated cytotoxicity. It should ideally be performed 5-6 days after peptide-stimulation of the transduced T cells. The

day before, target cells are plated at 1.5 x 10^5/mL. On the day of the experiment, target T2 cells are counted and loaded with 10 μM relevant CLG or irrelevant NLV peptide for 1 hour at 37°C and 5% CO_2. Then cells are labeled with 1.85 MBq chromium-51 (^{51}Cr) and incubated for an additional hour. Following incubation, cells are washed 3 times to remove excess ^{51}Cr. T cells are counted, washed and resuspended in RPMI at 1.25 x 10^5 cells in 100 μL before being added to a 96-well plate in a dilution series down to a concentration of 3.75 x 10^3 cells per 100 μL (in triplicate). Then target cells are added to each well at 5,000 cells per well, including 2 rows at the bottom for minimum ^{51}Cr release (target cells only) and maximum release (target cells plus 100 μL 1% trifluoroacetic acid for cell lysis). The plate is then centrifuged at 1300 rpm for 3 mins, after which it is placed in a designated radioactive incubator for 4 hours at 37°C and 5% CO_2. After incubation the plate is centrifuged again, and a new 96-well plate is prepared with 100 μL of scintillant added to each well. Fifty microlitres of supernatant is added to the scintillant and the plate is clearly labeled and left overnight in a designated room. The following morning, the plate is read in a Wallac 1450 Microbeta Plus analyser and the percentage cell lysis calculated as:

$$\text{Cell lysis} = \left(\frac{\text{sample lysis - spontaneous lysis}}{\text{maximum lysis - spontaneous lysis}}\right) \text{x } 100 \quad [55]$$

Equation 2-1: Equation used to calculate target cell lysis in the Chromium-51 release assay.

To assess the TCR-antigen mediated cytotoxicity against the transduced LMP2-GFP MDA-MB-231 cells, this assay was repeated using these cells in place of T2 cells, and omitting the peptide-loading step.

2.7. IL-2 and IFN-γ Enzyme-linked immunosorbent assay (ELISA)

ELISAs to measure IL-2 and IFN-γ secretion by activated EBV-TCR T cells were performed according to manufacturer's instructions (Abcam, UK). Briefly, the relevant capture antibody was appropriately diluted and used to coat a 96-well ELISA plate overnight at 4°C. The plate was then washed well with wash buffer and blocked with 200 μL assay diluent, whilst a dilution series of IL-2 and IFN-γ standards were prepared, starting at 500 pg/mL and 300 pg/mL

respectively. Assay diluent served as a zero standard. After blocking the plate was again washed with wash buffer, and 100 µL of each standard was added to the wells (in duplicate), including zero standards. Stimulated EBV-TCR T cell supernatant samples were diluted 1:5 in assay diluent, then 100 µL was added to the wells (in triplicate). EBV-TCR T cells were stimulated 24 hours before the assay by plating 1 x 10^5 T cells with 1 x 10^5 CLG peptide loaded T2 cells in 200 µL RPMI media in a 96-well plate.

After adding the samples, the plate was sealed and left room temperature for 2 hours, and then washed 5 times with wash buffer. The working detector was prepared by diluting appropriate concentrations IFN-γ/ IL-2 detection antibody in assay diluent and adding avidin-horseradish peroxidase conjugate. After washing, 100 µL working detector was added and the plate was sealed and left at room temperature for 1 hour. The plate was then washed 7 times in wash buffer, 100 µL of 3,3',5,5'-tetramethylbenzidine substrate solution was added to the wells and the plate incubated at room temperature, in the dark, for 10-30 minutes. When the colour had developed, 50 µL stop solution was added to the wells. The absorbance of each well of the plate was then read on an optical density reader at 450 nm. The results from the assay standards were used to plot a standard concentration curve using excel software, which was used to calculate the concentration of the samples.

2.8. Co-culture experiments

For all co-culture experiments, passage 9 or 10 MSC TRAIL were used. In 24-well plates, 5 x 10^4 MDA-MB-231 LMP2 cells were plated with a reducing ratio of MSC TRAIL, from 1:1 to 16:1. Control wells of tumour cells only, and tumour cells plated with MSCs that did not express TRAIL were included. Cells were plated in αMEM and left in a humidified incubator at 37°C, 5% CO_2, for 48 hours. Following incubation the cells were trypsinized, and all media and PBS was saved in order to keep the dead tumour cells for analysis. The cells were stained with Annexin V PE.Cy7 and PI to measure apoptosis and death, respectively. Briefly, the cells were suspended in 100 µL Annexin binding buffer and 5 µL Annexin V solution was added. The cells were left at room temperature in the dark for 20 minutes, after which another 400 µL of Annexin binding

buffer was added to the cells. Before running on the flow cytometer, 2 μL of 1 μg/mL PI solution was added.

The cells were run on a BD Biosciences™ LSR II flow cytometer using FACSDiva™ software, with appropriate signal colour controls used to set compensation. The tumour cells were identified by their expression of GFP, and gates were set defining the tumour cell population. The data was analysed using FlowJo software to give percentages of live, dead, apoptotic and dual stained tumour cells.

In order to complete further co-culture experiments exploring combined MSC TRAIL and EBV-TCR T cell killing, it was first necessary to establish the effect of culturing T cells in αMEM, rather than in RPMI (T cell media). 1 x 10^6 PBMCs were plated in 50:50 αMEM and RPMI, and 100% αMEM with IL-2 added to the media. After 48 hours a trypan blue death count was used to check cell survival.

To assess the affect of MSC TRAIL on EBV-TCR T cell survival, these cells were plated at a 1:1 ratio in a 24-well plate in αMEM for 48 hours. Following this, the T cells were stained with Annexin V and PI for apoptosis and death, as described above, and the cells were run on a BD™ LSR II flow cytometer as described above.

2.9. Conventional cell radiolabeling protocols

The cell labeling protocols followed for conventional radiolabeling were those used in clinical practice by the Radiopharmacy of the Institute of Nuclear Medicine at University College Hospital, London, and will be described in the relevant section. Cell labeling agents ^{99m}Tc-HMPAO and Indium-111 Tropolone were supplied by the Radiopharmacy at the Institute of Nuclear Medicine, University College Hospital.

2.10. Cell labeling with ^{99m}Tc-HMPAO

The ^{99m}Tc-HMPAO complex is lipophilic and in aqueous solution degrades into free ^{99m}Tc-pertechnetate and a hydrophilic ^{99m}Tc-HMPAO complex over time, hence it must be used to label cells within 20 minutes of preparation. The exact

mechanism of labeling is not understood but two methods have been proposed: 1) binding of ^{99m}Tc-HMPAO to non-diffusible organelles or cytoplasmic proteins, and 2) intracellular conversion of the lipophilic complex into the hydrophilic complex by reducing agents, such as glutathione, leading to sequestration within cells. [155]

For cell labeling, the ^{99m}Tc-HMPAO solution was freshly prepared and used within 20 minutes. A vial containing exametazime 0.5 mg (Ceretec^{TM}) was reconstituted with fresh ^{99m}Tc generator eluate (5mL in 0.9% saline) to form the labeling solution. Jurkat cells (40 x 10^6) were washed twice in PBS, before being spun down into a cell pellet. Immediately after the PBS on the cell pellet was discarded, the entire dose of ^{99m}Tc-HMPAO (123 MBq) was added onto the pellet and the cells were left at room temperature for 10 minutes, with occasional shaking. Afterwards, the cells were washed again with 10 mL PBS and the activity was counted in the cell pellet and the supernatant using a dose calibrator (Capintec). The cells were then resuspended in 1 mL PBS, left for 30 minutes, spun down again followed by gamma counting of the cell pellet and supernatant. Radioactivity in the cell pellet and the supernatant was measured over time, up to 24 hours. Death rates in the cells were also measured at each time point, in triplicate, using trypan blue.

2.11. Cell labeling with ^{111}In tropolone

The ^{111}indium-tropolone complex is neutral and lipid-soluble, allowing it to diffuse across the phospholipid bilayer to label cells. The mechanism of action for cell labeling is not fully defined, but is thought to involve an exchange reaction between tropolone and cytoplasmic components that are stronger chelating agents, such as lactoferrin. This theory is supported by the low stability constant of the ^{111}indium-tropolone complex. [178]

Jurkat cells (40 x 10^6) were washed twice with PBS then spun into a cell pellet and the PBS was discarded. Following the washes, 150 µL of tropolone solution was mixed with 30 MBq of indium-111 solution (volume 425 µL) and this was added to resuspend the cell pellet. The cells were incubated for 10 minutes at room temperature and agitated periodically, then washed with PBS and the

radioactivity measured in the cell pellet and supernatant using a dose calibrator. As before, the activity in the cell pellet and supernatant was measured over time. Death rates in the cells were also measured at each time point, in triplicate, using trypan blue.

Mesenchymal stem cells (5 x 10^6) were labeled in a similar fashion, with 20 MBq activity of Indium-111. For T cell imaging, EBV-TCR luciferase T cells (6 x 10^6 per mouse) were labeled separately with approximately 15 MBq of Indium-111.

2.12. Maleimide probe labeling protocol

The maintenance of extracellular thiol groups is supported by oxidation/reduction reactions and disulfide exchanges in the cell surface microenvironment. [179] Maleimide reacts specifically and irreversibly with thiol groups at a pH of 6.5-7.5, resulting in a stable thioether carbon-sulfur bond.

Jurkats or T cells were taken from suspension, washed twice with PBS and resuspended in PBS at 1 million cells/mL. The relevant concentration of the probe was spiked into the suspension and the cells left for 1 hour in the incubator at 37.5°C. The cells were finally washed twice in PBS, and then used for the experiment.

Rhodamine maleimide and Dansyl triazole maleimide will be the probes discussed in this thesis. For Rhodamine maleimide labeling the concentrations used were 1 nM - 1 μM. For Dansyl triazole maleimide cell labeling the concentrations used were between 1 μM to 1 mM. The choice of labeling concentration will be discussed further in chapter 5.

Secondary antibodies for flow cytometry were added after maleimide labeling as per the manufacturers protocol. Annexin-V Alexa Fluor®-647 or Annexin-V Alexa Fluor®-488 (Invitrogen), was used to measure apoptosis, and Propidium Iodide (PI) (Invitrogen) or 4',6-diamidino-2-phenylindole (DAPI) (Invitrogen), was used to measure cell death. Cells were transported on ice before flow cytometry.

2.13. CellTracker™ CM-DiI and DiR labeling

These membrane-bound fluorescent probes were used to label cells before injection for the *in vivo* experiments. Cells were labeled at 1 μL probe per 10^6 cells in 1 mL of serum–free media, for 15 minutes at room temperature, as per the maunfacturer's instructions (life technologies™, Paisley, UK). They were then washed twice in 10 mL PBS, before being resuspended in the desired volume ready for use.

2.14. Flow cytometry for maleimide-binding probes

A flow cytometer was used to analyse the percentage of maleimide labeled cells, and to measure other parameters, such as apoptosis (Annexin-V) and death (DAPI/PI). Rhodamine maleimide exhibits fluorescence at 610 nm and Dansyl triazole maleimide exhibits fluorescence at 525 nm, therefore, secondary fluorescent labels were chosen carefully so their fluorophores could be read in different channels, to avoid signal overlap. Unstained and single-stained controls were run for each experiment to determine gating parameters and compensation, after which the samples were run.

2.15. Fluorescent and confocal microscopy of labeled cells

For fluorescent microscopy, labeled cell samples were spun down at 1500 rpm for 5 minutes, and then re-suspended in 150 μl PBS. The suspension was dropped onto a SuperFrost® glass slide, and a number 1 coverslip (both VWR International, Lutterworth, UK) was placed on top. A Zeiss Axioskop 2, combined fluorescent and light microscope system was used to image cells in combination with QImaging software.

For confocal microscopy, cells labeled with the maleimide probes were counterstained with DAPI or Annexin V, and then spun down and resuspended to 10^6 cells in 200 μL. Using a Shandon Cytospin 2, 10^6 cells were spun onto a SuperFrost® glass slide at 400 rpm for 4 minutes, then the cells were covered with Immuno Mount™ (GeneTex Inc., Irvine, CA, USA) and a number 1 coverslip was placed on top. The cells were imaged with a Leica TCS SP2 upright confocal microscope (Leica Microsystems, Milton Keynes, UK).

2.16. 5,5'-dithiobis-(2-nitrobenzoic acid) (DTNB) assay for quantifying cell surface thiols

Jurkat cells were grown in suspension until they reached confluencies of 200,000, 400,000 and 800,000 cells per mL (in triplicate). Jurkat cells were then taken from suspension and washed twice with PBS, before being resuspended at 1 million cells/ 1ml PBS in eppendorf tubes, with 200 μM DTNB added. After a 5-minute reaction time, the cells were spun down and 100 μl of cell suspension from each was removed and added to a 96 well plate. The absorbance 2-nitro-5-thiobenzoic acid (TNB) a yellow coloured product, was measured using a plate reader set to 412 nm wavelength. The thiol groups present in the sample were quantified by reference to the extinction coefficient of TNB. (Equation 2-2) As the sample contained a known number of cells, the number of thiol groups per cell could be calculated.

$$\text{Molar absorptivity } (M^{-1}cm^{-1}) = \frac{\text{Absorbance}}{(\text{Path length (cm)} \times \text{Concentration (mol/L)})} \quad [180]$$

Equation 2-2: Equation used to calculate the concentration of thiol groups in the samples and hence the number of thiols per cell.

2.17. ^{125}I-Dansyl Triazole Maleimide labeling experiments

Jurkat cells were taken from suspension, washed twice with PBS and resuspended at 1 million cells in the required volume of PBS. Cells were then taken to the designated radioactive room for labeling. The ^{125}I-DM powder was dissolved in 500 μL dimethyl sulfoxide (DMSO), as it is insoluble in water, and the total activity measured using a dose calibrator (Capintec). The required activity was spiked into the cell suspension and the cells left for 1 hour in the incubator at 37.5°C. Following labeling, the cells were washed twice in PBS and re-suspended in media. All tubes used and supernatants were kept for gamma counter or dose calibrator measurements, in order to accurately measure labeling efficiency.

For initial cell labeling experiments the activity added to the cell suspension was 8 MBq (67 μL) or 2 MBq (16.8 μL). Labeling efficiency and activity over time

could then be measured using the dose calibrator. For cell labeling experiments with low activities, a gamma counter was used to measure the activities of the cell pellet and supernatant. The activity of probe used was within the range of ^{125}I measured accurately by the gamma counter as determined with a calibration experiment (Figure 2.2). Hence, 0.6 MBq of initial labeling activity was used for the experiments, accounting for a low labeling efficiency. The activity on the cell pellet, on the tube and in the supernatant was measured using the gamma counter, and the labeling efficiency was calculated using Equation 2-3.

$$\text{Labelling efficiency } (\%) = \frac{\text{CPM cell pellet}}{(\text{CPM tube} + \text{CPM supernatant} + \text{CPM cell pellet})} \text{ x100}$$

Where :

CPM = counts per minute

Equation 2-3: Equation used to calculate the labeling efficiency in all radiolabeling experiments.

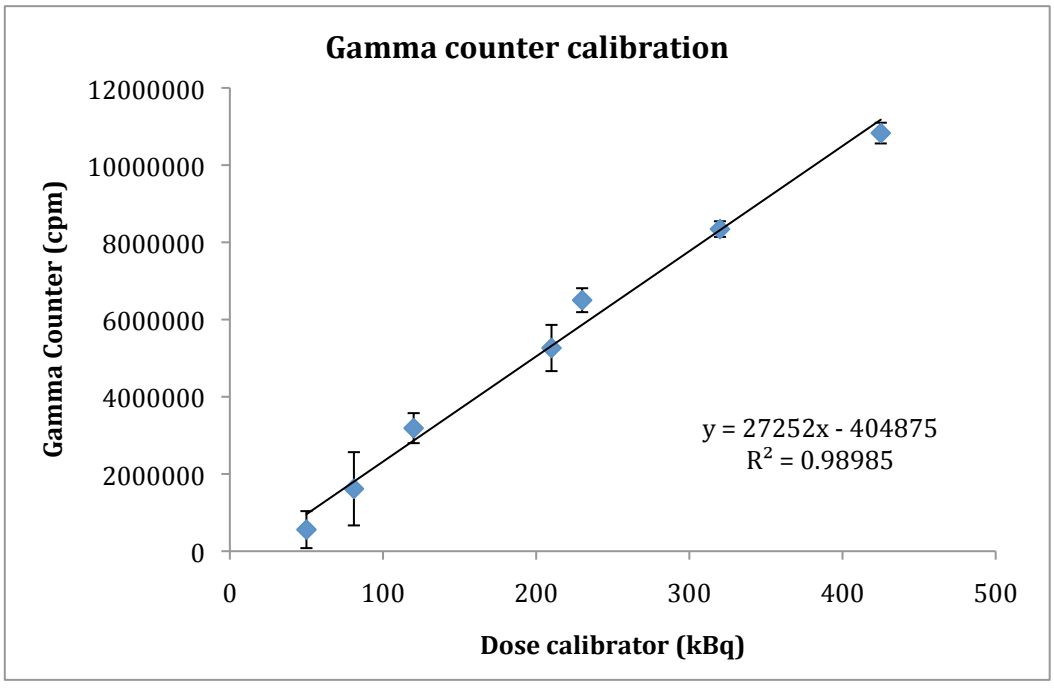

Figure 2.2: Calibration of the gamma counter for Iodine-125 using measurements of activity from the gamma counter and dose calibrator at CABI. A linear regression was performed using excel software (see equation).

2.18. *In vivo* Bioluminescence Imaging

Mice were anaesthetized with 2% isoflurane in 28% oxygen throughout imaging. An aqueous solution of D-luciferin (Regis Technologies Inc, Morton Grove, IL, USA) at 150 mg/kg in a volume of 200 µl was injected i.p. 10 minutes in advance. Imaging was performed using an IVIS® Lumina II (Caliper Life Sciences, Hopkinton, MA, USA) with the following parameters: f/stop 2 (aperture), maximum field of view (23 x 23 cm), acquisition time 60 s and 180 s. Quantification of the bioluminescent signal was performed using a region of interest (ROI) covering the whole thorax using Living Image 4.0 software (PerkinElmer).

2.19. *In vivo* Fluorescence Imaging

Mice were anaesthetized throughout imaging with 2% isofluorane. Fluorescence imaging was performed using an IVIS® Lumina II with an f/stop 2, maximum field of view, excitation wavelength 645 nm, ICG emission bandwidth and an exposure time of 10 seconds.

2.20. SPECT/CT Imaging

After labeling with the hot dansyl maleimide probe, 1 x 10^6 cells in PBS were spun down into a pellet in a microcentrifuge tube, and imaged using a NanoSPECT/CT system (Mediso, Budapest, Hungary) (Figure 2.3). CT was performed first, using a 45 kV X-ray source, with 500 ms exposure time in 180 projections, a pitch of 0.5 and an acquisition time of 11 min. SPECT using a 4-head scanner with 4 × 9 1.4 mm pinhole apertures in helical scan mode with an exposure time of 2400 s, obtained over 24 projections (100 s per projection), total acquisition time of 72 minutes. CT images were reconstructed in a 352 × 352 matrix using Bioscan InVivoScope version 1.44 (Bioscan, USA) software. SPECT images were reconstructed in a 256 × 256 matrix using HiSPECT (ScivisGmbH, Bioscan). Images were overlaid using InVivoScope software.

Figure 2.3: The NanoSPECT/CT system used for imaging, with physiological monitoring systems for *in vivo* imaging.

To track MSCs labeled with indium-111 tropolone, 5 x 10^6 MSCs were incubated for 10 minutes with 20.45 MBq Indium-111 (334 µL) and 150 µL tropolone, resulting in a labeling efficiency of 25.28% (5.17 MBq on the cell pellet after 2 washes with PBS). The control mouse received an intravenous injection of 5.08 MBq indium-111 in PBS, whereas the experimental mouse received an intravenous injection of 5 x 10^6 MSCs labeled with 5.17 MBq indium-111 tropolone in PBS. 30 minutes after intravenous injection the mice were imaged in a NanoSPECT/CT system. CT images were acquired first, using a 45 kV X-ray source, with 500 ms exposure time in 180 projections, a pitch of 0.5 and an acquisition time of 11 min. SPECT images were acquired using an exposure time of 1200 s, obtained over 24 projections (50 s per projection), using a 4-head scanner with 4 × 9 1 mm pinhole apertures in helical scan mode with a total acquisition time of 36 min. Image processing was carried out as described above, using HiSPECT and InVivoScope software.

To assess T cells survival during SPECT/CT tracking using indium-111 tropolone, PBMCs were transduced with EBV-TCR luciferase. These were

restimulated three times until the percentage of T cells expressing EBV-TCR luciferase was approximately 65%. Subcutaneous tumour bearing NSG mice (n=3) with small lung metastases were injected with 6 million T cells labeled with 150 μL tropolone and 173 μL indium-111 in saline solution, resulting in cell pellet activity of 10.62±1.37 MBq and an average labeling efficiency of 50.87±2.25%. Mice were imaged in a nanoSPECT/CT scanner (as described above), immediately after cell injection. To monitor cell survival *in vivo*, bioluminescence imaging was performed using a BioSpace Photon Imager (Paris, France) with the following parameters; acquisition time 5 minutes, 35 mm lens, f/stop 1.4. Fifteen minutes before imaging the mice received an intraperitoneal injection of the substrate D-luciferin (3 mg in 200 μL PBS). SPECT/CT and bioluminescence imaging was repeated using the same parameters at 24 hours to check the survival and location of the T cells.

2.21. Tumour models

Six-week old NOD/SCID mice (Harlan, Bicester, UK) were kept in filter cages in the Biological Services facility at the Centre for Advanced Biomedical Imaging, University College London, or in the Biological Services Unit at the Royal Free Hospital, depending on the location of the experiment. The mice were kept in a 12-hour light/dark cycle, with access to autoclaved food and water *ad libitum*. All studies were performed in accordance with UK Home Office procedural and ethical guidelines. For identification purposes, some in each cage mice received ear punches in the left ear, the right ear, or both.

For subcutaneous tumours, 10^6 MDA-MB-231 cancer cells transduced to express the LMP2 tumour antigen were injected subcutaneously into the right flank. The cells were suspended in 200 μL PBS and kept on ice before injection. The resulting tumours were measured every 3-5 days with calipers, and the tumour volume was calculated as $4/3\pi r^3$, where r denotes the radius measured in 3 orthogonal directions.

For the lung metastases model, 10^6 MDA-MB-231 LMP2 cancer cells were injected into the tail vein. The cells were suspended in 200 μL PBS and kept on ice until use.

2.22. Histological processing

Mice were sacrificed by sodium pentobarbital overdose (200 µL intraperitoneal injection), followed by laparotomy and exsanguination. To harvest the lungs the thoracic cavity was opened and the trachea was exposed and intubated using a 22G venflon. The lungs were insufflated with 4% (w/v) paraformaldehyde (PFA), following which the trachea was ligated and the trachea and lungs were removed from the thorax. The livers were removed after the lungs; both were weighed and then placed into 4% PFA overnight, followed by transfer to 70% ethanol solution. The livers and lungs were dissected into separate lobes, and then the samples were run overnight in a tissue-processing machine (Tissue-Tek®, Sakura, USA), with a programme consisting of multiple dehydration steps, clearing and paraffin wax infiltration. Following this the samples were embedded into blocks of paraffin wax, and 3 µm sections were cut using a microtome (Leica, Germany). Sections were placed on polylysine slides (VWR, Leicestershire, UK) for staining.

2.23. Haematoxylin and Eosin (H&E) staining

The prepared slides were run on an automatic tissue stainer with an H&E programme, followed by coverslipping on an automatic coverslipper (both Tissue-Tek®, Sakura, USA). The stained slides were imaged on a Nanozoomer-XR C12000 digital slide scanner (Hamamatsu, Hertfordshire, UK).

2.24. Immunofluorescence

For immunohistochemical staining, sections were dewaxed using an automatic tissue stainer. CM-DiI™ stained cells retained their fluorescence after histological processing, however the GFP signal from the MDA-MB-231 cells was amplified using anti-GFP immunostaining. Anti-luciferase immunostaining was used to locate luciferase expressing EBV TCR T cells.

Labeled slides with 3 µm sections of lung were dewaxed using an automatic tissue stainer, and were then washed in PBS. A hydrophobic circle was drawn around the area for staining using a PAP pen (Sigma-Aldrich, UK). An antibody blocking solution consisting of 5 mL FBS and 500 µL fish skin gelatin, in 45 mL

PBS, was applied to the slides to block non-specific background staining, and this was left for 1 hour at room temperature. Primary antibodies used were anti-GFP chicken Igγ (Invitrogen) (1:200) and rabbit polyclonal antibody to firefly luciferase (Abcam) (1:2000). A solution of these primary antibodies was made up in antibody blocking buffer and this was applied to the slides after antibody blocking. The slides were then left overnight in the dark at 2°C.

The following day the slides were washed for 5 minutes in PBS and then stained for 3 hours at room temperature in the dark with a solution of secondary antibodies (1:300), made up in antibody blocking solution. The secondary antibodies used were Rabbit anti-chicken Igγ FITC (Invitrogen) and donkey anti-rabbit IgG AlexaFluor 647 (Invitrogen). Following secondary antibody staining the slides were washed in PBS then counterstained with 1 μg/mL DAPI at room temperature for 5 minutes. They were then washed again in PBS for 5 minutes, followed by mounting with Mowiol and a size 1 coverslip.

3. Engineering T cells with tumour antigen specific T cell receptors

The first aim of this project was to engineer T cells with the EBV-TCR, in order to provide a tumour antigen specific cell therapy targeting LMP2-expressing cancer cells. This chapter presents data investigating the ability of transduced EBV-TCR T cells to release cytokines upon antigen stimulation and their ability to kill LMP2-expressing tumour cells *in vitro*. This is an important step, as it was necessary to verify the results observed by Hart et al. [64] before proceeding to *in vitro* combined tumour cell killing assays and *in vivo* work (Figure 3.1).

In tandem, I assessed the ability of MSC TRAIL to kill LMP2 expressing MDA-MB-231 tumour cells. Previous work by Loebinger et al. [104] had primarily investigated the action of MSC TRAIL against HeLa colorectal carcinoma cells *in vitro*, rather than MDA-MB-231 cells, before proceeding into an *in vivo* model of lung metastases using MDA-MB-231 cells. Furthermore, for EBV-TCR killing it was necessary to transduce the MDA-MB-231 cell line so the cells expressed the LMP2 antigen. Therefore, it was necessary to repeat the MSC TRAIL cancer cell killing assays, to prove that they were active against LMP2-expressing MDA-MB-231 cancer cells.

Finally, this chapter presents novel work examining the *in vitro* tumour cell killing potential of EBV-TCR T cells combined with MSC TRAIL.

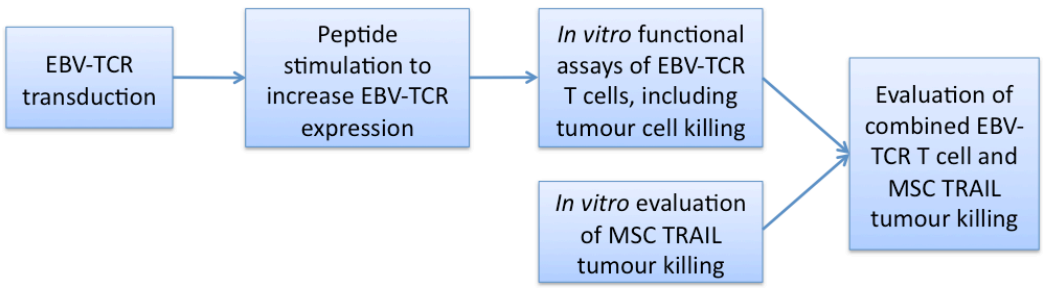

Figure 3.1: Experimental workflow for chapter 3.

3.1. Transduction of donor PBMCs to produce EBV-TCR T cells

The EBV-TCR specifically and with high affinity binds to the antigen latent membrane protein 2 (LMP2), which is characteristically expressed by EBV-associated tumours. This protein is poorly immunogenic and in patients normally leads to only weak cytotoxic T cell responses against the LMP2 antigen. However, rather than relying on the host T cell reactivity to LMP2, a new LMP2 specific TCR has been engineered, which redirects the antigen specificity of the engineered cells. The inserted EBV-TCR binds with high affinity to the LMP2 antigen, so the cells can be transferred as an adoptive immunotherapy.

Human donor peripheral blood mononuclear cells (PBMCs) were transduced with a modified retrovirus as described above in section 2.2 to express the EBV-TCR. Briefly, Phoenix Ampho cells were transfected with the EBV-TCR plasmid in order to produce retrovirus containing EBV-TCR plasmids. These were then collected and added to freshly defrosted PBMCs where the T cells had been activated and caused to proliferate by stimulation with interleukin-2 (IL-2) and anti-CD3 antibody. After 24 hours the media was changed and the transduction efficiency could be verified.

Flow cytometry was performed after each transduction to measure the percentage of EBV-TCR expression on T cells, using a fluorescent CLG pentamer that binds specifically to the EBV-TCR, and a fluorescent antibody against the murine constant region of the TCR β-chain (murine cβ). Additionally, fluorescent antibodies against CD4 and CD8 were used to assess the percentages of helper and cytotoxic T cells (discussed in section 2.3).

During flow cytometry analysis, the population of live cells was identified and a gate was drawn around them. Looking at live cells only, the percentage of CD4 and CD8 expressing cells was measured. Within each population of CD4 positive or CD8 positive cells, the expression of the murine cβ and the binding to CLG pentamer was measured. Cells were considered transduced with the EBV-TCR gene if they were double positive for murine cβ and CLG pentamer binding. After transduction, approximately 35% of CD4 and CD8 positive cells were

expressing the EBV-TCR, compared to 0% in the controls (Figure 3.2 and Figure 3.3).

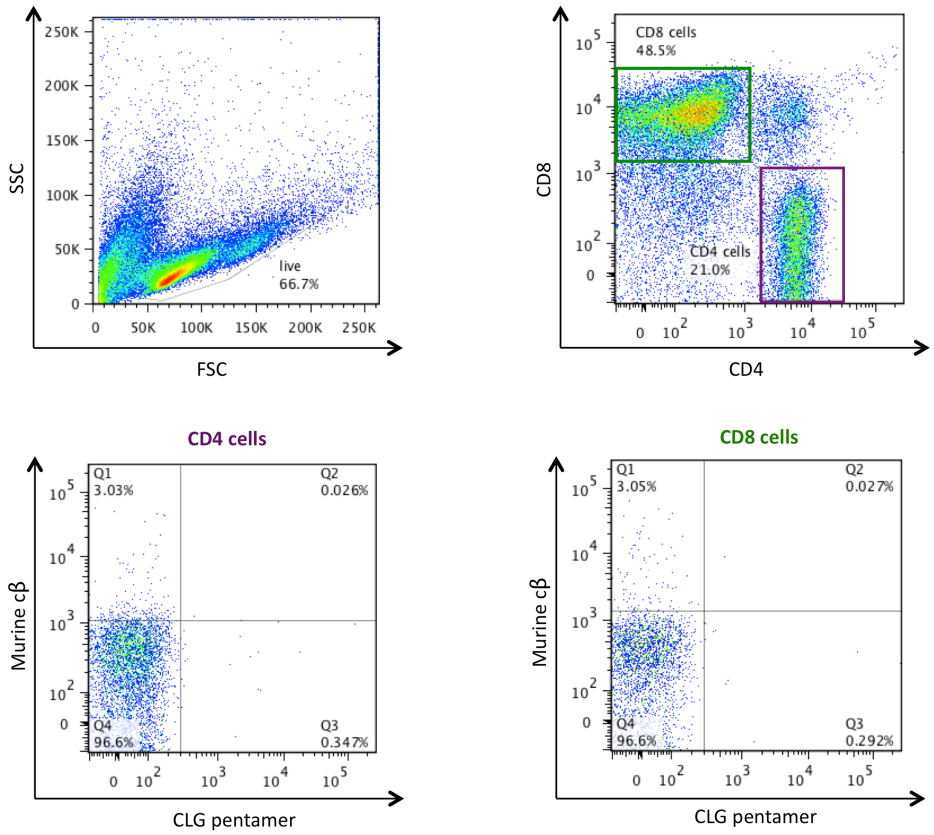

Figure 3.2: Mock untransduced cells stained with murine cβ and CLG pentamer.

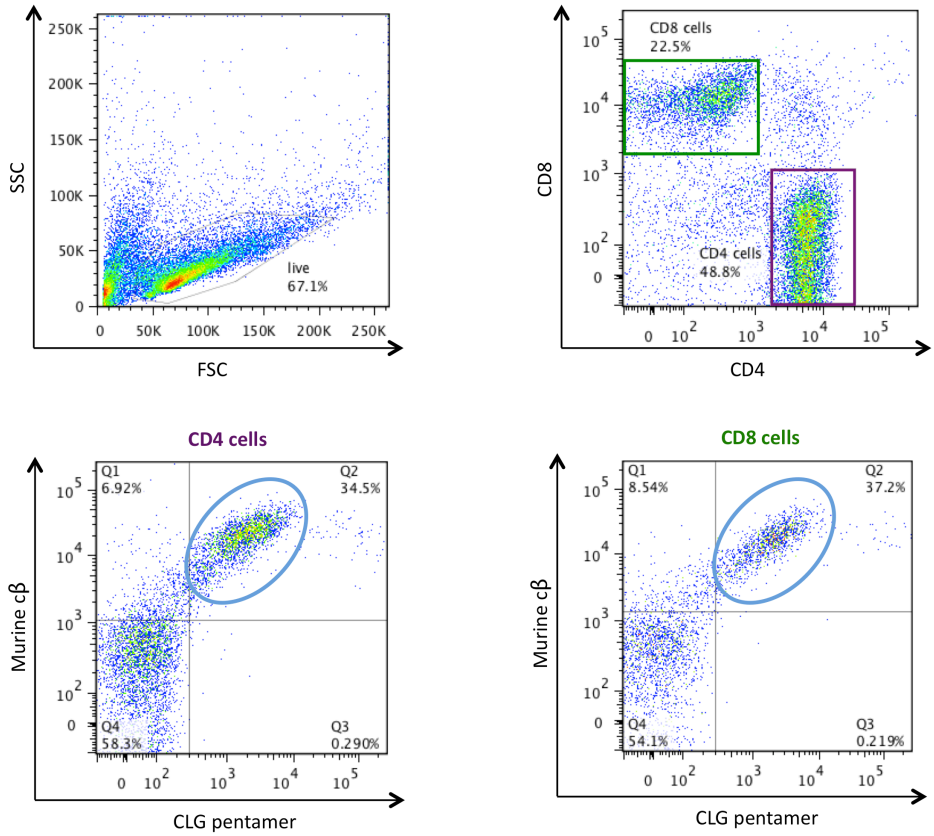

Figure 3.3: Transduced CD4 and CD8 positive cells are 34.5% and 37.2% respectively, dual positive for murine cβ and CLG pentamer, indicating expression of the EBV-TCR.

3.2. T cell stimulation increases the percentage of EBV-TCR positive T cells

Peptide stimulation is used to increase the percentage of EBV-TCR positive T cells, as described in section 2.4. In this protocol, T2 cells loaded with CLG peptide were used to stimulate proliferation and expansion of transduced cells. T2 cells are a human T cell leukemia/B cell line hybrid, which act as potent antigen presenting cells when loaded with peptide. Peptide loading is achieved by simply incubating the T2 cells with a high concentration of peptide for 2 hours at 37°C.

After CLG peptide loading, T2 cells were plated together with feeder PBMCs, IL-2 and the transduced T cells. T2 cells and feeder PBMCs were irradiated before plating to eliminate their expansion. After stimulation, flow cytometry analysis on these T cells showed 45.6% of CD4 positive T cells and 59.3% of

CD8 positive T cells expressed the EBV-TCR, indicating expansion of EBV-TCR expressing T cells (Figure 3.4). The percentage of T cells expressing the EBV-TCR after transduction and one round of stimulation was similar across different donor PBMCs (Figure 3.5). This data suggests that PBMCs from different donors can reliably be transduced to express the EBV-TCR, and that this expression can be increased using peptide stimulation.

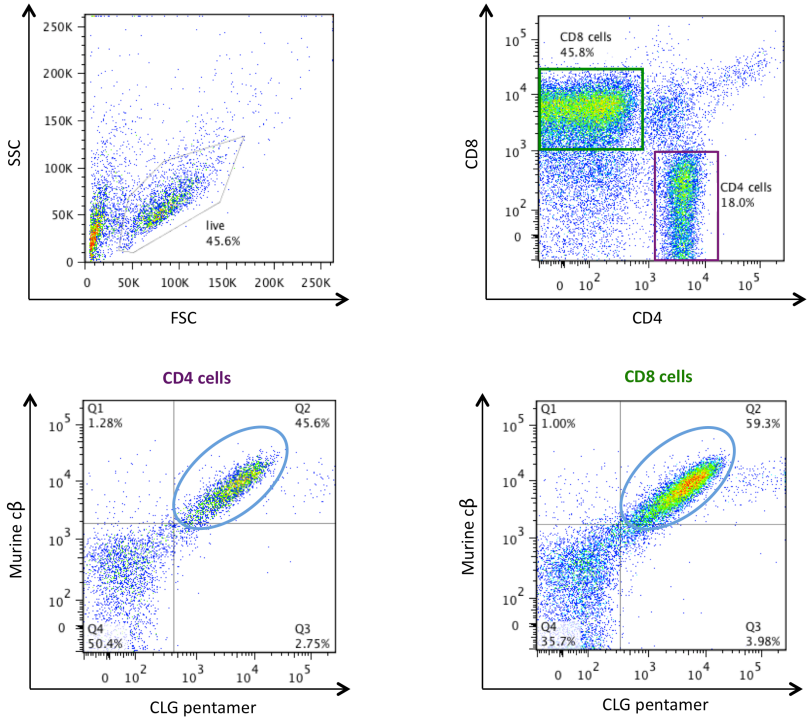

Figure 3.4: After one stimulation, the percentage of CD4 cells expressing the EBV-TCR increased to 45.6%, and CD8 to 59.3%.

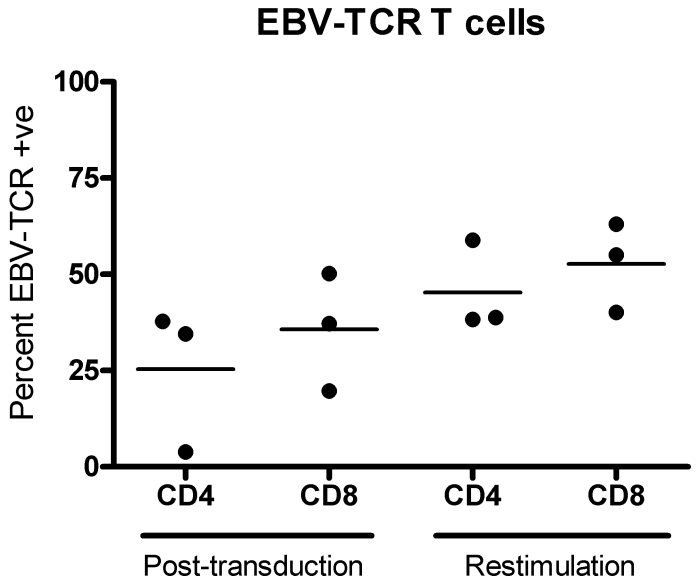

Figure 3.5: Percent EBV-TCR positive after transduction and stimulation in PBMC samples from three different donors.

3.3. *In vitro* T cell functional assays

3.3.1. Cytokine secretion assays

To assess the function of transduced EBV-TCR T cells, the secretion of cytokines after stimulation with antigen was measured. An ELISA measuring secretion of interleukin-2 and interferon-gamma was performed on EBV-TCR T cells. Transduced T cells (approximately 50% positive for the EBV-TCR after two stimulations) were plated overnight with T2 cells coated with irrelevant peptide (NLV) or relevant peptide (CLG). There was a significant increase in production of both cytokines when the transduced T cells were incubated with T2 cells expressing relevant peptide compared with control T2 cells expressing irrelevant peptide (Figure 3.6). Consequently, the EBV-TCR T cells produce cytokines in a peptide-specific manner.

3.3.2. Luciferase imaging of EBV-TCR T cells

Bioluminescence imaging of the T cells was performed *in vitro* to test the function of the luciferase plasmid before moving into *in vivo* experiments (Figure 3.7). Luciferase expressing EBV-TCR T cells, stimulated three times to

approximately 65% positive for the EBV-TCR, were plated in a 24-well plate in a dilution series from 2 x 10^6 cells to 31,250 cells, suspended in 2 mL RPMI media. Cells were treated with 2 mg D-luciferin for 15 minutes, before being imaged in a Xenogen IVIS® Lumina II system (f/stop 2, acquisition time 60 s). The resulting data was analyzed using PerkinElmer Living Image 4.0 software to measure photon radiance within regions of interest (ROI), represented by the red circles. The photon radiance was above the background signal of 2.11 x 10^4 at all dilutions, although the scale on the image was adjusted to display the highest concentration of EBV-TCR T cells. The *in vivo* dose of these T cells will be above 2 x 10^6, therefore it is possible that *in vivo* bioluminescence imaging could be used to assess the location and persistence of injected EBV-TCR T cells, if a large proportion of cells home towards a tumour or to lung metastases.

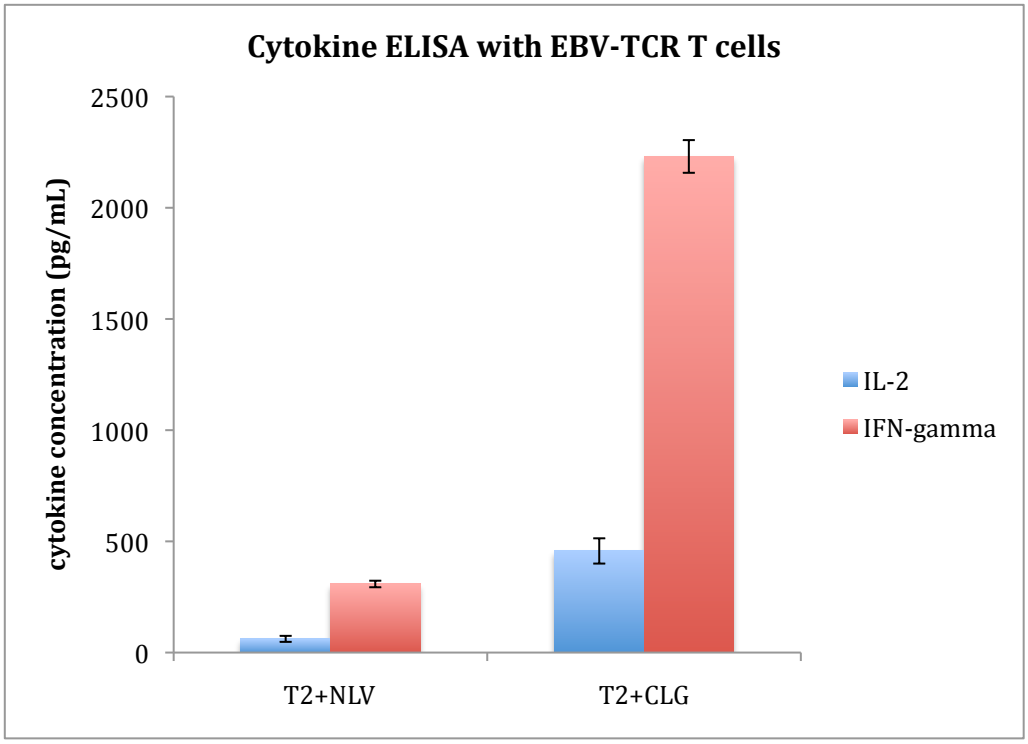

Figure 3.6: IL-2 and IFN-gamma ELISA of cytokine concentration in the cell culture media after incubation of transduced EBV-TCR T cells with T2 cells coated with irrelevant (NLV) or relevant (CLG) peptide, n=3 different donor PBMCs. EBV-TCR T cells secrete cytokines in peptide-specific manner.

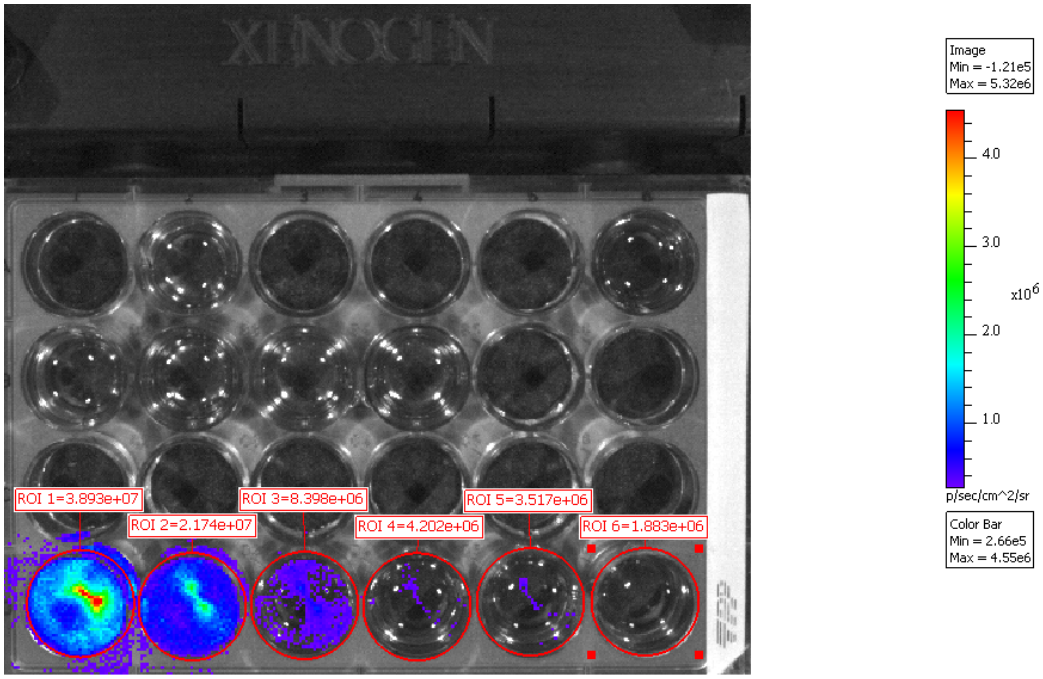

Figure 3.7: A dilution series of EBV-TCR luciferase T cells, suspended in T cell media (2 x 10^6, 1 x10^6, 500,000, 250,000, 125,000, 62,500). Cells were treated with 2 mg D-Luciferin in 200 µL PBS, for 15 minutes, before being imaged in a Xenogen IVIS® Lumina II system (f/stop 2, acquisition time 60 s). The red circles represent ROI drawn over each well and the signal is measured as photon radiance. The background signal was 2.11e+04 and the photon radiance scale was adjusted to optimize the image for the first EBV-TCR T cell dilution. Control wells contained PBS (second well from left, top row), RPMI media (right well, top row) and control untransduced PBMCs in a dilution series from 2 x 10^6 to 2.5 x 10^5 (second row, left to right).

3.3.3. EBV-TCR T cell killing assays

A chromium-51 assay was used to assess the capability of the transduced EBV-TCR T cells to kill target cells. To quantify the cytotoxicity of different concentrations of T cells, target cells are labeled with chromium-51, which is then released into the media when the cell is lysed by a cytotoxic T cell. The resulting chromium-51 activity in the media can be measured using a scintillation counter.

This assay was performed first with relevant and irrelevant peptide loaded T2 cells, to test specific TCR-antigen mediated killing (Figure 3.8). Plating T2 cells coated with CLG peptide with transduced EBV-TCR T cells resulted in between 60.19% (±14.0%) to 100% (±8.88%) lysis of T2 tumour cells at all dilutions of T cells. Plating T cells with T2 cells coated with irrelevant peptide (NLV) resulted in a low, non-specifc tumour cell lysis average of 17.0% (±2.67%). Therefore,

EBV-TCR T cells can kill target cells in a peptide-specific fashion. This also occurs in a dose-dependent fashion, with lower ratios of EBV-TCR T cells to T2 cells causing less percentage lysis.

Tumour cells express fewer antigens on their cell surface membrane than T2 cells coated with peptide. In order to assess the capability of transduced T cells to kill tumour cells, it was first necessary to transduce the tumour cell line of choice to express the LMP2 antigen. The EBV-TCR selectively binds to the LMP2 antigen to cause cell death. The cancer cell line used for all *in vitro* and *in vivo* experiments was the human breast cancer cell line MDA-MB-231. This tumour cell line will form lung metastases several weeks after subcutaneous injection of tumour cells, or directly if the cells are injected intravenously. The MDA-MB-231 cells were transduced with a retroviral vector to express latent membrane protein-2 (LMP2) and green fluorescent protein (GFP). GFP signal could then be measured using flow cytometry to assess the number of transduced cells, which was 63.6% (Figure 3.9).

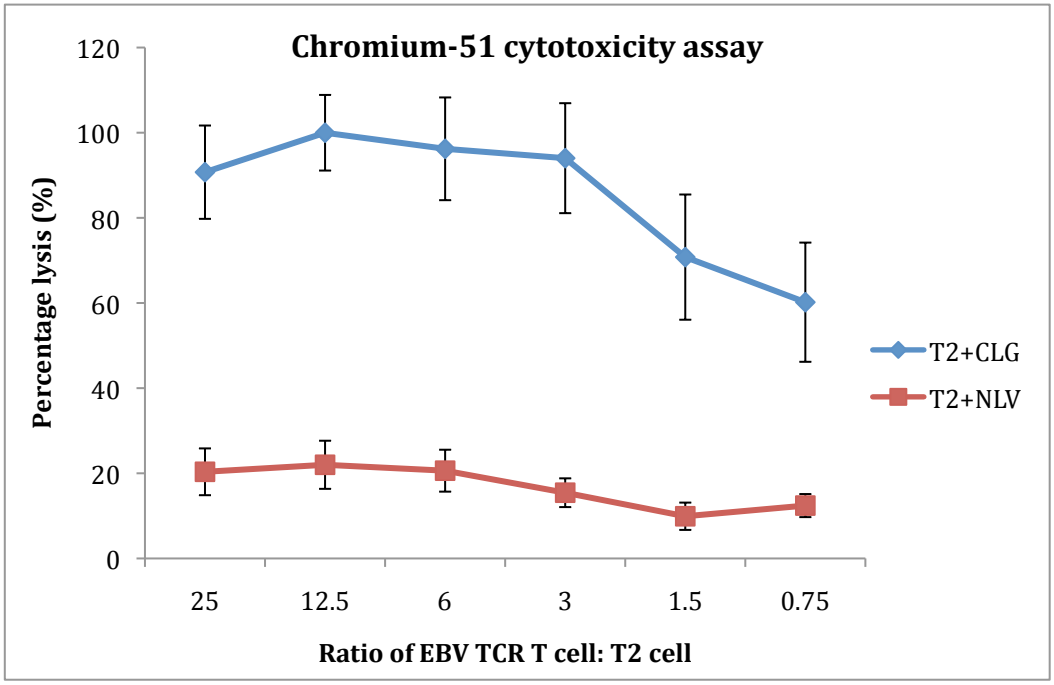

Figure 3.8: Chromium-51 assay showing TCR-antigen mediated killing against T2 cells expressing relevant peptide (T2+CLG) and non-specific background lysis of T2 cells coated with irrelevant peptide (T2+NLV), n=3 different donor PBMCs.

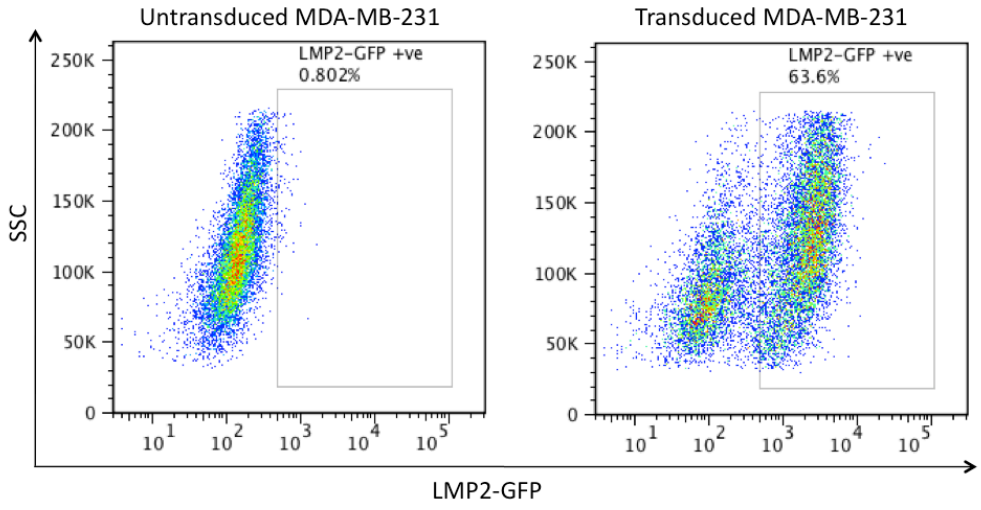

Figure 3.9: Flow cytometry analysis of MDA-MB-231 cells after transduction with LMP2-GFP.

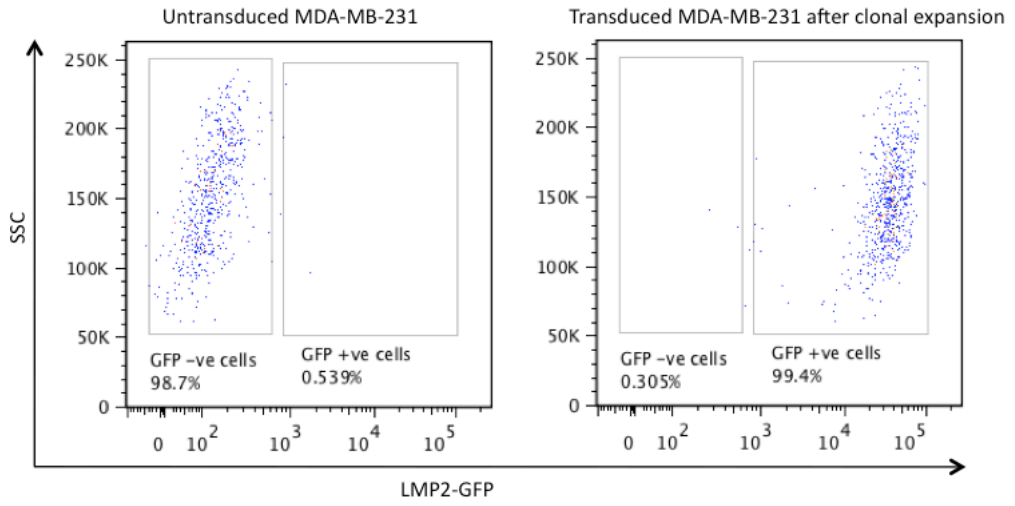

Figure 3.10: Flow cytometry analysis of MDA-MB-231 cells after clonal expansion for LMP2-GFP. The successful cell colony after clonal expansion (right) is 99.4% positive for LMP2-GFP. These cells were expanded and used for further *in vitro* and *in vivo* experiments.

After transduction it was necessary to do a clonal expansion to isolate and expand a pure LMP2-GFP expressing population, resulting in a population of cells where 99.4% expressed LMP2-GFP (Figure 3.10). This allowed more accurate *in vitro* and *in vivo* testing of the transduced EBV-TCR T cells, since the T cells could target all tumour cells, rather than a population of tumour cells.

After expansion of a clonal population of the LMP2-GFP positive tumour cells, the chromium-51 assay was repeated using control MDA-MB-231 cells and MDA-MB-231 LMP2-GFP cells, to assess T cell killing of tumour cells. These cells express a lower concentration of surface antigen than peptide loaded T2 cells, resulting in a lower maximum percentage lysis of 76.04% (±8.64%), compared with an average background lysis of 9.10% (±2.22%) (Figure 3.11). However, this data shows that EBV-TCR T cells can specifically lyse MDA-MB-231 LMP2 cells, compared to a low background lysis of MDA-MB-231 control cells, and that this occurs in a dose-dependent fashion.

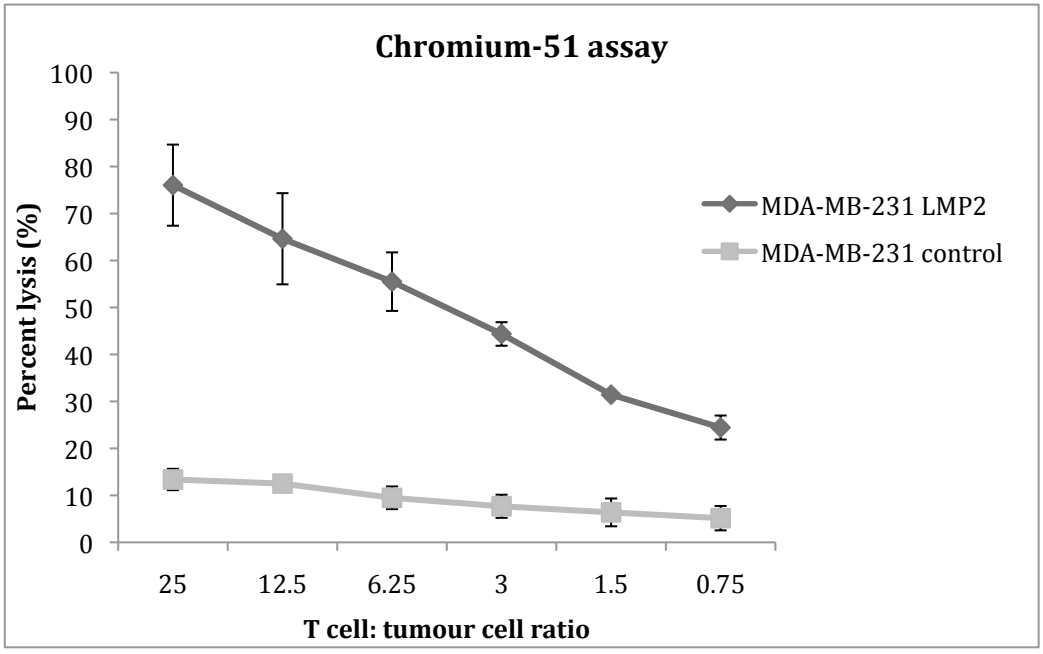

Figure 3.11: Chromium-51 assay showing T cell TCR-antigen mediated tumour cell killing. Background lysis of control tumour cells is low, however, lysis of LMP2 expressing tumour cells is high, n=3 different donor PBMCs.

3.4. *In vitro* co-culture assays of combined EBV-TCR T cells and MSC TRAIL tumour killing

To test the combined killing capacity of EBV-TCR T cells and MSC TRAIL, I used co-culture experiments followed by analysis of apoptosis and death using flow cytometry. Annexin V is a probe used to detect cells expressing phosphatidylserine on their cell surface membrane, an event that occurs soon after induction of apoptosis. Fluorescent conjugates of Annexin V can be used with a flow cytometer to indicate the percentage of apoptotic cells. Propidium iodide and 4'6-diamidino-2-phenylindole (DAPI) are fluorescent nuclear staining dyes that can be used for flow cytometry to indicate dead cells, since they cannot enter live cells. Cells that were Annexin V negative and PI/DAPI negative were recorded as live, cells that were Annexin V positive but PI/DAPI negative were recorded as apoptotic, and cells that were Annexin V and PI/DAPI positive were considered to be dead.

Co-culture experiments were necessary due to the time taken for MSC TRAIL to produce measurable tumour cell death (48 hours). The co-culture assay was previously developed by Loebinger et al. [104] and was modified to include EBV-TCR T cells. In contrast, the chromium-51 assay for T cell cytotoxicity requires just 4 hours.

A typical co-culture experiment consisted of 5 x 10^4 MDA-MB-231 LMP2 tumour cells plated with a decreasing ratio of MSC TRAIL or EBV-TCR T cells in a 6-well plate. The cells were left for 48 hours in αMEM media in the incubator, before being trypsinised and stained for flow cytometry. Appropriate single colour controls were used to set compensations and gates.

3.4.1. MSC-TRAIL only co-culture experiments

Co-culture experiments were performed to test if MSC TRAIL could kill MDA-MB-231 LMP2 tumour cells. In these experiments, 5 x 10^4 MDA-MB-231 LMP2 tumour cells were plated with 5 x 10^4 MSC TRAIL (1:1 ratio), 2.5 x 10^4 MSC TRAIL (1:2 ratio), 1.25 x 10^4 MSC TRAIL (1:4 ratio), 6.25 x 10^3 MSC TRAIL (1:8 ratio) and 3.125 x 10^4 MSC TRAIL (1:16 ratio), in αMEM media.

All the MSC TRAIL cells used in these experiments were passage 8 or 9. During the analysis of flow cytometry data, all cells were taken, but debris was excluded in the side scatter, forward scatter plots. Tumour cells were distinguishable from MSC TRAIL by their expression of GFP (Figure 3.12).

The results show that MSC TRAIL can kill MDA-MB-231 cells in a dose-dependent fashion similar to that observed with T cell killing (Figure 3.13). Control tumour cells showed a baseline apoptosis of 14.8% (±0.38%) and death of 2.6% (±1.46%), whereas tumour cells plated with MSC not expressing TRAIL showed a small but not significant rise in apoptosis and death, with apoptosis of 17.9% (±2.41%) and death of 6.0% (±0.53%).

Tumour cells treated with a 1:1 ratio of MSC TRAIL showed a significant increase in apoptosis and death, with apoptosis of 50.06% (±1.09%) and death of 12.16% (±1.94%). This rate of apoptosis and death is higher than that observed by Loebinger et al. [104] with HeLa cancer cells at the same ratio. Tumour cells plated at 2:1, 4:1 and 8:1 ratios with MSC TRAIL also showed a significant increase in apoptosis ($p<0.01$).

Tumour cells plated at a ratio of 2:1 with MSC TRAIL showed apoptosis of 40.27% (±1.13%) and death of 5.66% (±0.50%), and those plated at a ratio of 4:1 showed apoptosis of 35.13% (±1.38%) and death of 2.21% (±0.35%). Lastly, tumour cells plated at a ratio of 8:1 with MSC TRAIL showed apoptosis of 28.93% (±1.36%) and death of 1.77% (±0.15%), whereas those plated at 16:1 with MSC TRAIL showed apoptosis of 15.27% (±2.66%) and death of 0.826% (±0.10%), very similar to control cell death and apoptosis rates.

Therefore, MSC TRAIL is capable of killing MDA-MB-231 cancer cells expressing the LMP2 antigen, in a cell ratio dependent effect. A significant

increase of tumour cell apoptosis and death was observed even at high tumour cell to MSC TRAIL ratios of 4:1 and 8:1. However, at a tumour cell to MSC TRAIL ratio of 16:1, tumour cell apoptosis and death was not significantly altered compared to control tumour cells, or tumour cells plated with MSC.

This cell ratio effect accounts for the significantly reduced subcutaneous tumour growth seen by Loebinger et al. when MSC TRAIL was co-injected with MDA-MB-231 tumour cells, as the tumour cell to MSC TRAIL ratio was 2.66:1. [104] However, if the MSC TRAIL was activated 25 days after co-injection, there was no change in tumour growth compared to controls, probably as the MSC TRAIL to tumour ratio was then too low. Unfortunately, this low ratio of MSC TRAIL to tumour cells is likely to occur with the *in vivo* lung metastases model. It is encouraging that Loebinger et al. saw a significant reduction or clearance in lung metastases after 4 intravenous doses of MSC TRAIL in their *in vivo* model. The suggests that other factors *in vivo* assist MSC TRAIL mediated cancer cell death, possibly cytokines in the extracellular environment.

The combination of MSC TRAIL with EBV-TCR T cells may therefore increase the clearance of lung metastases, as the activated EBV-TCR T cells will secrete cytokines and lyse cancer cells, reducing the tumour cell to MSC TRAIL ratio.

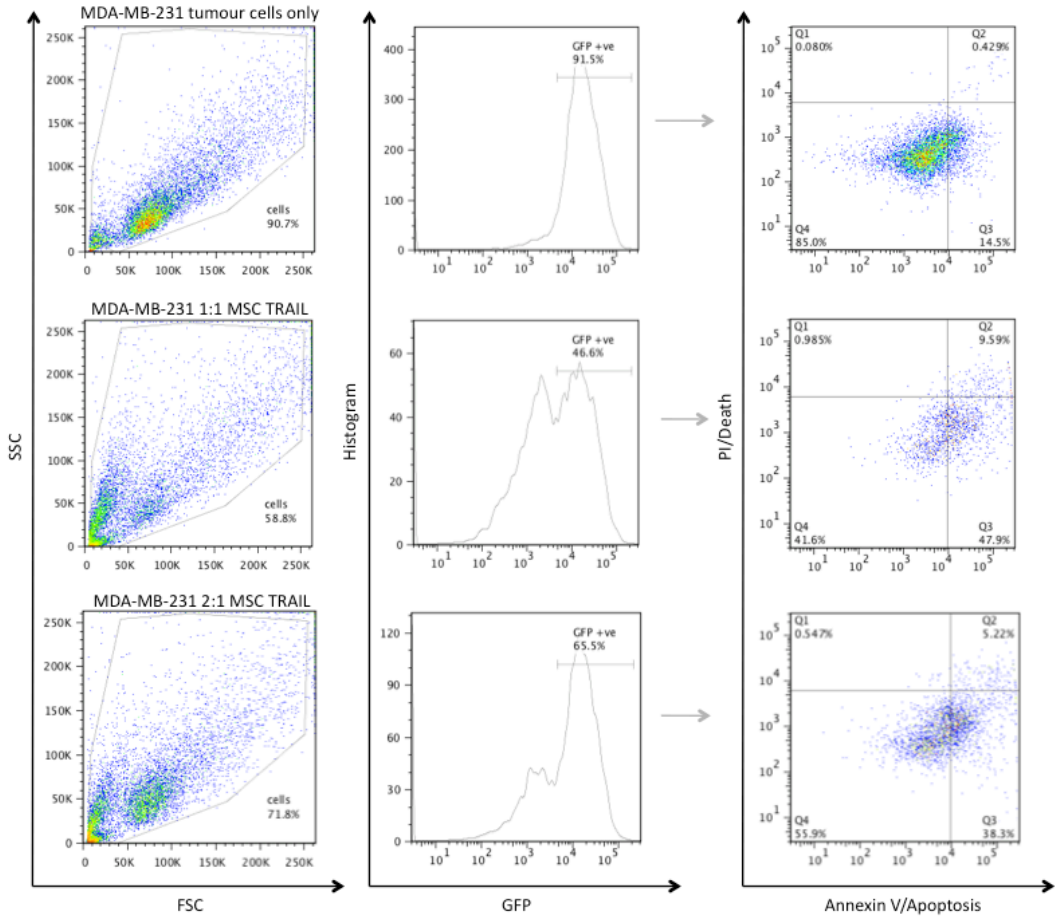

Figure 3.12: Representative flow cytometry plots of the MSC TRAIL and tumour cell co-culture experiments. Only debris was excluded in the side scatter, forward scatter plots, then the LMP2-GFP positive tumour cells were gated on and the population staining for Annexin V and PI was recorded.

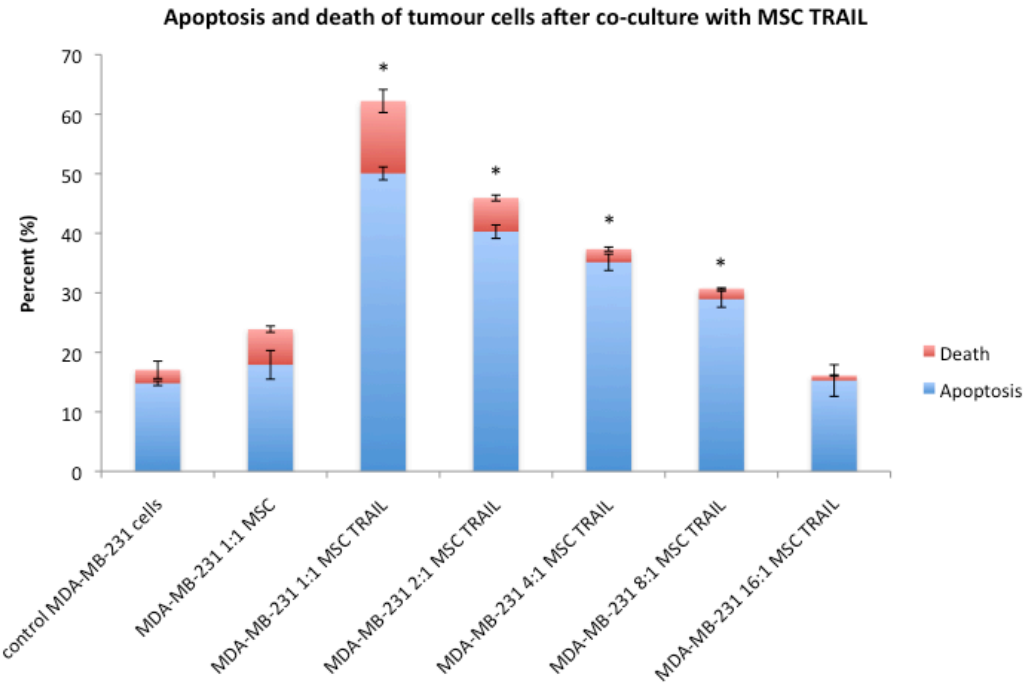

Figure 3.13: Bar chart showing the results of co-culture experiments measuring MDA-MB-231 LMP2 cell death and apoptosis using Annexin V and PI, 48 hours after plating with MSC TRAIL (*significant difference in apoptosis against control, p<0.01).

3.4.2. Choice of culture media does not effect PBMC survival

Before starting co-culture experiments testing combined killing of EBV-TCR T cells and MSC TRAIL it was first necessary to establish if culturing T cells in αMEM would result in any survival disadvantage. To test this, 10^6 PBMCs in triplicate were plated in a 24-well plate in RPMI only, 50:50 RPMI and αMEM, and αMEM only, with Roche IL-2 added. After 48 hours, trypan blue viability counts were performed to assess cell survival (Figure 3.14). Trypan blue cannot cross intact cell membranes, hence only dead cells are stained. There was no significant difference in death rates between the groups; therefore, αMEM with IL-2 supplements was used in subsequent co-culture experiments.

3.4.3. MSC TRAIL does not effect EBV-TCR T cell survival *in vitro*

The next co-culture experiment determined whether plating with MSC TRAIL resulted in any survival disadvantage for the EBV-TCR T cells. EBV-TCR T cells alone and MSC TRAIL and EBV-TCR T cells combined at a 1:1 ratio, were plated in a 24-well plate in αMEM for 48 hours. Following this the cells were

stained with Annexin V and PI to assess apoptosis and death, and the cells were run on a flow cytometer. There was no significant difference in cell survival between the groups plated with or without MSC TRAIL after 48 hours (Figure 3.15).

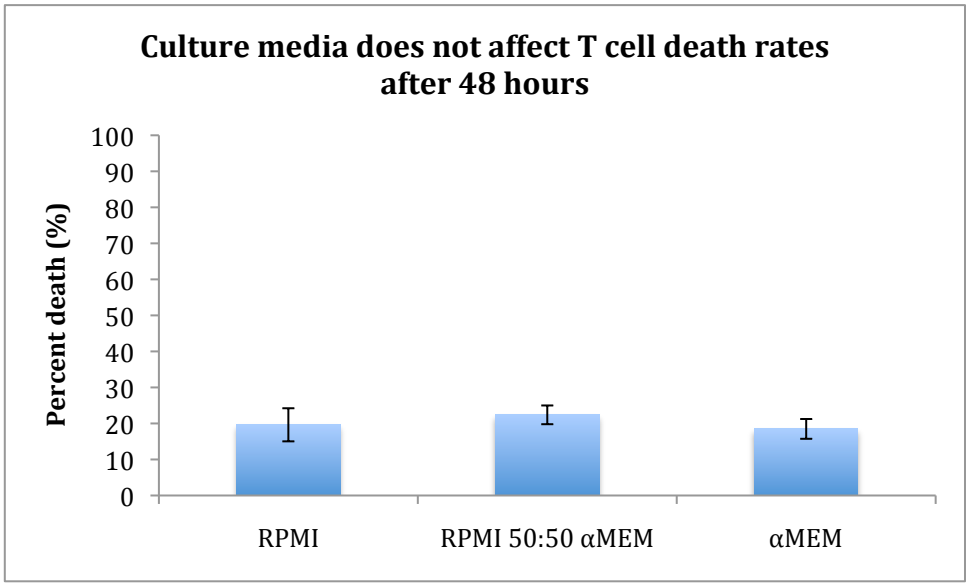

Figure 3.14: Trypan blue assessment of T cell survival after 48 hours of culture in different culture media. There is no significant difference in cell death between any of the groups, n=3.

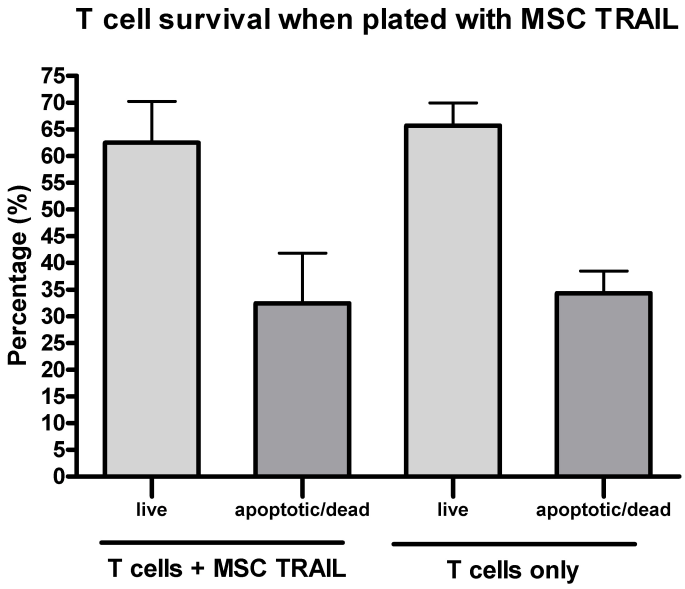

Figure 3.15: Bar chart showing T cell survival (live cells and apoptotic/dead cells), 48 hours after plating with MSC TRAIL at a 1:1 ratio, n=3.

3.4.4. EBV-TCR T cell co-culture experiments

Before assessing combined tumour cell killing with EBV-TCR T cells and MSC TRAIL *in vitro*, the capability of EBV-TCR T cells alone to cause tumour cell apoptosis and death in a 48 hour co-culture experiment was characterized. Previous chromium-51 assays demonstrating tumour cell lysis used a T cell/tumour cell incubation period of just 4 hours, and greater ratios of T cell to tumour cell than what was used in co-culture experiments. Therefore, co-culture experiments were performed with the same ratios of EBV-TCR T cell to tumour cell as the co-culture experiments performed with MSC TRAIL, to allow a direct comparison.

In these experiments, 5 x 10^4 MDA-MB-231 LMP2 tumour cells were plated with 5 x10^4 EBV-TCR T cells (1:1 ratio), 2.5 x 10^4 EBV-TCR T cells (1:2 ratio), 1.25 x 10^4 EBV-TCR T cells (1:4 ratio), and 6.25 x 10^3 EBV-TCR T cells (1:8 ratio). Cells were plated in αMEM, with 2 μl/mL IL2 added.

Flow cytometry was performed as described above, with gates to identify the GFP positive tumour cell population, and measure their death and apoptosis. The results demonstrate 86.50% (±1.50%) tumour cell death and 6.82% (±0.68%) apoptosis at a 1:1 EBV-TCR T cell, to tumour cell ratio. At a 1:2 ratio, there was 78.63% (±3.71%) tumour cell death and 10.17% (±1.48%) apoptosis, and at a 1:4 ratio there was 74.93% (±2.21%) tumour cell death and 10.09% (±0.56%) apoptosis. Finally, at a 1:8 ratio there was 65.43% (±1.22%) cell death and 16.07% (±0.64%) apoptosis (Figure 3.16).

These results show markedly superior tumour cell killing using the EBV-TCR T cells, when compared with MSC TRAIL. The EBV-TCR T cells caused a significant increase in cell death at all ratios within the 48-hour incubation, whereas incubation with MSC TRAIL resulted in a significant increase of apoptosis at all ratios, and a significant increase in cell death only at the 1:1 ratio. If cell death and apoptosis are combined, EBV-TCR T cells again result in a much greater cell death/apoptosis rate than MSC TRAIL (93.32% versus 62.22% at a 1:1 ratio).

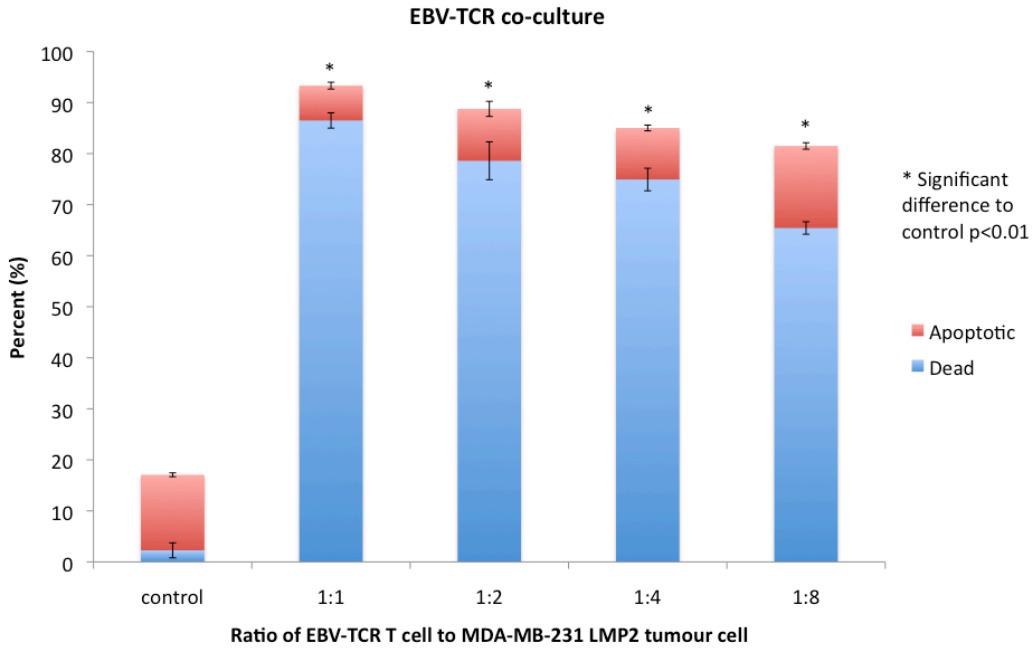

Figure 3.16: Bar chart of results from co-culture experiments measuring MDA-MB-231 LMP2 cell death and apoptosis, with PI and Annexin V, 48 hours after incubation with EBV-TCR T cells (n=3).

3.4.5. Combined EBV-TCR T cell and MSC TRAIL co-culture experiments

The last set of co-culture experiments sought to determine whether adding EBV-TCR T cells to MSC TRAIL enhanced *in vitro* tumour cell death. In these experiments 5 x 10^4 MDA-MB-231 LMP2 tumour cells were plated with reducing ratios of MSC TRAIL and EBV-TCR T cells as described above, from 1:1:1 to 1:1:4. As before, these were plated in triplicate and left in the incubator for 48 hours, followed by the retrieval of all cells and subsequent Annexin V and PI staining. T cells had received four rounds of restimulation and were approximately 65% positive for the EBV-TCR. Passage 9 or 10 MSC TRAIL were used for all experiments.

Flow cytometry analysis of the cells was performed as described above, with gates drawn on the GFP positive tumour cell population, and apoptosis and death measured in the tumour cell population (Figure 3.17). The results show that in a 1:1:1 ratio (5 x 10^4 cells), 91.43% (±0.17%) of tumour cells are dead, with 3.74% (±0.43%) of cells undergoing apoptosis, compared with a control tumour cell apoptosis of 14.80% (±0.38%) and death of 2.27% (±1.47%). With 2.5 x 10^4 T cells and MSC TRAIL, at a 1:1:2 ratio, 79.77% (±0.41%) of tumour cells were dead, and 7.33% (±0.81) were apoptotic. At the lowest ratio of 1:1:4 (1.25 x 10^4 T cells and MSC TRAIL), 67.03% (±1.28%) of tumour cells were dead, and 9.72% (±0.47%) were apoptotic.

The results show superior killing of tumour cells compared with MSC TRAIL alone. However, while the combined cell death and apoptosis rates at the 1:1:1 and 1:1:2 ratios are comparable with those observed with EBV-TCR T cells alone at similar ratios, cell death and apoptosis are slightly reduced at a 1:1:4 ratio compared with a 1:4 ratio of tumour cells to EBV-TCR T cells (76.76% versus 85.03%). However, this difference was not significant using a paired sample student's t-test.

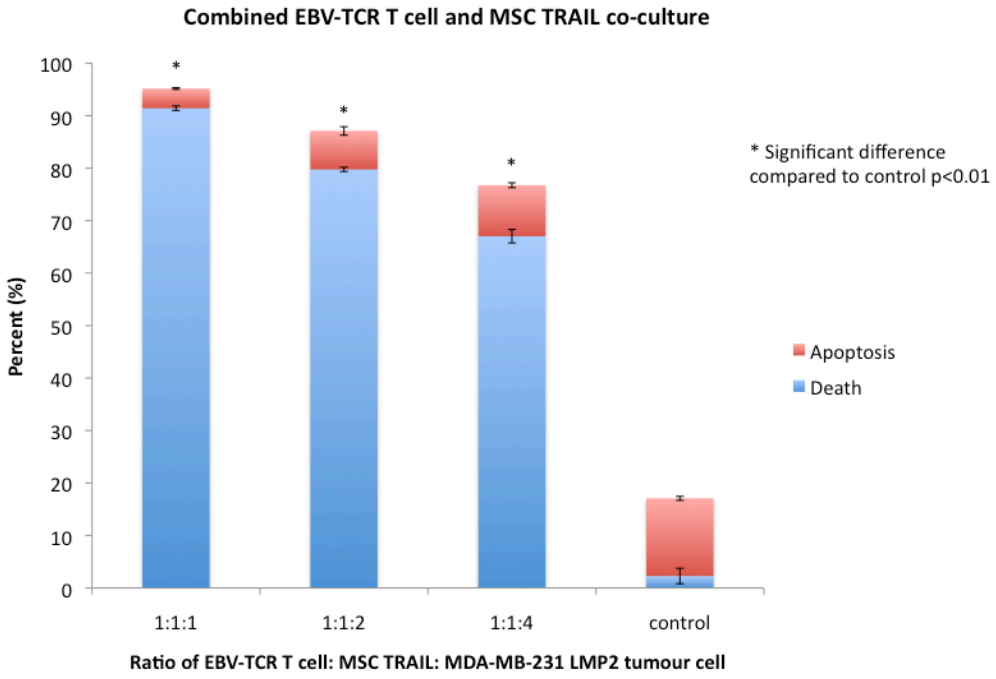

Figure 3.17: Bar chart of co-culture experiment results showing MDA-MB-231 LMP2 cell death and apoptosis measured with Annexin V and PI, after 48 hours of incubation with EBV-TCR T cells and MSC TRAIL, n=3.

3.5. Summary

This chapter has demonstrated that:

- Donor PBMCs can readily be transduced to express the EBV-TCR
- Peptide stimulation increases the percentage of EBV-TCR positive CD4 and CD8 T cells
- Transduced EBV-TCR T cells secrete cytokines when stimulated by the target cells expressing the relevant peptide, but not when exposed to irrelevant peptide.
- Transduced EBV-TCR T cells can specifically kill T2 cells labeled with CLG peptide and MDA-MB-231 cells transduced to express the LMP2 antigen via antigen-TCR mediated cell killing.
- MSC TRAIL kills MDA-MB-231 LMP2 tumour cells in a dose dependent fashion, with a 1:1 ratio causing the greatest increase in cell death and apoptosis, and a 16:1 ratio resulting in only baseline apoptosis and death.
- MSC TRAIL do not cause any significant adverse effects on EBV-TCR T cell death and apoptosis during co-culture.
- EBV-TCR T cells provide superior tumour cell killing to MSC TRAIL at all ratios.
- MSC TRAIL in combination with EBV-TCR T cells provide far superior tumour cell killing compared with MSC TRAIL alone, but no significant killing benefit to EBV-TCR T cells alone.

3.6. Discussion

Adoptive cell transfer is a promising technique in cancer immunotherapy. Retroviral insertion of genes coding for TCRs with high antigen affinity and specificity can result in the generation cytotoxic T cells which are highly active against tumour antigens. In this chapter I have shown that human donor PBMCs can be consistently transduced to express the EBV-TCR, and that during peptide stimulation the population of EBV-TCR positive T cells are expanded. These cells can efficiently kill T2 cells coated in the relevant peptide target and produce cytokines. More importantly these cells are also able to specifically kill tumour cells expressing the LMP2 antigen, in a dose-dependant fashion. Further increases in target cell lysis may have been possible with a pure population of EBV-TCR T cells, however, enrichment by FACS sorting inevitably resulted in T cell death so this was abandoned after 3 attempts.

In addition, MSC TRAIL can also kill tumour cells, and do not have any adverse effects on T cell survival *in vitro*. In fact, TRAIL expression is seen in many cells of the innate and adaptive immune system, including dendritic cells, natural killer cells, T cells and macrophages, and its expression is dependent on their stimulation. [181] Many studies have shown that activated CD8+ T cells express membrane-bound TRAIL, and that this expression is induced by anti-CD3 and type I interferon. [182, 183] Resting T cells have also been shown to express the decoy TRAIL receptor DcR2, whereas on activation death receptor DR5 becomes the predominant TRAIL receptor. Despite the expression of DR5 in activated T cells, both resting and activated T cells are resistant to TRAIL-mediated apoptosis. [183, 184] This is thought to be due to their expression of FLIP, an inhibitor of the extrinsic apoptotic pathway activated by TRAIL (see Figure 1.4). [183]

The EBV-TCR T cells used in the co-culture experiment were activated, and hence should express both DR5 and membrane-bound TRAIL. In keeping with the work of Mirandola et al. regarding T cell resistance to TRAIL, exposure to external TRAIL (from the TRAIL-expressing MSCs), did not result in any significant T cell toxicity.

An interesting but perhaps not surprising finding is that EBV-TCR T cells provide more efficient tumour cell lysis at equivalent cell ratios than MSC TRAIL. To my knowledge there are no papers examining the difference in efficiency between TRAIL-mediated and TCR antigen-specific cytotoxicity, however, cytotoxic T cells are known to be serial killers that are capable of initiating apoptosis within 5 minutes of antigen-TCR binding. Cytotoxic T cells most often use the granule exocytosis pathway to kill target cells, although they can also affect target cell death using FAS or TRAIL to activate the caspase cascade. [185] The granules are prepackaged within the cytoplasm of the T cell and hence can cause more rapid target cell apoptosis than through the binding of death ligands. Therefore, it is possible that the mechanism of death significantly impacts the overall efficiency of target cell killing in co-culture experiments.

When MSC TRAIL were used in combination with EBV-TCR T cells, up to 95% of tumour cells were dead or apoptotic. However, tumour cell death was not increased by the dual EBV-TCR T cell and MSC TRAIL, compared with EBV-TCR T cells alone. This could be a result of the extremely high rate of apoptosis and death seen within the samples in both experiments, with 95% target cells apoptotic or dead with either the EBV-TCR cells alone or with dual therapy at 1:1 cell ratios.

The advantage of co-culture experiments is that they offer quantification of cytotoxic activity that would be impossible in an *in vivo* model. However, *in vitro* co-culture tumour cell killing assays do not accurately represent the true tumour microenvironment *in vivo*, and may underestimate or overestimate the killing effect of a dual cell therapy. Of particular relevance is the 2-dimensional nature of co-culture experiments, which differs significantly from the *in vivo* scenario.

These cells will be used in an *in vivo* model of LMP2 expressing MDA-MB-231 lung metastases, to test their therapeutic activity. Although no benefit with combined cell therapy was seen *in vitro*, the *in vivo* treatment of established lung metastases could present a different scenario.

4. Cell labeling and tracking using conventional methods for Nuclear Medicine

There is a pressing need to track and quantify the transfused cells during adoptive immunotherapy, in order to evaluate homing efficiency, biodistribution and the functionality of a cell therapy after administration. The next aim of my project was to explore conventional nuclear medicine cell tracking techniques used for labeling and imaging leucocytes. These radiotracers are in routine clinical use; hence using them to track a cell therapy poses no regulatory hurdles. Furthermore, nuclear imaging is more sensitive than MRI for cell tracking, and allows quantification of the accumulation of radiolabeled cells (although SPECT imaging is semi-quantitative compared with PET imaging which is fully quantitative).

This chapter presents cell labeling experiments comparing the two most common leucocyte direct labeling agents, indium-111 tropolone and technetium-99m HMPAO. Direct labeling techniques are generally easier, quicker and cheaper than indirect methods, but their disadvantage is that they cannot be used to repeatedly image cells over long periods due to gradual elution of the label out of the cell. Any novel agent that could be used to track a cell therapy must therefore prove superior to the methods currently available.

4.1. Conventional cell labeling

Conventional cell labeling for leucocyte tracking using nuclear imaging relies on the use of chelated metal ions, namely indium-111 and technetium-99m. Once chelated the radioactive compound is lipophilic and crosses the cell membrane. Inside the cell these compounds dissociate because they are inherently unstable, resulting in radioactive cell labeling and the diffusion of the chelating agent out of the cell. In the case of indium-111, cell labeling efficiency is further helped by the indium-111 ion binding directly to nuclear and cytoplasmic proteins, giving good label retention, whereas the technetium-99m ion will diffuse out of cells, resulting in a higher leakage of activity over time. [186]

For cell labeling studies, I used the Jurkat T cell leukaemia line, as the cells were cheap to produce and less precious than transduced T cells, whilst being similar in size and morphology. Cell labeling with technetium-99m hexamethylpropyleneamine oxime (HMPAO) and indium-111 tropolone was achieved following a clinical protocol supplied by the Radiopharmacy of the Nuclear Medicine Department at University College Hospital.

To label Jurkat cells with technetium-99m, 40 x 10^6 cells in a pellet were incubated with 123 MBq of a technetium-99m HMPAO mixture. The clinical guidelines for technetium-99m HMPAO cell labeling state that the expected labeling efficiency is between 40-80% for 200 x 10^6 leucocytes labeled with 750-1,000 MBq activity (corresponding to 3.75-5 Bq/cell). [155] Jurkat cell labeling with technetium-99m at approximately 3 Bq/cell, resulted in a 31.88±2.1% labeling efficiency, but the activity diffused out of cells (loss of 25% activity with decay correction after 5 hours), and the short half-life of technetium-99m (6 hours) contributed to the rapid loss of activity retained in the cells (Figure 4.1).

To label with indium-111 tropolone, 40 x 10^6 cells in a pellet were incubated with 30 MBq of indium-111, with 150 μL tropolone added. The clinical guidelines for indium-111 labeling state that the expected labeling efficiency is between 50-80% for 200 x 10^6 leucocytes labeled with 20 MBq activity (corresponding to 0.1 Bq/cell). [178] Jurkat cell labeling with indium-111 tropolone at 0.75 Bq/cell resulted in a labeling efficiency 60.77±1.9% (Figure 4.2).

Swirski et al. have demonstrated greater than 90% viability of Indium-111 labeled monocytes after 24 hours at activities ranging from 0.6-3.7 Bq/cell. [187] Hence, I increased the initial labeling activity in my experiment to maximize the labeling efficiency. Due to the longer half-life of 2.8 days, there was more activity on Indium-111 labeled cells after 24 hours, making it preferable for cell tracking. However, the decay corrected curves illustrate that there is actually more elution of label from Indium-111 labeled cells compared with Technetium-99m labeled cells, with 46.2% elution at 5 hours versus 25% with the Technetium-99m label.

Therefore, any new technique for direct cell labeling must improve on these currently used methods, by giving better cell labeling efficiency, improved retained activity over time, or reducing the administered radiation dose to the nucleus of the labeled cell.

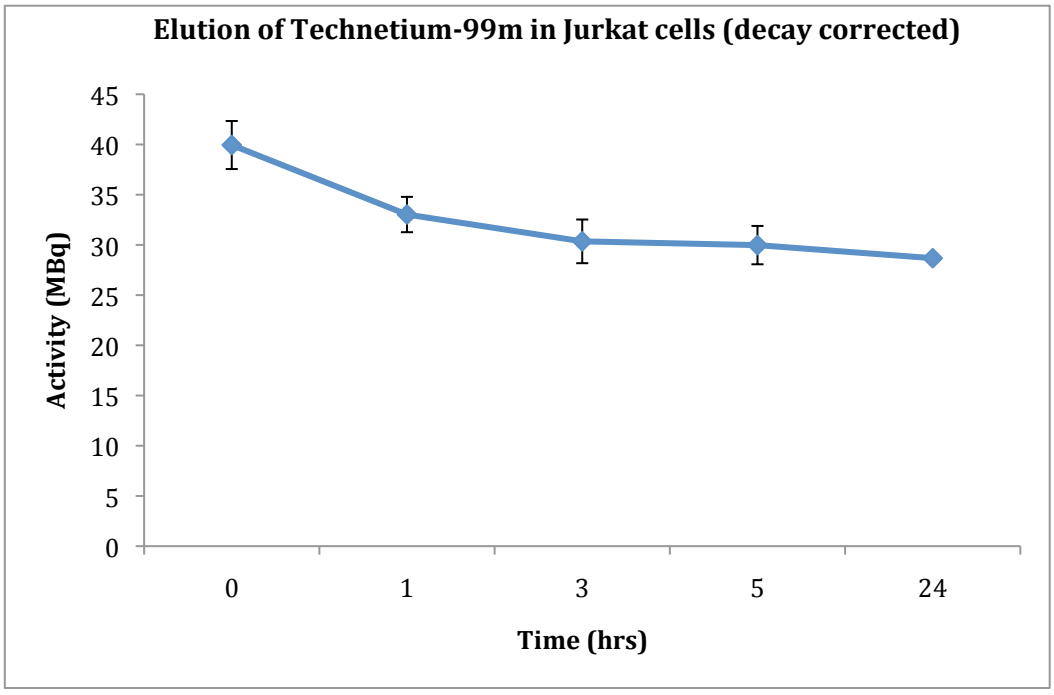

Figure 4.1: Representative graph showing retained activity over time in 40 x 10^6 Jurkat cells after labeling with technetium-99m HMPAO measured using a dose calibrator. Cell labeling efficiency at time 0 was 31.88% +/-2.1% of added activity. After 5 hours the activity remaining on the cells was 12.48 +/-1.91 MBq and at 24 hours it was just 1.21 +/-0.31MBq.

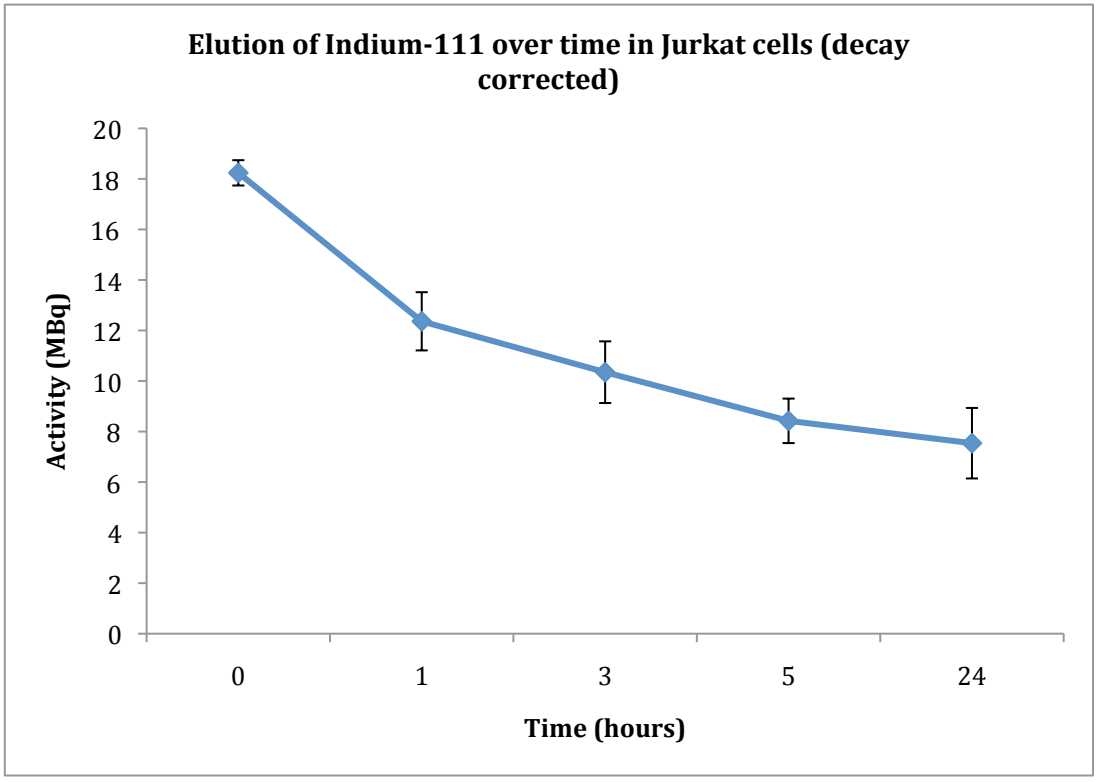

Figure 4.2: Representative graph showing activity on 40 x 10^6 Jurkat cells over time after labeling with indium-111 tropolone. Cell labeling efficiency was 60.77% +/-1.9% of added activity. After 5 hours the activity remaining on the cells was 7.60 +/-0.88 MBq and at 24 hours it was 3.55 +/-1.40 MBq.

4.2. Imaging MSCs labeled with Indium-111 Tropolone

To assess if tracking cells labeled with indium-111 tropolone to the lungs was possible using our small animal SPECT/CT system, a pilot study was carried out using 2 mice.

The control mouse received an i.v. injection of 5 MBq indium-111 alone in PBS (Figure 4.3), whereas the experimental mouse received an i.v. injection of 5 million MSCs labeled with an activity of approximately 5 MBq indium-111 tropolone in PBS, corresponding to 1 Bq/cell (Figure 4.4). MSCs were washed twice in PBS before injection to wash off excess unbound activity, and the labeling efficiency in this experiment was 25% (original labeling activity was 20 MBq).

A previous study by Gildehaus et al. also reported a labeling efficiency of 25% using indium-111 oxine to label MSCs, and no effect on cell viability at a labeling activity of 10 Bq/cell, although their migratory capacity was reduced. [156] Additionally, another study by Bindslev et al. also reported a labeling efficiency of 25%, and no effects on MSC doubling time or intracellular markers after labeling with indium-111 tropolone in the activity range of 15-260 Bq/cell. [188] However, for the purposes of this pilot study, a total activity of 5 MBq was adequate for *in vivo* imaging.

Approximately 30 minutes after i.v. injection the mice were imaged in a NanoSPECT/CT system as described in section 2.20.

Cell imaging using indium-111 tropolone as a labeling reagent allowed visualization of labeled MSCs trapped in the small capillary bed of the lungs after injection into the caudal vein and subsequent passage through the right side of the heart. Kidd et al. report that intravenous injection of luciferase transduced MSCs into a murine model lacking any environments of inflammation, results in the majority of the cells trapped in the lungs at day 1, observed using bioluminescence imaging. [189] At day 3 the cells still are still present predominantly in the lungs, with a threefold decrease in signal, followed by a further decrease in lung signal with small population in the liver at day 5 and then all of the injected cells in the liver or spleen at day 7. Therefore, this is the expected location of MSCs immediately after i.v. injection. However, there is a large activity of free indium-111 in the bladder, illustrating the significant loss of activity over time from labeled cells.

There are three possibilities to explain the free indium-111 in the bladder. Firstly, this could be the result of a leakage of activity out of labeled cells over time. Secondly, this could be a result of cell death and membrane permeability, allowing free indium-111 to leak out into the circulation. Lastly, it is possible that two washes in PBS was not adequate to wash off excess unbound indium-111 from the cells, so this free activity could have been injected alongside the labeled cells.

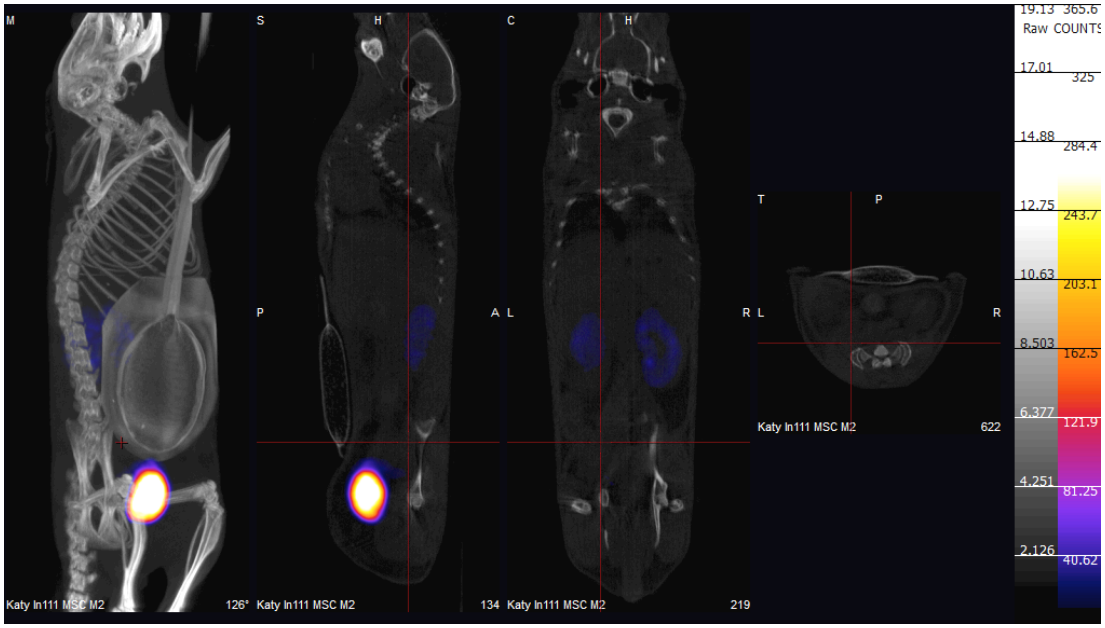

Figure 4.3: SPECT/CT image of the control mouse, 30 minutes after an i.v. injection of 5 MBq ^{111}In. Excretion of free ^{111}In can be seen in the kidneys and bladder.

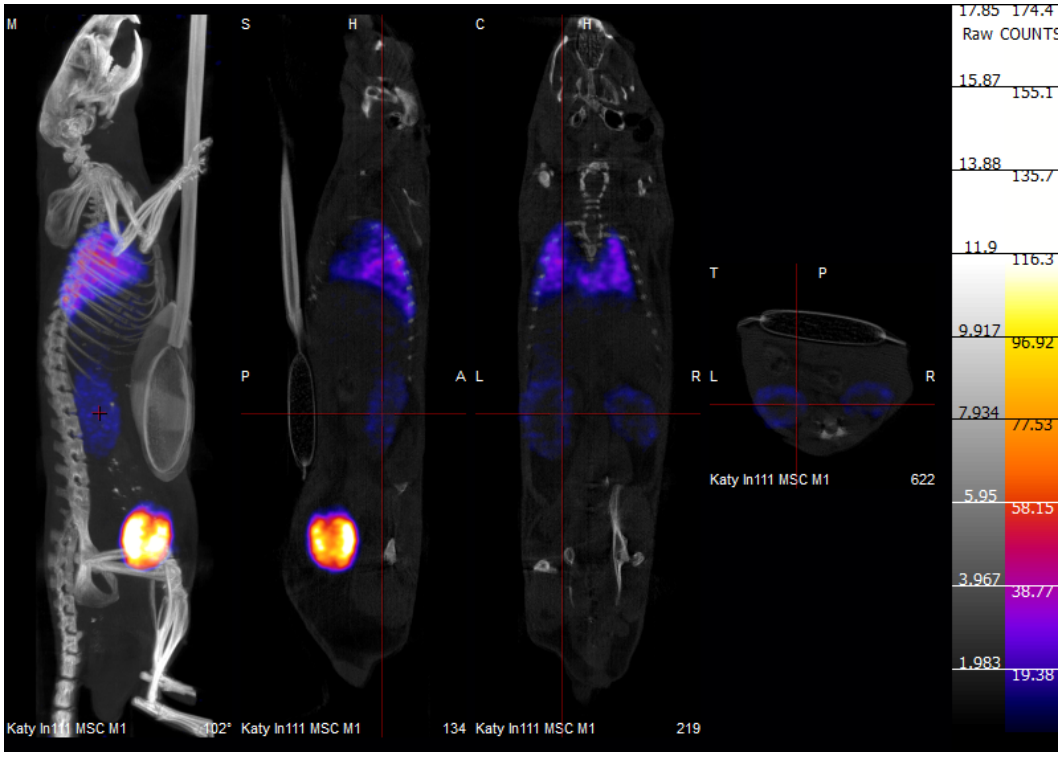

Figure 4.4: SPECT/CT image of the experimental mouse 30 minutes after i.v. injection of 5 x 10^6 MSCs, labeled with 5.0 MBq ^{111}In, 1 hour after i.v. injection. MSCs are seen primarily in the lung fields, with free ^{111}In secreted by the kidneys into the bladder.

4.3. Imaging T cells labeled with Indium-111 Tropolone

To assess SPECT/CT tracking of T cells using indium-111 tropolone and accurately measure cell survival *in vivo*, PBMCs were transduced with the EBV-TCR luciferase plasmid. These were peptide stimulated three times until the percentage of T cells expressing EBV-TCR luciferase was approximately 65%. A subcutaneous tumour lung metastases model was chosen for this pilot study in an attempt to observe the T cells residing in the lungs after delivery and homing to a tumour. A murine model of T cell homing using Gaussia bioluminescence imaging to image T cells homing to subcutaneous A20 mouse lymphoma tumours showed the majority of the bioluminescence signal located in the lungs up to day 2, then a small proportion of T cells in the subcutaneous tumour at day 5, with a maximum signal in the tumour at day 7, when there was negligible signal in the lungs. [190] Therefore, if EBV-TCR luciferase T cells could be visualized in the lungs at 7 days and subcutaneous tumour at 5 days, this would be strong evidence of tumour homing.

Subcutaneous MDA-MB-231 LMP2 tumour bearing NSG mice (n=3) with small lung metastases were injected with 6 million T cells labeled with indium-111 tropolone (average labeling efficiency 36.1%), corresponding to an average activity of 10.1 MBq per 6 x 10^6 cells, and 1.68 Bq/cell. Mice were imaged in a nanoSPECT/CT scanner as described in section 2.20 (Figure 4.5), immediately after cell injection. To monitor cell viability *in vivo*, bioluminescence imaging was performed (Figure 4.6). At 3 hours post i.v. injection, the average bioluminescent signal in the lung fields was 9.79 x 10^3 counts per minute (acquisition time 5 minutes, 35 mm lens, f/1.4).

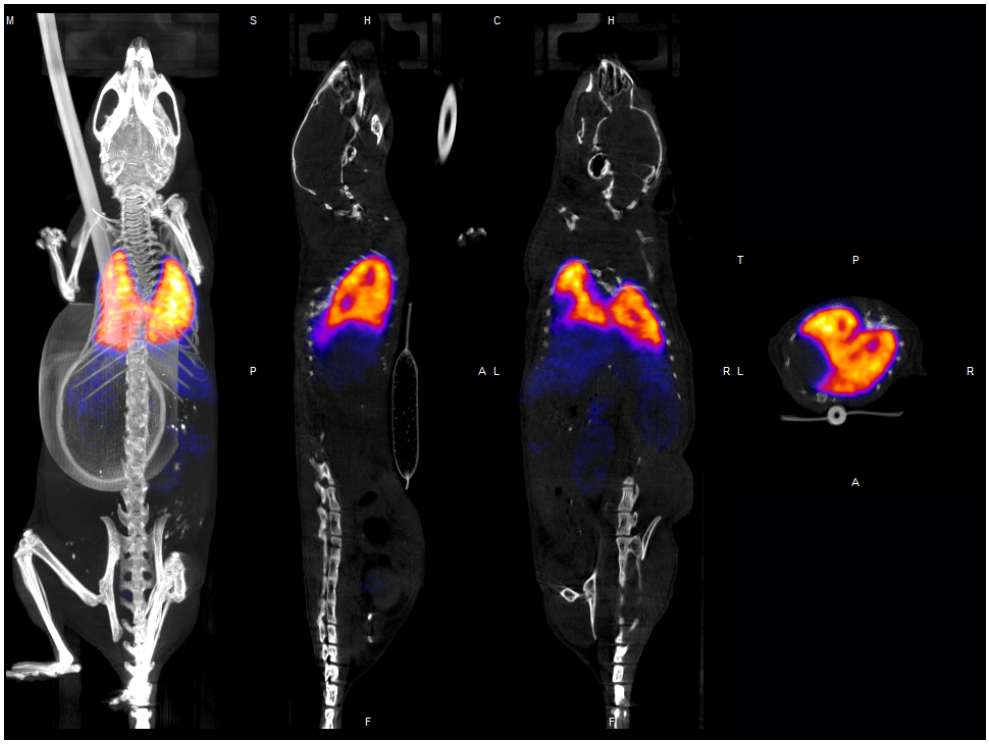

Figure 4.5: Representative SPECT/CT image of a mouse injected with 6 x 10^6 T cells labeled with 10 MBq indium-111 tropolone. Immediately after cell injection the majority of the activity is within the lung fields.

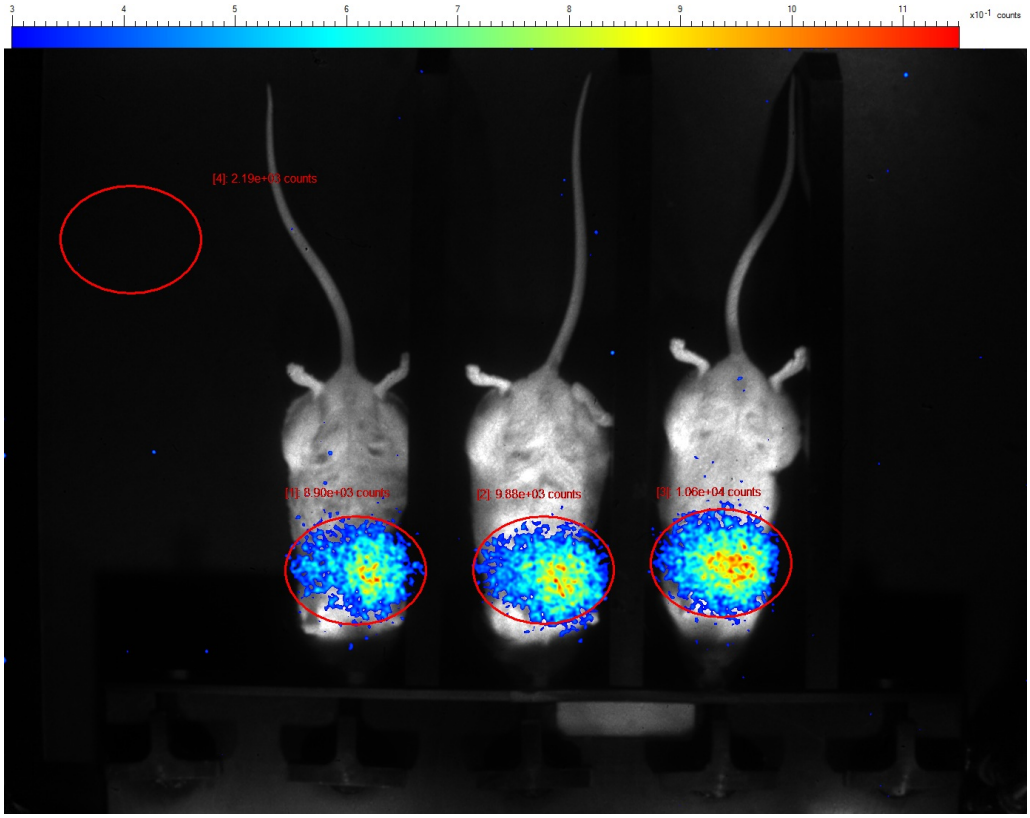

Figure 4.6: Bioluminescence image of the three NSG mice injected with 6 x 10^6 EBV-TCR luciferase transduced T cells. The image was taken 3 hours after i.v. injection of the cells.

After 24 hours, the mice were scanned in the SPECT/CT again to check the location of the T cells (Figure 4.7). The signal was located primarily in the liver and spleen, with a small amount of signal in the kidneys. Bioluminescence imaging was repeated to check the viability of the T cells (acquisition time 5 minutes, 35 mm lens, f/1.4). No bioluminescence signal was seen *in vivo* at 24 hours (Figure 4.8). This indicates that the injected cells died; probably due to the radiation dose they received. Further evidence of T cell death is provided in the location of the indium-111 signal in the liver and spleen. Free indium-111 would be excreted, hence localized in the kidneys and bladder as seen in Figure 4.3. Therefore, the signal in the liver and spleen is likely to be damaged cells that have been phagocytosed by specialized macrophages responsible for clearing cell debris, such as Kupffer cells in the liver, which represent 80-90% of the total tissue associated macrophages in the body. [191]

In vitro data of T cells labeled with 1.68 Bq/cell of ^{111}In tropolone shows approximately 80% cell death after 24 hours, and 100% cell death after 48 hours (Figure 4.9). In an early paper investigating indium-111 labeling of human lymphocytes, Wagstaff et al. recommend a maximum activity of 0.015 Bq/cell. [192] Botti et al. reported 90% viability at 4 hours but close to 100% cell death of T cells at 6 days after labeling with 0.28 Bq/cell. [193] Therefore, it seems that compared with MSCs, T cells are extremely sensitive to radiation dose. In the previous study, lowering the initial activity on the cells from approximately 0.28 Bq/cell to 0.007 Bq/cell improved T cell viability and proliferation; however, this was at the expense of labeling efficiency, and the authors did not attempt to image radiolabeled cells *in vivo*. Such low activity per cell is likely to make SPECT/CT tracking of the transferred cells impossible in an *in vivo* mouse model.

Contradicting these studies, van Monfrans et al. reported that ^{111}In oxine labeling of T cells at approximately 1 Bq/cell resulted in no loss of T cell function *in vivo* since they homed to a murine model of experimental colitis after 48 hours. [194] However, the authors did not specifically monitor T cell viability.

These pilot studies demonstrate that indium-111 is a good choice of labeling agent for MSC tracking, since MSCs seem fairly resistant to radiation injury.

However, indium-111 is not a good label for T cell tracking unless the activity on cells is very small. At a labeling dose sufficient for *in vivo* longitudinal tracking using SPECT/CT, it is likely that all the transferred cells will die after 48 hours. However, there are studies with contradicting data regarding ^{111}In T cell labeling, and its effect on homing and viability.

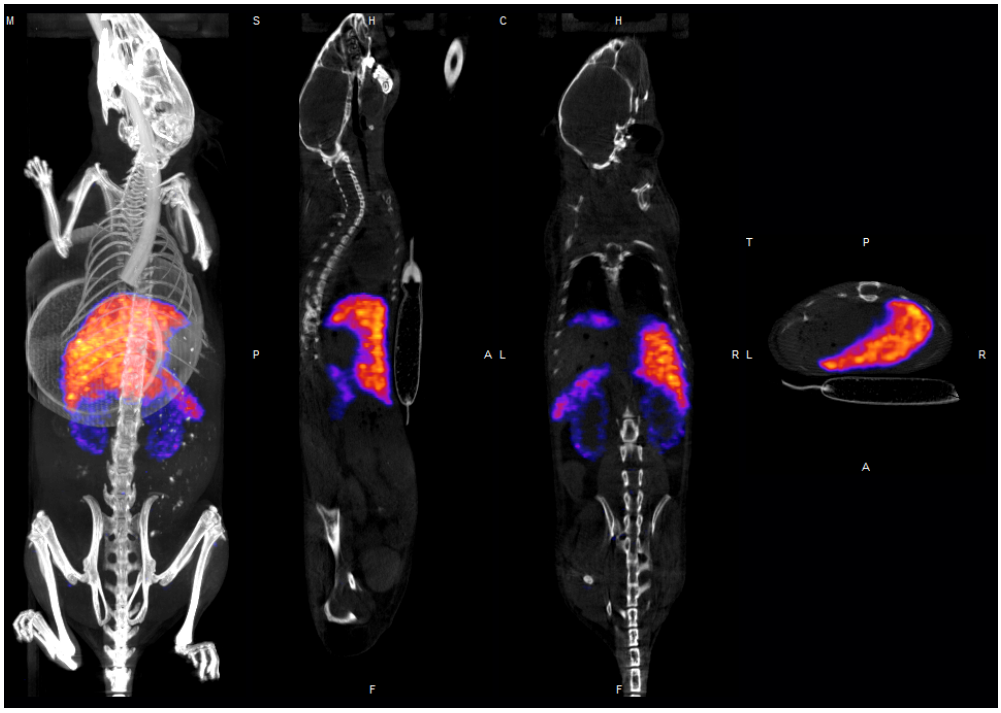

Figure 4.7: SPECT/CT image of the same mouse, 24 hours after i.v. injection of 6 x10^{6} EBV-TCR luciferase T cells labeled with ^{111}In-tropolone. Signal is now located in the liver, kidneys and spleen.

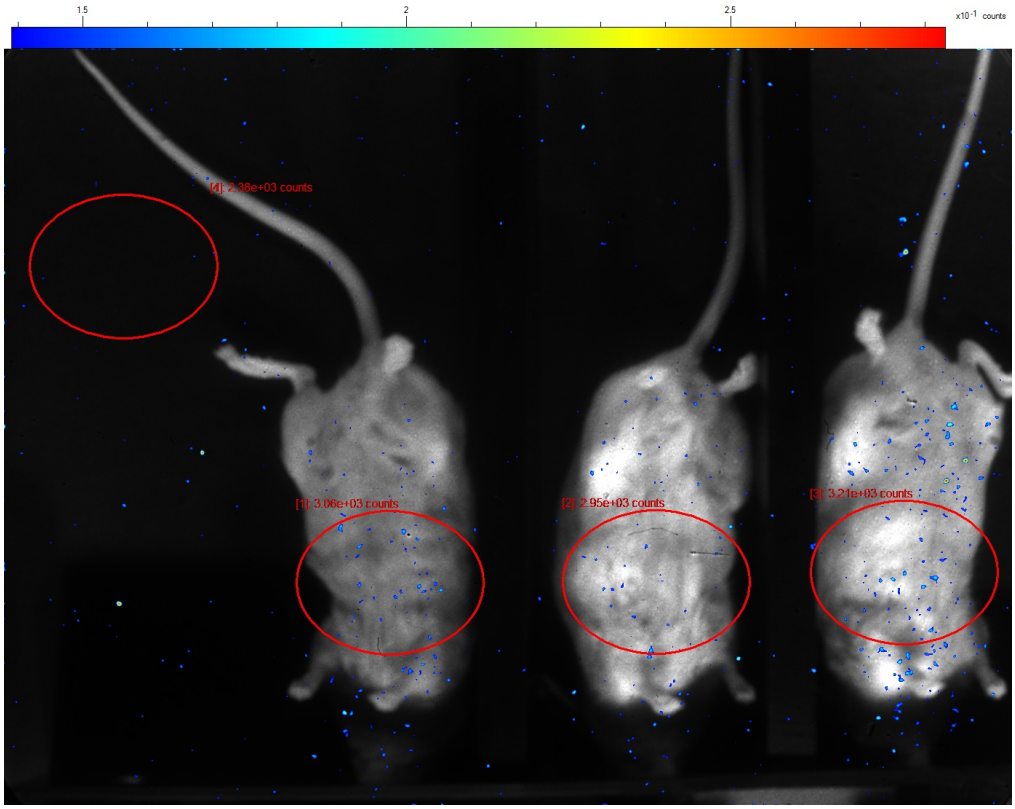

Figure 4.8: Bioluminescence image of the three NSG mice injected with 6 x 10^{6} EBV-TCR luciferse transduced T cells. The image was taken 24 hours after i.v. injection of the cells. There is no measurable bioluminescence signal, indicating death of all the injected cells.

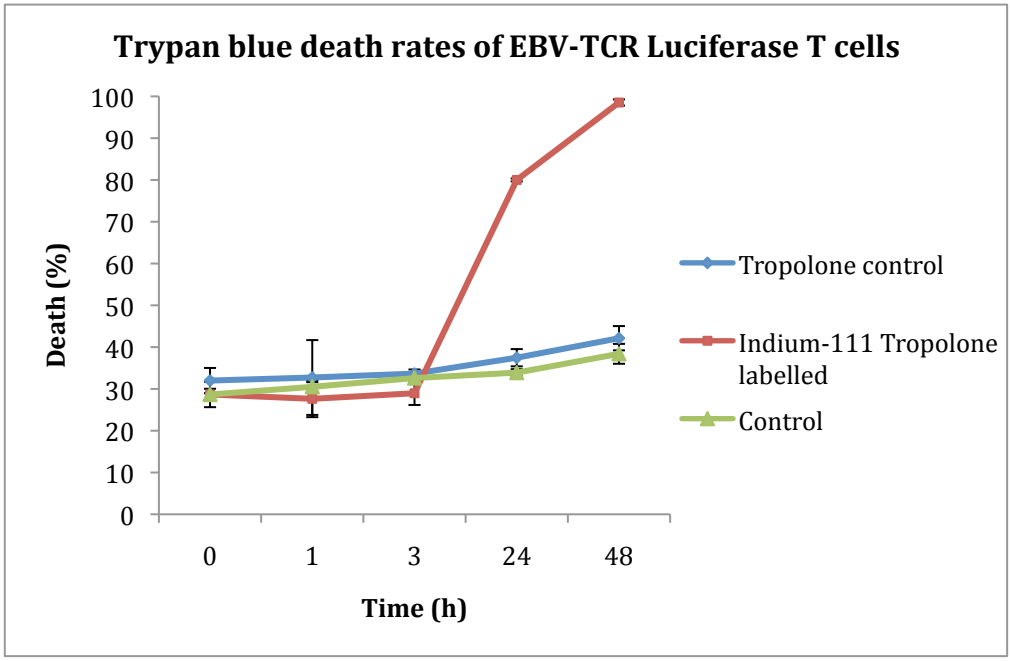

Figure 4.9: Cell death rates using trypan blue staining after labeling with indium-111 tropolone or tropolone only (n=3).

4.4. Summary

This chapter demonstrates that:

- Conventional cell radiolabeling strategies result in leakage of activity from the cells over time; however, indium-111 tropolone is superior to technetium-99m HMPAO in terms of retained activity on the cells after 24 hours.
- Indium-111 can be used to track injected MSCs and T cells in murine models, however, bioluminescent imaging of injected T cells indicates a large percentage of cell death after 24 hours.
- Indium-111 toxicity resulting in T cell death was confirmed with *in vitro* viability assessments of the labeled cells, which showed approximately 80% cell death at 24 hours after labeling.
- Hence, despite having a half-life of 2.8 days, indium-111 is not a suitable agent for longitudinal T cell tracking in a small animal SPECT/CT system. Various studies have reported that very low doses of ^{111}In activity per cell are required to avoid detrimental effects on T cell function,

homing and viability. Taking into account the elution of activity from the cells over time, it is likely that this would preclude longitudinal T cell tracking using ^{111}In.

4.5. Discussion

In order to modify and optimize a cell therapy, it is useful to assess the location, numbers and viability of the transferred cells. Many clinical protocols for adoptive immunotherapy favour several divided doses of cells, [195-197] therefore, a measure of the transferred cells proximity to the tumour and their numbers would be useful to tailor the next treatment.

While conventional cell radiolabels have previously been used to image cell therapies, these have many disadvantages, such as a high radiation dose to the sensitive cell nucleus and detrimental effects to cell proliferation and function. In addition, as shown in this work, there is elution of the label out of the cells over time and significant cell toxicity associated with radiolabeling. The short half-life of ^{99m}Tc and ^{111}In also precludes longitudinal cell tracking studies.

For adoptive immunotherapy studies, the viability and function of the transferred cells are of paramount importance. An estimate of the internal dose from ^{111}In cell labeling is 14.8 Gy, derived from low energy Auger electrons during the radioactive decay process, and which the cell absorbs. In contrast, the external radiation dose from characteristic x-rays and γ-radiation is estimated at 1 Gy. [149] Lymphocytes are known to be radiosensitive and many groups have demonstrated reduced viability, chemotaxis, cytotoxic function and proliferation after cell radiolabeling with ^{99m}Tc [198] and ^{111}In. [199]

As a result, these cell labeling techniques have not been widely adopted for adoptive immunotherapy trials, with some groups preferring to use flow cytometry analysis of blood samples instead to estimate the numbers of persisting cells. [197] A direct cell label that is not carried intracellularly could minimize the damage to the cells by limiting radiation dose to the cell nucleus. This will be discussed in the next chapter.

5. A novel tri-functional radiolabel for cell tracking

The third aim of the project was to test a novel tri-functional probe, developed by UCL's Radiochemistry department, and to compare the results to conventional labeling techniques. This chapter presents data exploring the use of this probe for T cell tracking.

To improve on conventional cell labeling strategies, I tested a probe for direct cell labeling that would bind to thiols on the cell surface membrane, keeping activity on the outside of the cell and limiting the dose to the radiosensitive nucleus. The probes were synthesized by Dr Ran Yan (UCL Department of Chemistry and Radiochemistry) and consisted of a maleimide group for cell membrane thiol conjugation, iodide-125 and a fluorescent reporter (Figure 5.1). Two fluorescent reporters were tested, rhodamine and dansyl. The purpose of the fluorescent reporter is to allow measurement of cell labeling and survival *in vitro* using flow cytometry, and *ex-vivo* cell localisation within tumours using fluorescent microscopy after histological processing. The iodine-125 reporter is useful for *in vivo* cell imaging using SPECT/CT and its long half-life of 59.4 days could allow long-term tracking.

The method describing one-pot synthesis of a probe that can be used for both nuclear and optical imaging has already been published by Yan et al. and will not be discussed here. [174] This had previously been tested as a tri-functional ^{125}I and rhodamine labeled A5B7 antibody, targeting carcinoembryonic antigen in a mouse xenograft model with subcutaneous colorectal tumours. The probe used in this work was modified version, with a maleimide group replacing the A5B7 antibody fragment, and was also synthesized using the one-pot method (see Figure 1.6 for a chemical diagram).

For cell labeling studies, I used the Jurkat T cell leukaemia line, because the cells were cheap to produce and less precious than transduced T cells, whilst being similar in size and morphology. They also express 4 nmol of cell surface thiol groups per 1 x 10^6 cells [200], equivalent to the expression of thiols by lymphocytes. [167]

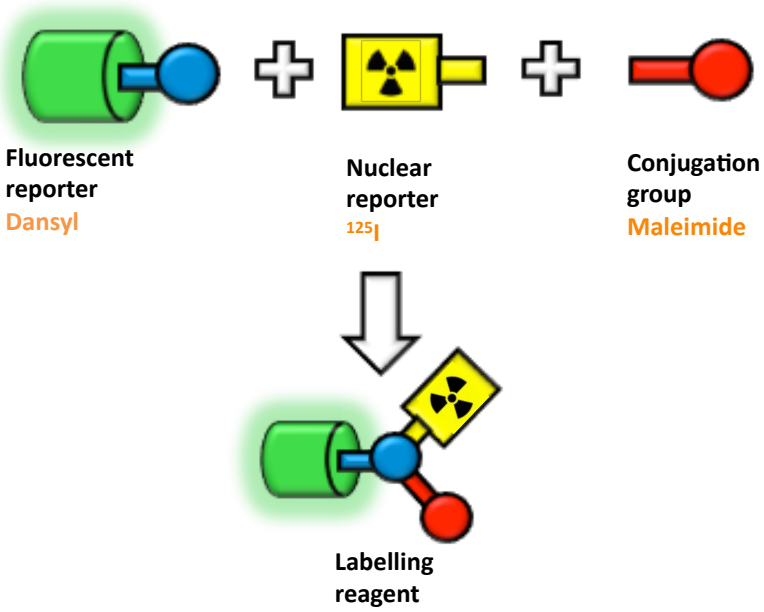

Figure 5.1: Schematic diagram of the ^{125}I-DM tri-functional probe.

5.1. Expression of thiols on Jurkat cells is dependent on cell density

A 5,5'-dithiobis-(2-nitrobenzoic acid) (DTNB) assay is used to quantify the number of thiol groups in a sample. The chemical DTNB reacts with thiols leading to the formation of yellow 2-nitro-5-thiobenzoate (NTB), the absorbance of which can be measured in a microplate reader at 412 nm. The absorbance is used to calculate the mols of thiol in the sample, with reference to the extinction coefficient of NTB.

This assay was performed on samples of Jurkat cells to measure the quantity of thiols available for labeling. Firstly, it was important to measure how many thiol groups were present on Jurkat cells to judge if thiol labeling would result in detectable fluorescence signal using flow cytometry. Secondly, research by Sahaf et al. suggests that the extracellular environment is more important than the redox status of the cell in determining cell surface thiol expression. [167] Therefore, I hypothesized that cell culture density would effect cell surface thiol expression, hence the cell culture protocol would almost certainly effect the expression of thiols and might need to be adjusted for optimal labeling. Since Jurkat cells are grown in suspension the effect of trypsinization, used to lift off

adherent cells, could be ignored. However, trypsinization has been shown to reduce cellular glutathione, [201] which may alter cell surface thiol expression, as the expression of cell surface thiols is linked to redox status. [202]

A DTNB assay was performed on samples of Jurkat cells grown at increasing cell densities for 24 hours (Figure 5.2). These cell densities were chosen since they are typical densities of Jurkat cells in culture. In fact the American Type Culture Collection recommends that Jurkat cells should be cultured at cell densities between 100,000-1,000,000 cells per mL.

The results of the DTNB assay show that increasing cell densities per millilitre of cell culture medium results in a significant decrease in the number of thiol groups expressed. Therefore, further *in vitro* thiol labeling experiments were performed with cells grown at low confluency (approximately 200,000 cells per mL of cell culture media).

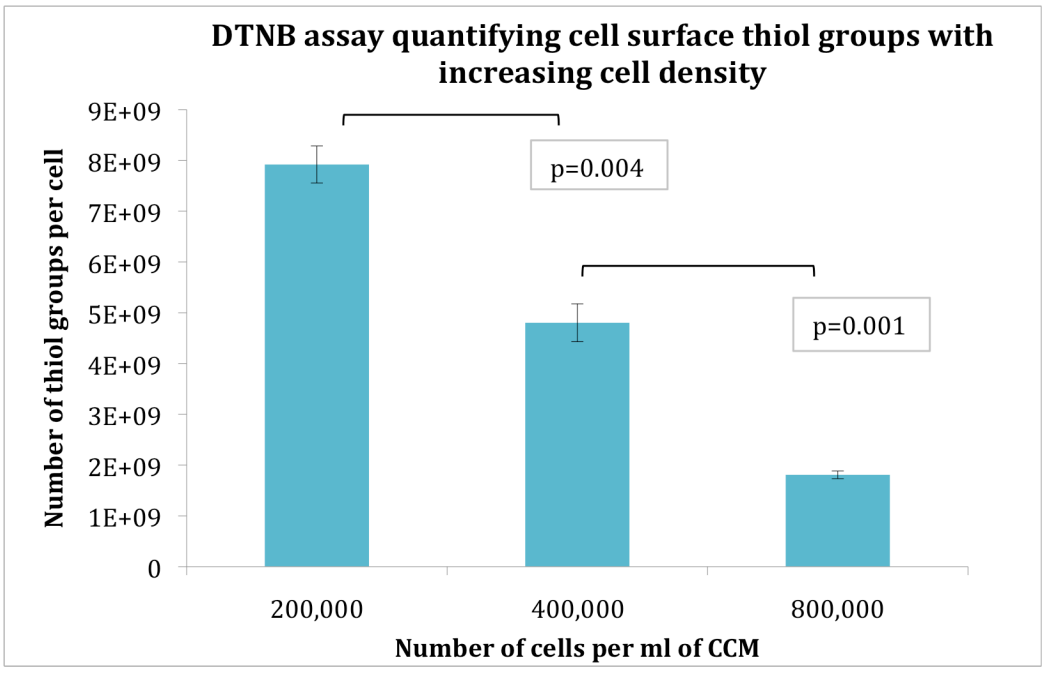

Figure 5.2: DTNB assay on Jurkat cells suspended at different confluences shows a significant decrease in thiol expression with increasing numbers of cells per ml of CCM.

5.2. Cell labeling with Iodide-Rhodamine Maleimide (I-RM)

Jurkat cell membrane thiol labeling was first assessed using rhodamine as a fluorescent reporter. Rhodamine has a high quantum yield and good photostability, making it a good choice for flow cytometry and fluorescence microscopy studies.

Flow cytometry was used to assess I-RM cell labeling as described in section 2.14, with Annexin V and DAPI counterstaining for apoptosis and death. One million Jurkat cells were labeled in 1 mL PBS at room temperature for 30 minutes with concentrations of probe in the nanomolar range (Jurkat cells express 4 nmol of cell surface thiol groups per 1 x 10^6 cells [200]), and the resulting toxicity was measured (Figure 5.3). The majority of labeled, rhodamine positive cells died within the period between cell labeling and flow cytometry analysis (2 hours). This toxicity was not reduced using decreasing concentrations of probe. A possible reason for this toxicity could be transport of the probe inside of the cell and interaction of the rhodamine or maleimide group with intracellular contents. Rhodamine is a cationic molecule and is selectively accumulated in the mitochondria of cells due to their trans-membrane potential. [203] A toxicity study by Nestmann et al. reported that a rhodamine B labeling concentration of 960 nM for 1 hour resulted in 100% cell death of Chinese hamster ovary cells. [204]

Attempting to reduce the toxicity associated with cell labeling, the cells were labeled with 10 nM of probe on ice to arrest active membrane transport and this was compared to labeling at 37°C and at room temperature (Figure 5.4). Again, all rhodamine stained cells were positive for Annexin V and DAPI, indicating cell death. No difference in cell survival was seen between the different labeling conditions, revealing that the cell labeling is dependent on molecular charge or chemical maleimide-thiol interaction, rather than an active process by the cell. Maleimide-thiol interaction is particularly important because many peptides, nanoparticles and probes modified to express thiols show enhanced cellular uptake. [205] Unfortunately, the mechanisms involved in the cellular uptake of molecules interacting with exofacial thiols have not yet been discovered,

although the redox status of the thiols seems to be important, with oxidization increasing cellular uptake. [206]

To determine if cell labeling with I-RM was resulting in intracellular accumulation of the probe, confocal microscopy images were taken of I-RM labeled Jurkat cells counterstained with DAPI (Figure 5.5). The images reveal that as well as binding to the cell surface membrane, the probe has entered the cells and bound to intracellular organelles. This data confirms the hypothesis that internalization of the I-RM probe is resulting in cell death.

In conclusion, although the I-RM probe labels cells very efficiently, the poor cell survival after labeling makes it undesirable for tracking a cell therapy. Its toxicity is due to the internalization of the probe, probably through maleimide-thiol interactions. Once inside the cell membrane, the toxicity could be explained by the reactivity of the rhodamine fluorescent group, since it is negatively charged and lipophilic, or the interaction of the maleimide group with intracellular glutathione. Therefore, to elucidate whether rhodamine was the main cause of toxicity, the tri-functional probe was modified with an alternative fluorophore.

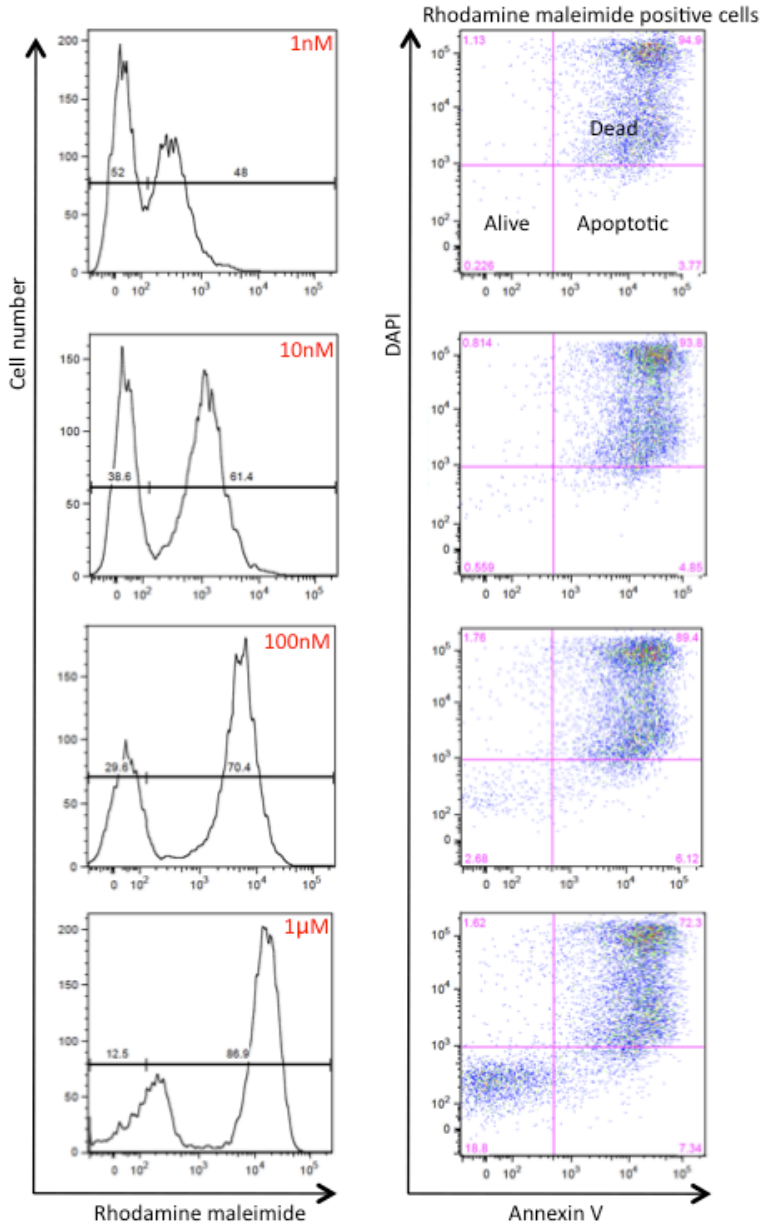

Figure 5.3: Representative flow cytometry plots of I-RM cell labeling at different concentrations of probe (red), (n=3). Cell labeling increases with concentration, however the survival of the cells after labeling is very poor.

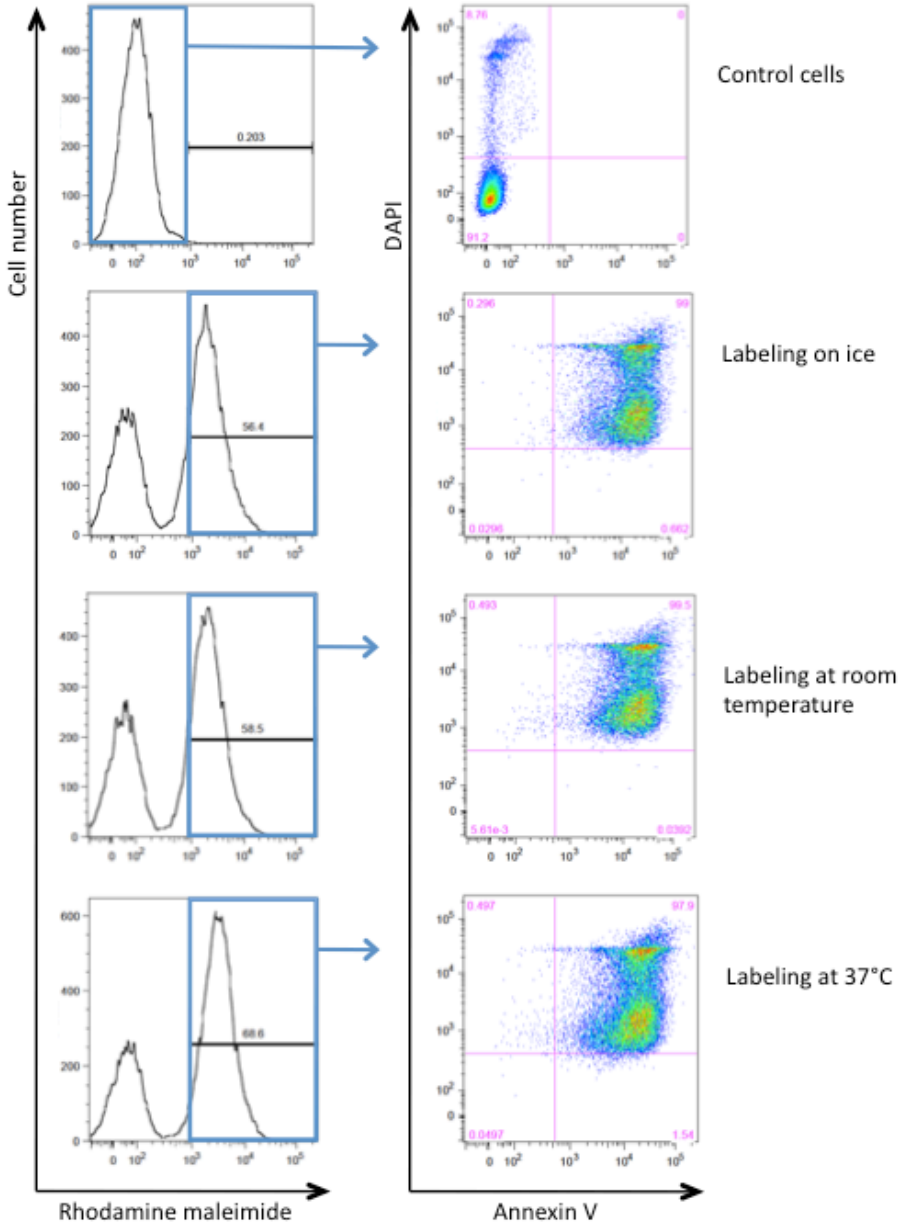

Figure 5.4: Representative flow cytometry plots of cells labeled with 10nM I-RM on ice, at room temperature and at 37°C (n=3). The poor survival of the cells is unchanged by the labeling conditions.

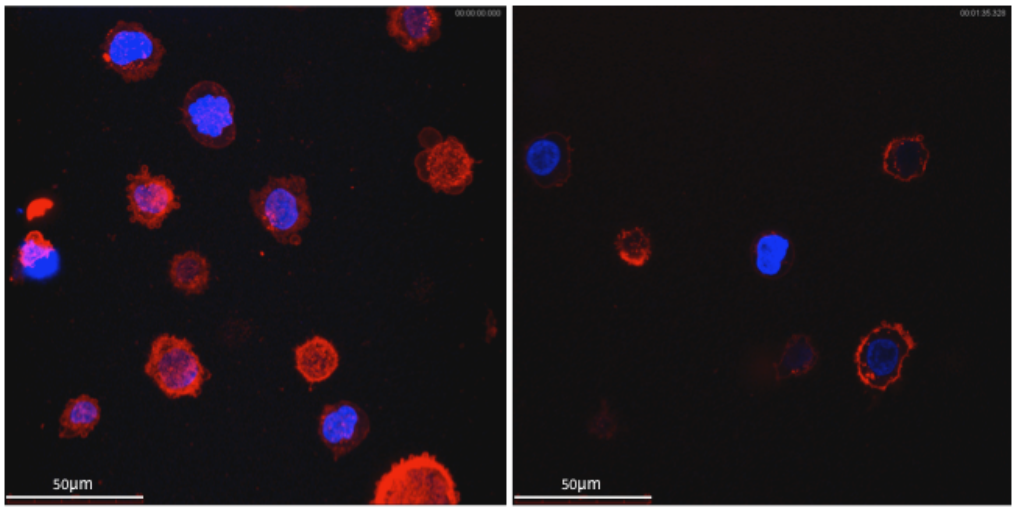

Figure 5.5: Confocal microscopy image of Jurkat cells labeled with 10nM I-RM (red), counterstained with DAPI (blue) to highlight the cell nucleus of dead cells. The left image is a maximum intensity projection through all imaging slices, and the right image is a single slice. All cells are dead or undergoing apoptosis with blebbing of the cell membrane. Rhodamine fluorescence can be seen inside the cell membrane, indicating internalization of the probe.

5.3. Cell labeling with Iodide-Dansyl Triazole Maleimide (I-DM)

The fluorophore dansyl has a neutral charge, although it is lipophilic. Therefore, the tri-functional probe was modified to contain a dansyl fluorescent reporter. Cell labeling at nanomolar concentrations did not result in detectable fluorescence using flow cytometry, hence cells were labeled at micromolar concentrations.

Flow cytometry was used to assess I-DM cell labeling as described in section 2.14, with Annexin V and Propidium Iodide (PI) counterstaining for apoptosis and death, respectively. Due to spectral overlap with dansyl fluorescence, DAPI could not be used to measure cell death in these experiments. The same cell labeling protocol was followed, 30 minutes incubation with the probe in PBS.

Cell labeling was observed in the micromolar concentration range and above (Figure 5.6). A labeling concentration of 1mM resulted in increased cell death, seen by a shift of the population up the y-axis (PI fluorescence). However, cell labeling at probe concentrations between 10-100 μM resulted in a large percentage of alive and labeled cells (76-85.8% survival after 2 hours). This positive finding enabled further evaluation of the I-DM probe and provided the rationale to proceed to labeling experiments using T cells. In subsequent experiments, 10 μM I-DM was chosen as the optimum labeling concentration, because it was shown to provide approximately 81% labeling and 86% survival at 2 hours after labeling.

As a result of this favourable data, I-DM was used to label T cells, to assess its suitability for T cell tracking *in vivo*.

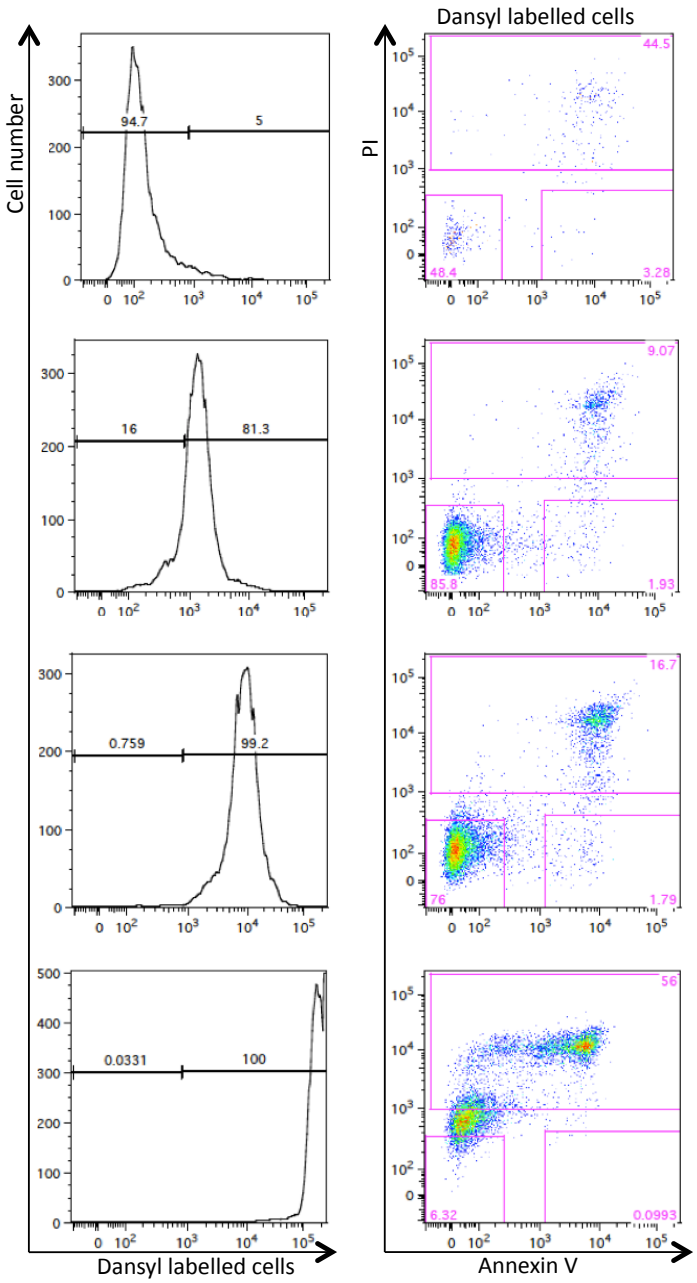

Figure 5.6: Representative flow cytometry plots of I-DM labeling (n=3), two hours post-labeling. Cell labeling increases with concentration, shown by the histogram plot moving right along the axis of dansyl positive signal. After gating on the dansyl positive population, apoptosis and death plots are shown in the right-hand column.

5.4. T cell survival after I-DM labeling

In order to assess the suitability of the probe for long-term tracking of T cells, T cells were labeled with 10 μM I-DM, and the survival of the cells at 24 hours was assessed using flow cytometry. The results indicate that although T cells can be labeled with I-DM with approximately 65% of labeled cells alive at 2 hours, unfortunately no cells survive at 24 hours post-labeling (Figure 5.7).

To assess if the probe was entering the cell cytoplasm instead of being restricted to the cell membrane, T cells labeled with 10 μM I-DM were imaged using confocal microscopy (Figure 5.8). This clearly showed I-DM inside the cells, bound to organelles and within cytoplasm, as well as bound to the cell membrane. Therefore, the toxicity of the I-DM is likely to be due to the entry of the probe into the cells.

In an attempt to assess whether the dansyl group or the maleimide binding group was responsible for the delayed toxicity at 24 hours, T cells were labeled with Alexa Fluor® 488 maleimide. Unfortunately, there is a paucity of data regarding the toxicity of Alexa Fluor 488 itself, [207] however, the Alexa Fluor family of dyes are advertised as being non-toxic labeling probes. The results show markedly inferior cell labeling compared with the I-DM probe, with 24.2% cells labeled at 10μM of Alexa Fluor® 488 maleimide, and 85.6% cells labeled at 10μM I-DM (Figure 5.9). However, with both labels close to 100% cell labeling was achieved with 10mM of probe. Similar to the results achieved with I-DM cell labeling, the majority of cells were dead after 24 hours. This result points to a possible conclusion that the maleimide group is responsible for the toxicity of these probes, rather than any interaction of the dansyl group with the cell. The mechanism of death could be interaction of the maleimide group with intracellular redox processes, in particular, binding to intracellular glutathione. However, toxicity of the dansyl group alone has not be excluded and further testing of dansyl toxicity and maleimide toxicity is required.

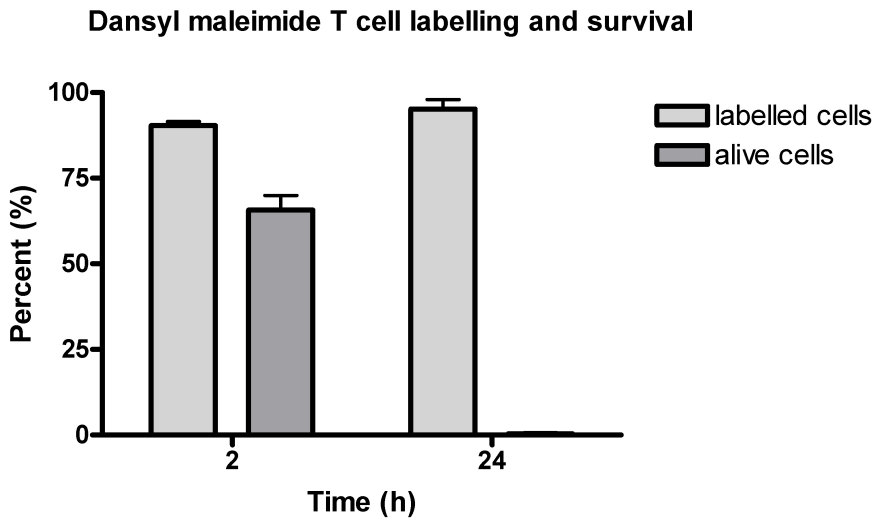

Figure 5.7: T cell survival after labeling with 10µM I-DM, assessed using flow cytometry (n=3).

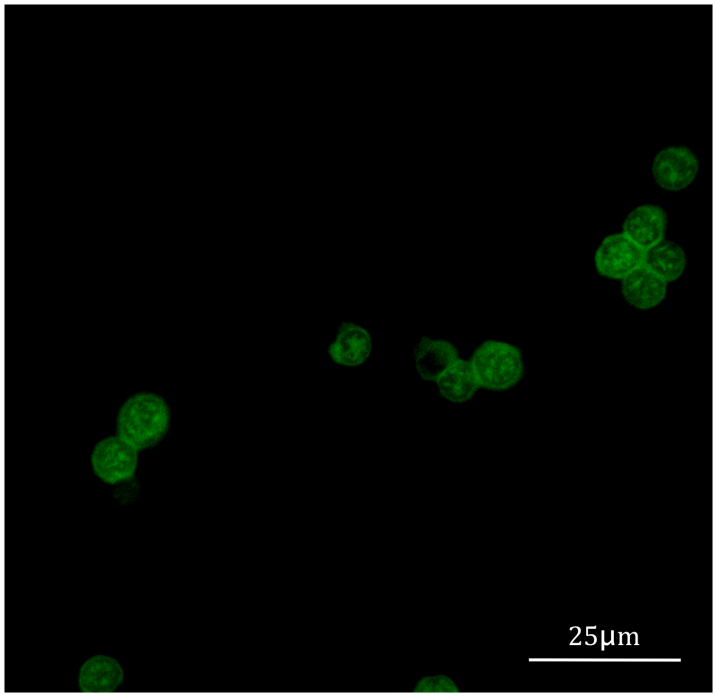

Figure 5.8: Confocal microscopy maximum intensity projection image (x100) of I-DM labeled human T cells after 24 hours, showing I-DM probe (green) binding to the cell membrane, as well as to intracellular organelles, with probe present in the cytoplasm.

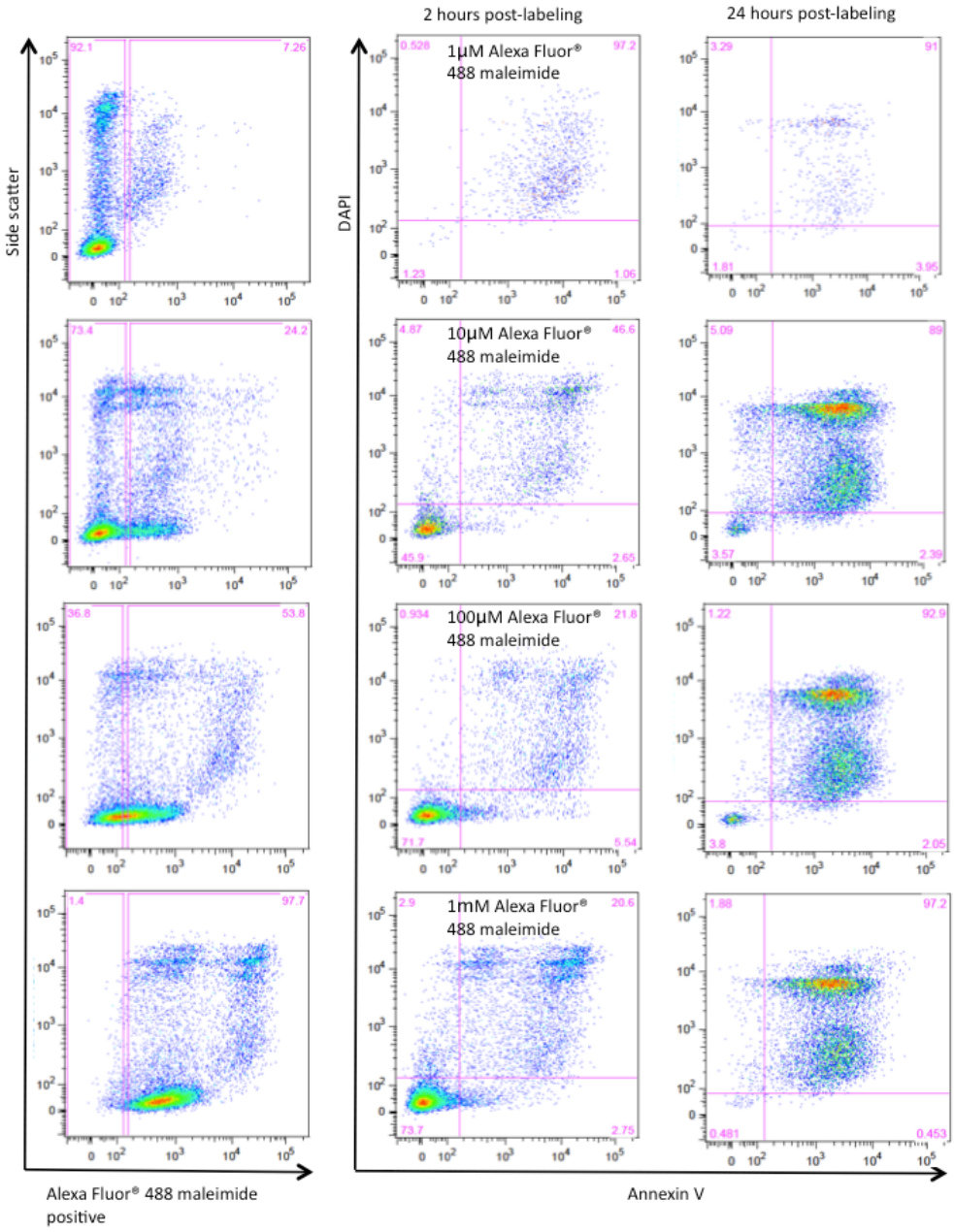

Figure 5.9: Representative flow cytometry plots of cell labeling with Alexa Fluor® 488 maleimide (n=3), 2 hours post-labeling. Cell labeling increases with probe concentration, shown by the movement of the cell population along the x-axis in the left column. After gating on the labeled cells, cell death (DAPI) and apoptosis (Annexin V) is shown in the right columns, at 2 hours and 24 hours post-labeling.

5.5. T cells labeled with ^{125}I-DM can be imaged using SPECT/CT

Due to the sensitivity of SPECT/CT imaging, a much lower concentration of radioactive probe can be used than that required for fluorescence labeling bright enough to be detected by flow cytometry (10 μM). Therefore, labeling cells in the nanomolar range was explored for SPECT/CT imaging, and in an attempt to avoid cell toxicity.

To assess if the label was retained after labeling, Jurkat cells were labeled using the radioactive ^{125}I-DM probe in PBS or cell culture media, and the activities of the cell pellets were measured over time (section 2.17). The labeling efficiency with 8 MBq of probe incubated with 1 x 10^6 Jurkat cells was 25.6 ±0.8 % of added activity (specific activity of the ^{125}I-DM sample was unknown, I received 43.0 MBq activity in 1 mL DMSO from Radiochemistry). This is inferior to the labeling efficiency of 51.5 % observed using indium-111 tropolone. However, at 24 hours after labeling with ^{125}I-DM, 64.5 % of the original activity immediately after labeling was retained on the cell pellets (Figure 5.10). Leakage of the activity from the cells over time was small and therefore favorable for imaging. In contrast, only 19.5 % of the original retained activity of indium-111 was on the cell pellets at 24 hours, which will result in reduced sensitivity of imaging.

In an attempt to maximize cell survival after labeling, small activities of ^{125}I-DM were tested for cell labeling and imaging. Jurkat cells (1 x 10^6) were labeled with 0.6 MBq ^{125}I-DM (n=3), resulting in a labeling efficiency of 38.45 ±3.77% (specific activity of the ^{125}I-DM sample was unknown, I received 24.84 MBq activity in 963 μL DMSO from Radiochemistry). Control Jurkat samples were labeled with 0.6 MBq of ^{125}I only (n=3), resulting in a labeling efficiency of 39.43 ±6.77%.

After labeling these were spun into a cell pellet and imaged using a nanoSPECT/CT system (Figure 5.11). Although imaging results were good, cell death in the samples was found to be 43.3 ±3.3 %, 5 hours post-labeling (n=3), with a control death rate of 5.9 ±1.6 % (n=3). In contrast the retained activity in the ^{125}I labeled cells was 0.83 ±0.47% at 5 hours, with a death rate of 8.8 ±2.4% (n=3).

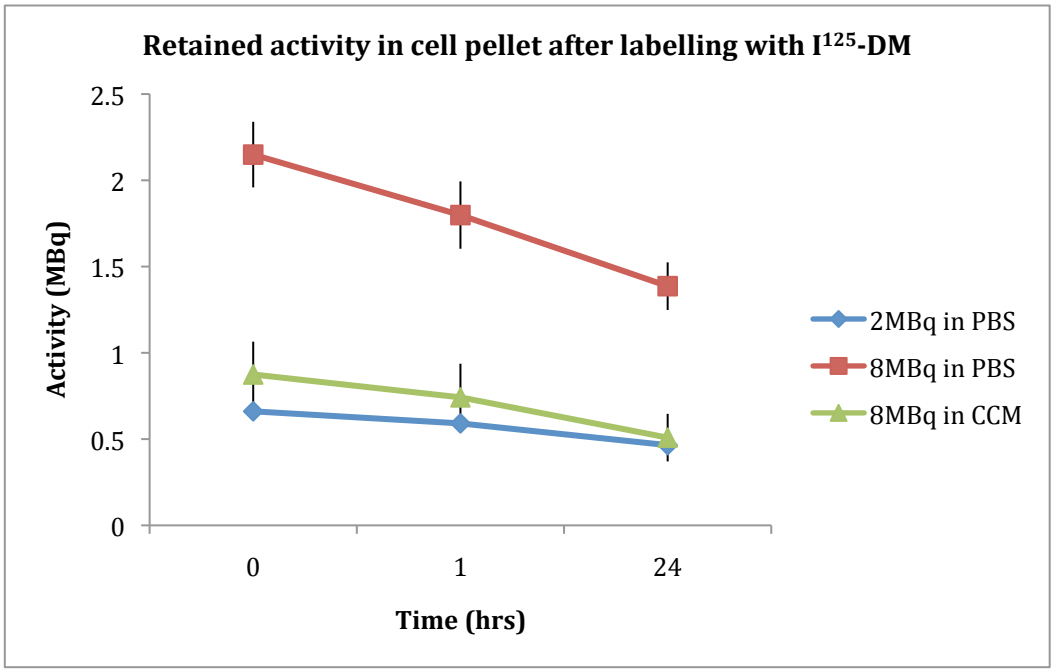

Figure 5.10: Activity of ^{125}I on 1 x 10^6 Jurkat cells measured over time after labeling with 2 MBq/8 MBq ^{125}I-DM in PBS or 8 MBq ^{125}I-DM in cell culture media (CCM), n=3.

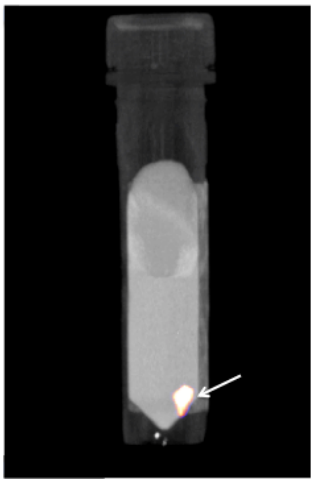

Figure 5.11: SPECT/CT image of 1 x 10^6 Jurkat cells (arrowed) in an eppendorf, labeled with 0.6 MBq ^{125}I-DM.

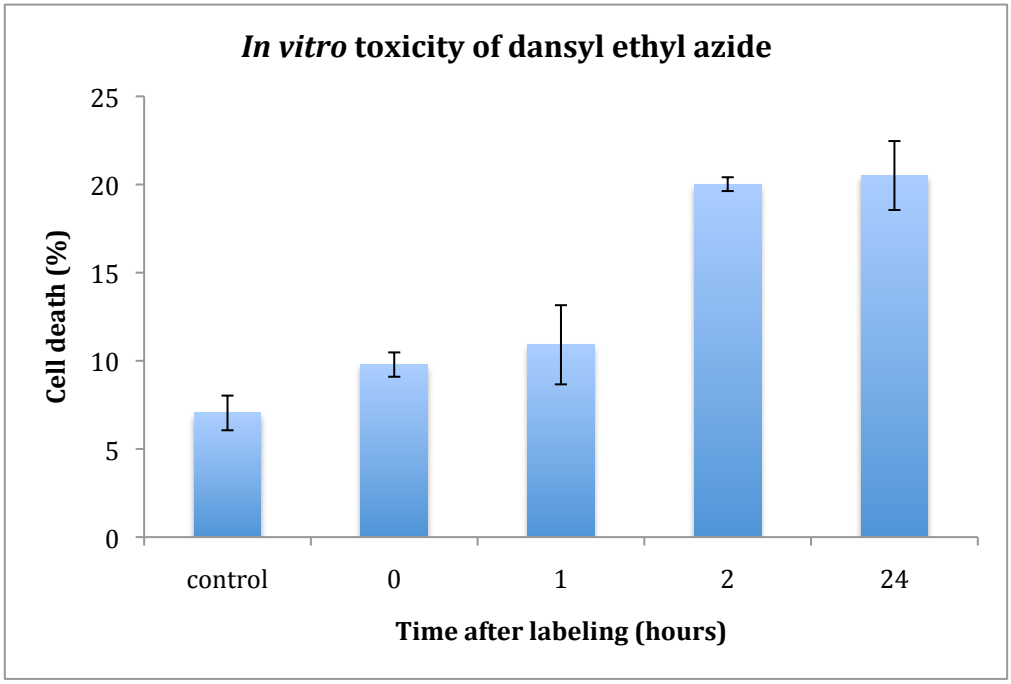

Figure 5.12: Bar graph of cell death (using trypan blue), after labeling 1 x 10^6 Jurkat cells with 10µM Dansyl chloride dye for 1 hour in PBS, n=3.

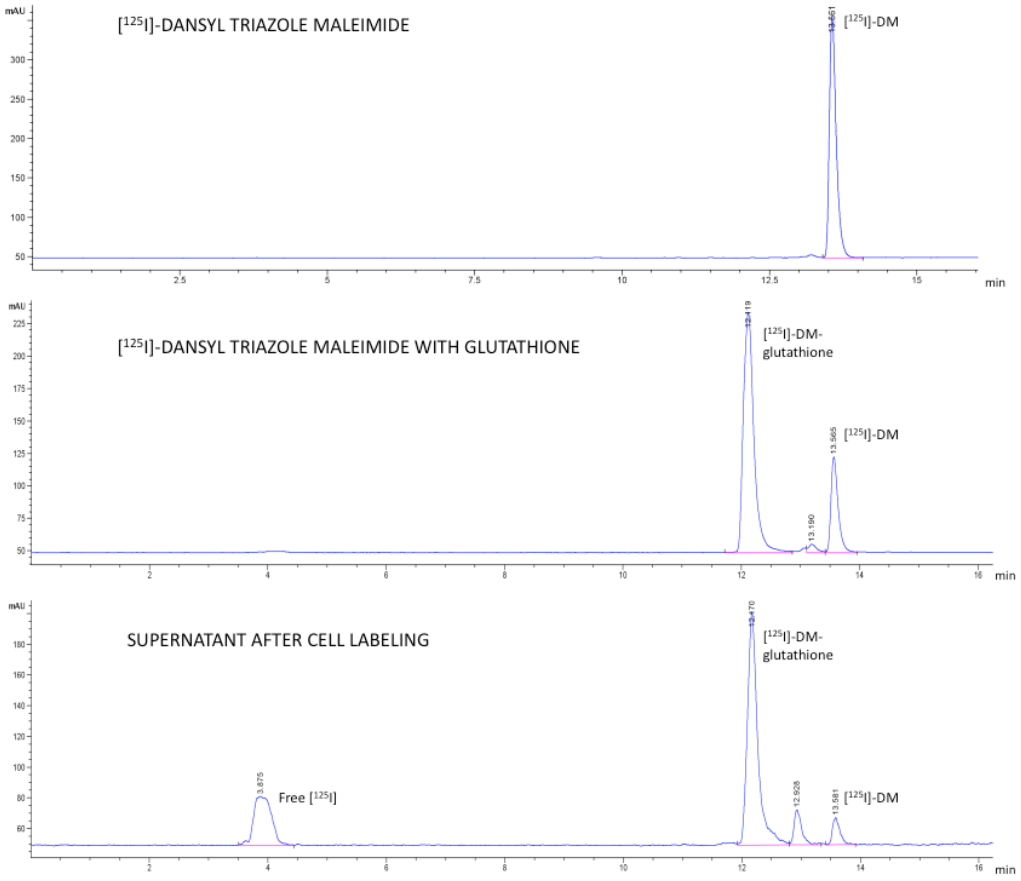

Figure 5.13: HPLC analysis of the supernatant after labeling Jurkat cells with 0.6 MBq ^{125}I-DM.

In order to assess the toxicity arising from the dansyl component of the I-DM probe, T cells were incubated with 10μM Danzyl ethyl azide dye for 30 minutes in PBS, as per the cell labeling protocol. In fact, labeling with Dansyl ethyl azide dye alone (10 μM) results in significant toxicity of approximately 20% within 2 hours (Figure 5.12), although after 24 hours the cell death does not increase. Therefore, the dansyl fluorophore component is only responsible for a proportion of the overall toxicity.

To further assess the consequences of maleimide binding to the cells, high perfomance liquid chromatography (HPLC) was performed on the cell supernatant 1 hour after labeling with ^{125}I-DM, and this was compared to reference HPLC data of the ^{125}I-DM probe alone, and the ^{125}I-DM probe reacted with glutathione. HPLC analysis on the cell supernatant 1 hour after ^{125}I-DM labeling revealed approximately 60% abundance of a ^{125}I-DM-glutathione complex (Figure 5.13). This implies that once inside the cell, the probe is binding intracellular glutathione followed by excretion of the complex from the cell. The multidrug resistance-associated protein 1 (MRP1) pump is an ATP-binding cassette transporter, which actively translocates glutathione, glucuronate and sulfate conjugates across the cell membrane. [208] The MRP1 pump is widely expressed in human tissues and is also expressed by Jurkat cells, [209] making it the most likely candidate transporter responsible for the active excretion of the ^{125}I-DM-glutathione complex. Glutathione is the most important and prevalent thiol/disulfide redox buffer in the cell, and depletion of glutathione in an oxidizing environment leads to apoptosis. [210] Therefore, the high toxicity of the probe is probably multifactorial, in part due to the dansyl fluorophore and also due to binding of the maleimide group to intracellular glutathione and subsequent depletion of intracellular glutathione leading to oxidative stress.

After much deliberation with my colleagues at UCL Radiochemistry, this probe was not carried forward and the project was closed. The novel tri-functional probe design did not achieve the objective of dual fluorescence and nuclear imaging, as the high concentrations of probe required for good fluorescent labeling resulted in cell death. Furthermore, using the probe for radiolabeling, even at nanomolar concentrations, still resulted in 43% cell death after 5 hours. Therefore, this probe is not a suitable long-term cell-tracking agent, although it

could be used to label a small minority of injected cells to image the delivery of transfused cells within the first few hours.

5.6. Summary

This chapter demonstrates:

- Thiol targeting maleimide probes can be used for cell labeling, however the probe enters the cells resulting in significant toxicity.
- Despite this, retained activity on the labeled cells is very good compared with conventional cell labeling techniques.

Unfortunately, the further development of this probe was halted, as it is not a suitable tracking agent for a cell therapy.

5.7. Discussion

Despite promising cell labeling at nanomolar concentrations, the toxicity of the I-RM probe was soon discovered and this limited any *in vivo* applications of this probe. One proposed advantage of our tri-functional probe design was to keep the iodine-125 restricted to the cell membrane, thus decreasing radiation dose to the radiosensitive nucleus. Therefore, internalization of the probe was an unwanted consequence of cell labeling. Once inside the cell, rhodamine can cause toxicity by interrupting mitochondrial function and binding to DNA. I concluded after the I-RM experiments that the toxicity of the I-RM probe could be due to the rhodamine reporter; hence, other fluorescent reporters were tested.

Initial results with the cold I-DM probe looked promising, with 81% cells labeled at 10μM and 86% cells alive after 2 hours. However, when the probe was used to label T cells and their survival was traced over a prolonged period (24 hours), 100% of the labeled cells died within that period. On confocal microscopy imaging of the labeled cells, intracellular dansyl staining was observed. However, despite this result I proceeded to experiments testing cell labeling with the ^{125}I-DM probe, since lower probe concentrations could be used with

sufficient activity for cell imaging. Unfortunately, despite adequate labeling efficiency and activity on the cell pellets, toxicity was still problematic, with cell death in the samples found to be 43.3%, 5 hours post-labeling, with a control death rate of 5.9%.

Further work was required to understand the mechanism of cell toxicity and to distinguish if the toxicity was primarily due to the fluorescent reporter or the maleimide group. Cell labeling with the dansyl ethyl azide fluorescent reporter alone also resulted in some cell toxicity, although this was only approximately 20% cell death. Therefore, the fluorescent group alone cannot account for the high toxicity of the I-DM probe.

Cell labeling with Alexa Fluor 488 maleimide resulted in close to 100% cell death after 24 hours. Unfortunately, it is difficult to assess whether toxicity is exclusively a result of maleimide labeling, since there is little evidence regarding the stability and toxicity of Alexa Fluor 488 itself. However, this result adds weight to the above evidence suggesting that binding of the maleimide probe to cell membrane thiols results in internalization of the probe and cell death.

Following ^{125}I-DM labeling, HPLC analysis performed on the cell supernatant showed an interesting result, a large amount of a ^{125}I-DM-glutathione complex. This indicates that as well as entering the cell and binding to organelles, the probe is also binding to intracellular glutathione and then exiting the cell. This suggests that the toxicity of the probe could result from disruption of the cell's delicate redox balance.

Redox homeostasis is essential for many intracellular processes, including gene transcription, DNA synthesis and enzyme activation. The cell must also counteract the large number of reactive oxygen species that are generated during normal biological reactions, such as oxidative phosphorylation in mitochondria. As a result, the intracellular redox status is tightly regulated, and the most important component of this system is glutathione (existing at intracellular concentrations of 0.5-10mM), which can be either oxidized or reduced by reactions of its thiol group. [211] Therefore, a large concentration of maleimide probe (1μM- 1mM in these experiments) binding to intracellular glutathione

would result in an inability to reduce reactive oxygen species, oxidative stress and finally, cell death.

The multi-drug resistance protein-1 pump (MRP1) is a member of the ATP-binding cassette superfamily of transport proteins, and exports glutathione compounds formed during oxidative reactions to maintain cell redox homeostasis. [212] Therefore, it is likely that the MRP1 pump is responsible for the export of the ^{125}I-DM-glutathione complex, in an attempt to regulate the redox environment in the cell after labeling.

In conclusion, it is likely that the maleimide group of the tri-functional probes causes significant toxicity, as well as the fluorescent reporter, which contributes to a smaller extent. Strategies to prevent the probe entering the cell could be employed to reduce toxicity, for example, making the probe too large to enter the cell easily. However, this is likely to result in a reduced labeling efficiency, so these avenues of research were not explored.

6. In vivo imaging of a combined T cell and MSC TRAIL therapy

The final aim of my project was to combine engineered EBV-TCR T cells and MSC TRAIL as a dual cell therapy for lung metastases. This dual cell therapy is a novel contribution in the field of cell therapies for cancer. Furthermore, this is the first *in vivo* study using T cells expressing the chimeric EBV-TCR, and to my knowledge, the first application of tumour antigen specific T cells to target lung metastases. It is also the first use of bioluminescence imaging to track a T cell therapy homing to lung metastases.

Due to the toxicity problems associated with direct labeling with conventional cell radiolabels and the tri-functional probes, bioluminescence imaging was used instead to track the T cells *in vivo*. Although this is an indirect labeling method that is not currently translatable into clinical imaging, bioluminescence imaging offers fast, sensitive, repeatable and highly specific imaging of the transfused cells. [213] In addition, fluorescent probes can be used alongside bioluminescence imaging to track multiple cell types.

6.1. Tumour models in NOD/SCID mice

NOD/SCID mice have a severe combined immunodeficiency (SCID), on the background of a non-obese diabetic (NOD) genotype. The immunodeficiency is caused by a lack of functioning B cells and T cells, as well as defective macrophages and natural killer cells, and this allows the growth of human cancer cells *in vivo*. [214]

6.1.1. A subcutaneous tumour model

Subcutaneous tumours were set up in NOD/SCID mice by injecting 10^6 MDA-MB-231 LMP2 cells into the right flank of 6 mice. The resulting tumours occurred in all mice within 2 weeks. These were measured regularly, and the tumour volume was calculated (Figure 6.1). After sacrifice at day 30, all mice had multiple, small lung metastases (Figure 6.2). However, for the purpose of testing cell therapies for lung metastases, a shorter, more direct method was needed. Accordingly, I set up a tumour model with intravenous injection of tumour cells that would result in immediately delivery of cancer cells into the lungs.

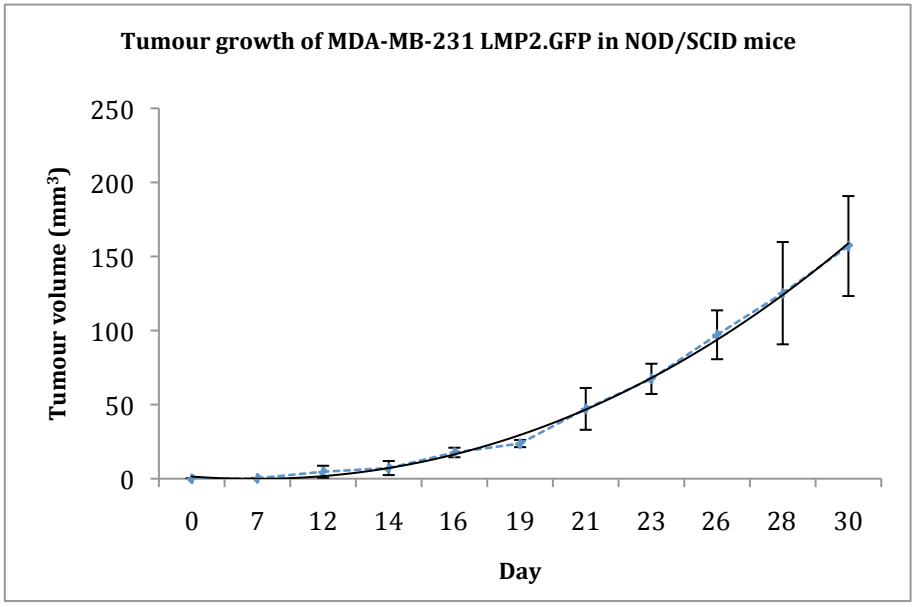

Figure 6.1: Subcutaenous tumour growth after injection of 10^6 MDA-MB-231 LMP2 cells into the right flank (n=6).

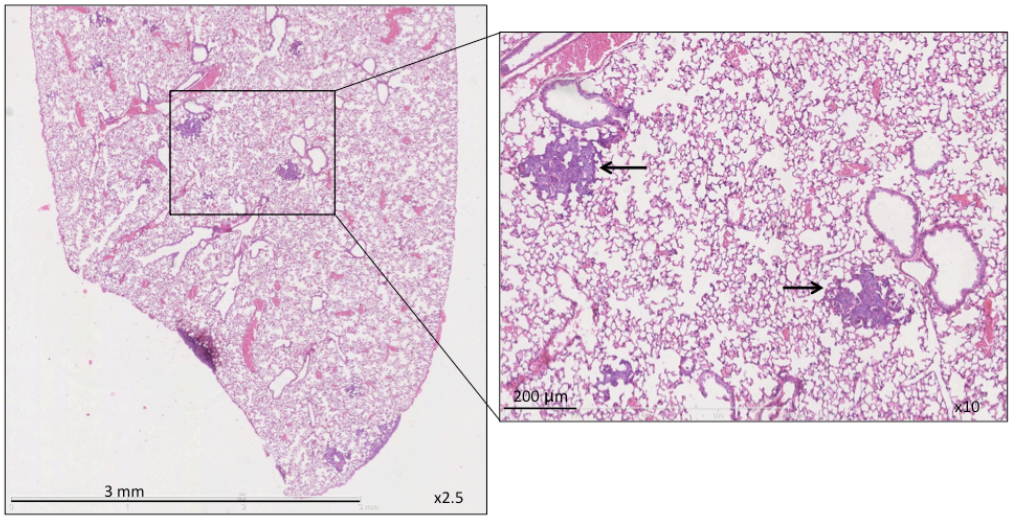

Figure 6.2: Representative H&E staining of a 3 µm lung section showing multiple small lung metastases at day 30 (arrowed).

6.1.2. An intravenous delivery lung metastases model

To set up a direct lung metastases model, I injected 10^6 MDA-MB-231 LMP2 into the caudal vein. This resulted in the formation of multiple lung metastases in all mice by day 20 (Figure 6.3).

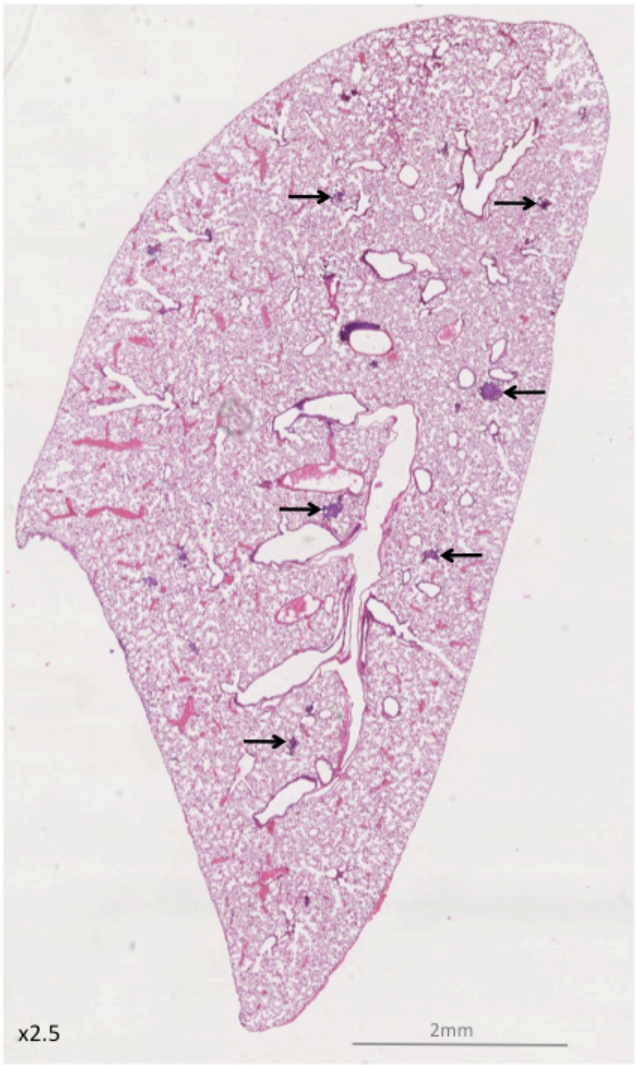

Figure 6.3: Representative H&E staining of a 3 µm section of lung showing multiple small lung metastases (see arrows for examples) after tail vein injection of MDA-MB-231 LMP2 tumour cells.

6.1.3. DiR imaging biodistribution pilot study

DiR is a lipophilic, near-infrared fluorescent dye that can be used to label cell membranes. Imaging in the near-infrared spectrum significantly reduces background fluorescence caused by tissue, and the resulting photons can be transmitted through a greater thickness of tissue. [215] DiR fluorescence imaging can be used to non-invasively track the fate of labeled stem cells *in vivo*. [216] However, I decided to use DiR imaging to track the fate of injected MDA-MB-231 cancer cells, in order to simultaneously monitor the tracking ability of luciferase expressing EBV-TCR T cells.

Before using DiR to label and image MDA-MB-231 LMP2 tumour cells, I conducted a pilot study looking at the biodistribution of free DiR after tail vein injection. Briefly, 1 µL of DiR was suspended in 200 µL PBS and this was injected into the tail vein of 3 NOD/SCID mice. These mice underwent serial fluorescence imaging on a Xenogen IVIS® Lumina II system with constant camera settings (f/stop 2, exposure time 10 s, excitation 745 nm, emission ICG).

This data can be compared to the DiR signal from injected labeled tumour cells, in order to distinguish free DiR from tumour cell membrane bound DiR. This would help determine if the cells are intact after injection. After free DiR injection, the signal is diffuse throughout the mouse for up to 5 days, with areas of high signal located in the lungs and liver (Figure 6.4). After 25 days the signal localizes to the liver. It is interesting that there is still strong DiR fluorescent signal even after 25 days in the mouse. This suggests that DiR is either metabolized or excreted by the liver very slowly.

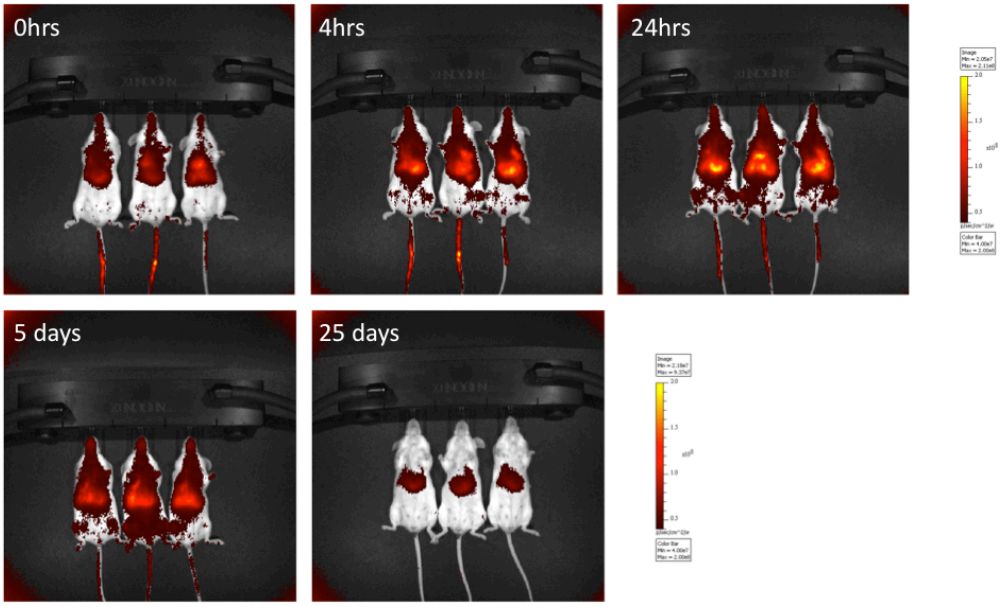

Figure 6.4: Pilot study of free DiR biodistribution. NOD/SCID mice (n=3) received a tail vein injection of 1 µL DiR in 200 µL PBS. These were then imaged repeatedly on a Xenogen IVIS® system at the same settings.

6.2. In vivo effects on lung metastases of a combined cell therapy with EBV-TCR T cells and MSC TRAIL

NOD/SCID mice were first irradiated with 2.5 Gy to eliminate any residual immune cells. After 24 hours, all mice had 10^6 DiR labeled MDA-MB-231 LMP2 cells injected into the caudal vein. After DiR fluorescence imaging of all mice to establish successful delivery of tumour cells, mice were randomized into 4 groups (Figure 6.5). One week following tumour cell delivery, mice received either no cells, 5 x 10^6 EBV-TCR luciferase T cells, 10^6 MSC TRAIL, or 5 x 10^6 EBV-TCR T cells combined with 10^6 MSC TRAIL. Mice were imaged throughout the experiment to monitor luciferase signal (EBV-TCR T cells) and DiR signal (MDA-MB-231 LMP2 cells). At day 14 and 21, mice in the groups treated with MSC TRAIL received further doses of 10^6 MSC TRAIL.

At day 23 the mice were sacrificed and final Bioluminescence imaging (BLI) and Fluorescence imaging (FLI) was performed with the chest cavity open and the heart removed. Following imaging, the lungs were insufflated with 4% paraformaldehyde (PFA), before removal and storage in PFA for histology. All livers were also removed and fixed in PFA, due to the large amount of DiR signal present. The spleens were removed in each mouse, and put into RPMI media before being mashed, stained for T cell markers and run on the flow cytometer.

Fluorescence imaging after DiR labelled tumour cell injection showed a large amount of signal in the liver and lungs, and often also at the injection site in the tail (Figure 6.6). There was no diffuse background signal as seen with injection of free DiR (Figure 6.4), indicating that these cells were successfully delivered intact to the lungs. This is where most of the cells are likely to be trapped, due to the pulmonary first pass effect. [217] The presence of signal in the liver is puzzling and is similar to that observed with injection of free DiR. This could be due to free DiR that was not successfully washed from the cell pellet during the preparation of cells, or fragments of dead cells within liver macrophages.

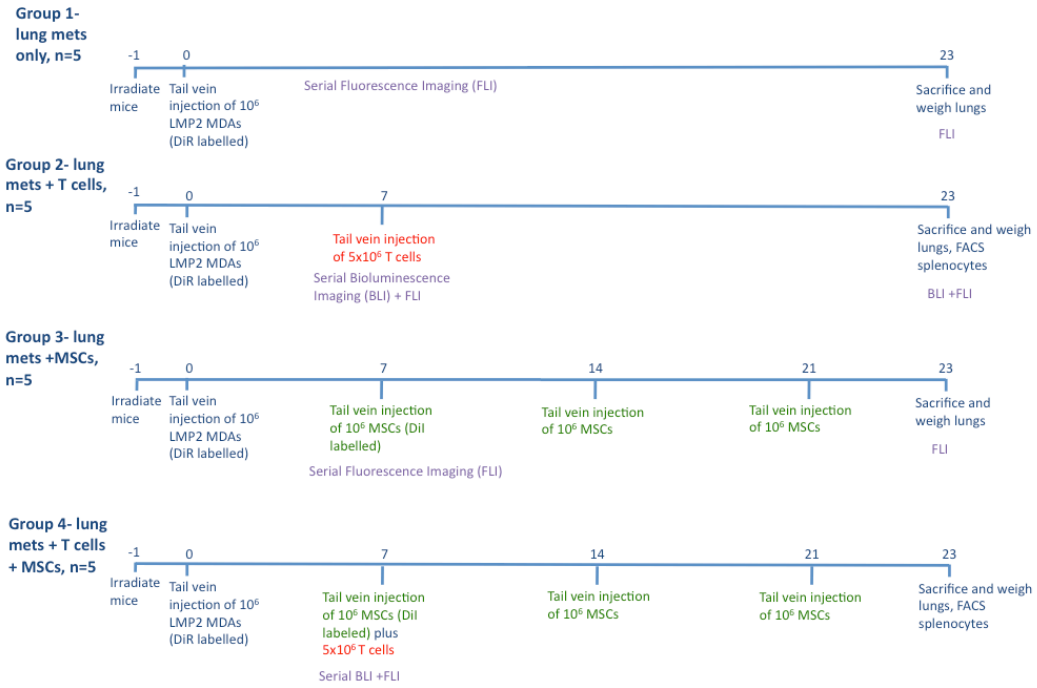

Figure 6.5: Experimental outline for the first *in vivo* experiment

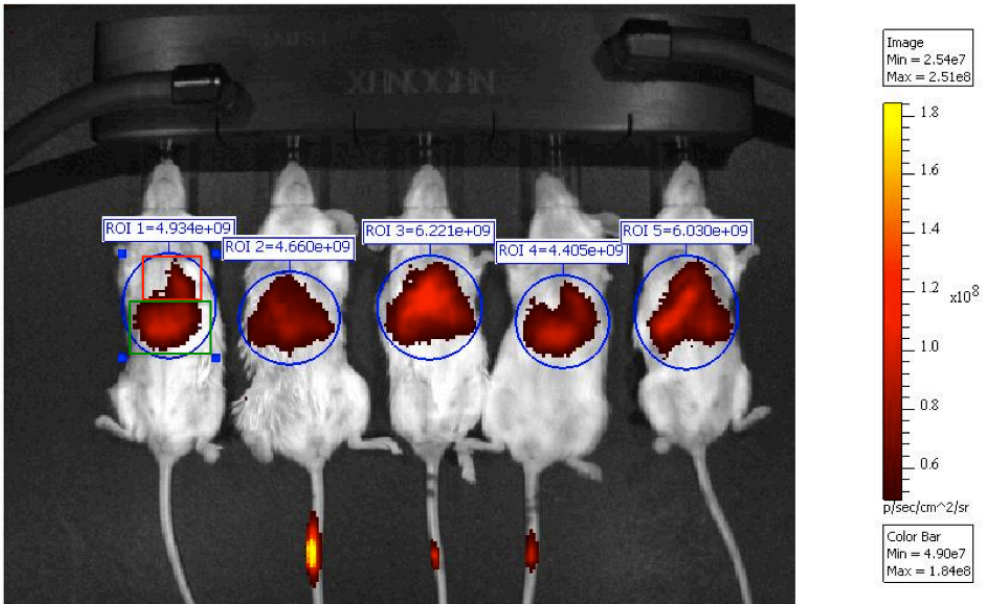

Figure 6.6: FLI imaging of group 3 mice after tumour cell injection (day 0). DiR signal can be seen in the liver and the lungs, as well as residual signal in the tail after injection. DiR imaging looked similar between groups and the signal characteristics did not change over the time-course of the experiment, remaining mainly in the liver (green box) and the lungs (red box). DiR signal in the liver is free DiR or dead cell fragments, whereas the signal in the lungs is a result of the delivered MDA-MB-231 cells.

Serial DiR fluorescence imaging did not reveal any significant changes in signal after treatment, or any difference in signal between treatment groups (Figure 6.7). Fluorescence signal was measured using regions of interest (ROI) drawn around the livers and lung in each mouse.

In contrast, bioluminescence imaging after the delivery of EBV-TCR luciferase T cells showed maximum signal in the lungs immediately after injection, and a subsequent decrease in signal. Analyzing the data using ROIs drawn over the lungs (Figure 6.8) shows that photon radiance (photons per square metre per second per steradian) is maximal at injection, followed by decreasing signal over time, indicating a lack of *in vivo* proliferation of the T cells. This trend was seen in the T cell only group, and the T cell plus MSC TRAIL group (Figure 6.9). Although two mice from the T cell only group died unexpectedly at day 11 before the end of the experiment, this is unlikely to have effected the average bioluminescence signal for the group as the standard errors for each data point are very small. Background autoluminescence is not very well understood, but research has suggested that it is in part due to the white fur of the mice. [128] Autoluminescence is known to be higher in the regions of the thoracic cage and liver, which may explain why the lung signal does not entirely reach background autoluminescent levels.

Bioluminescent signal was seen at sacrifice in the lungs of only one mouse in the T cell only group. (Figure 6.10) Human T cells are not thought to survive much longer than 3 weeks in a NOD/SCID mouse, so this data is in keeping with the work of others. [55]

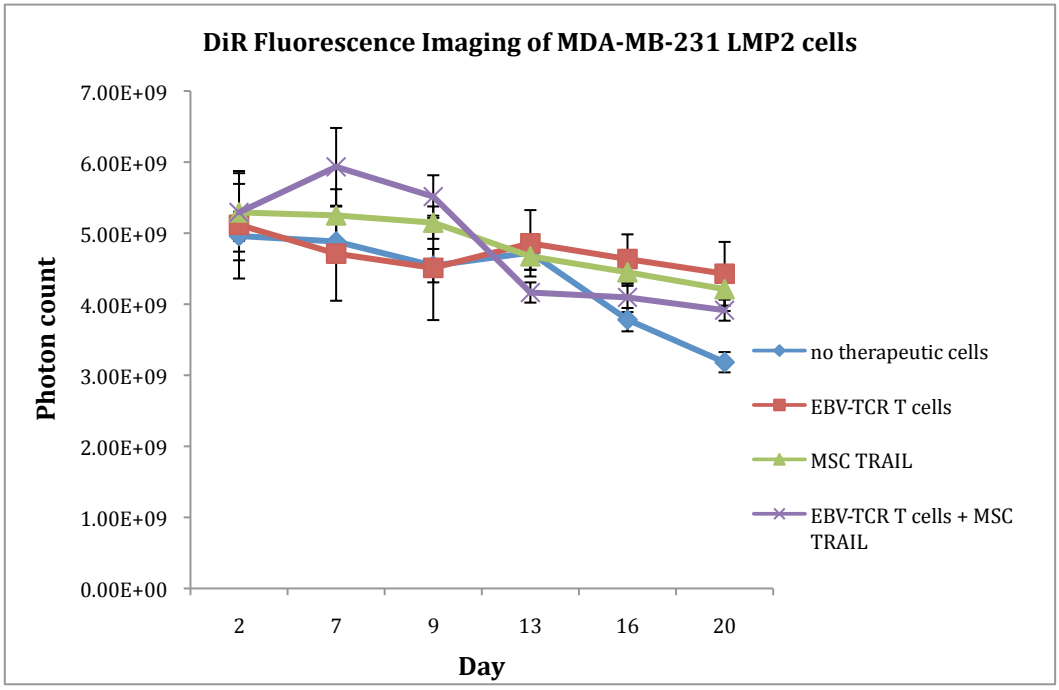

Figure 6.7: Average DiR fluorescence photon count in the liver and lungs over time, per group. There is no significant difference in the signal between different treatment groups.

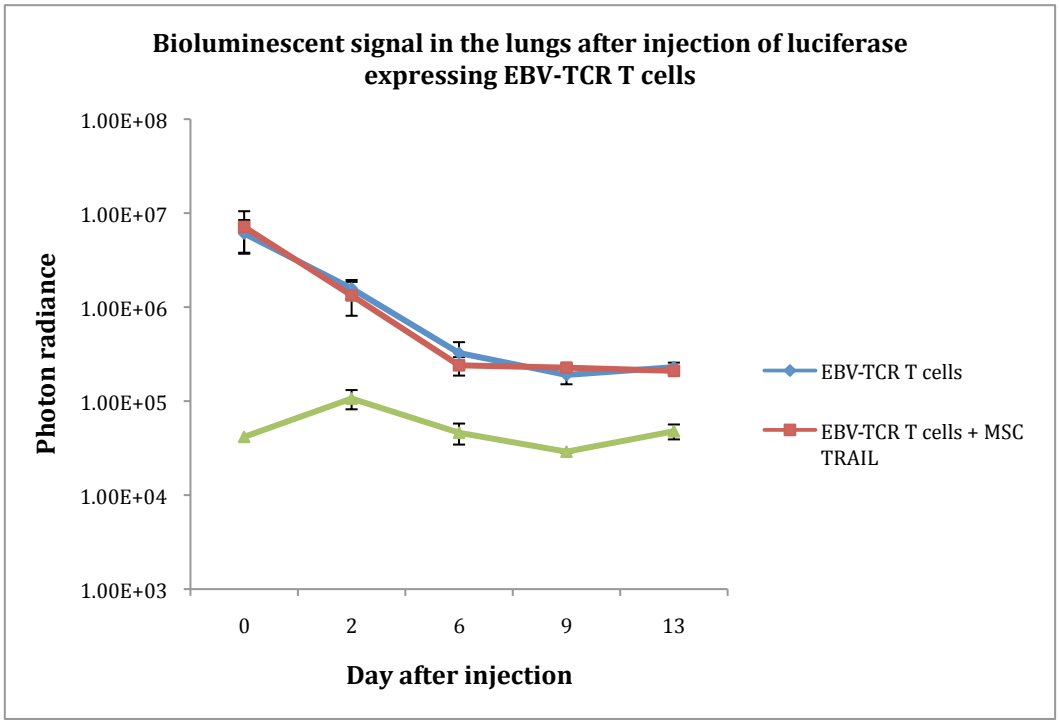

Figure 6.8: Average bioluminescence photon count in the lungs of groups 2 and 4 over time. There is a slow decrease in signal until 6 days post-injection after which the signal is close to background autoluminescence signal levels.

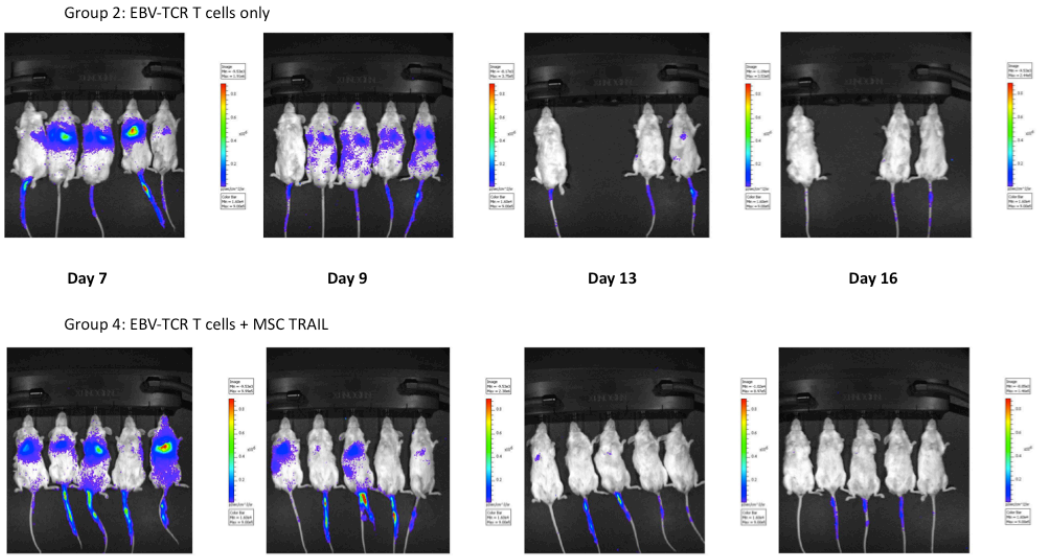

Figure 6.9: Bioluminescence images of groups 2 and 4 over time (left to right- day 7 immediately after injection of T cells, day 9, day 13, day 16). Signal in the lungs is lost after day 16, indicating death of the T cells.

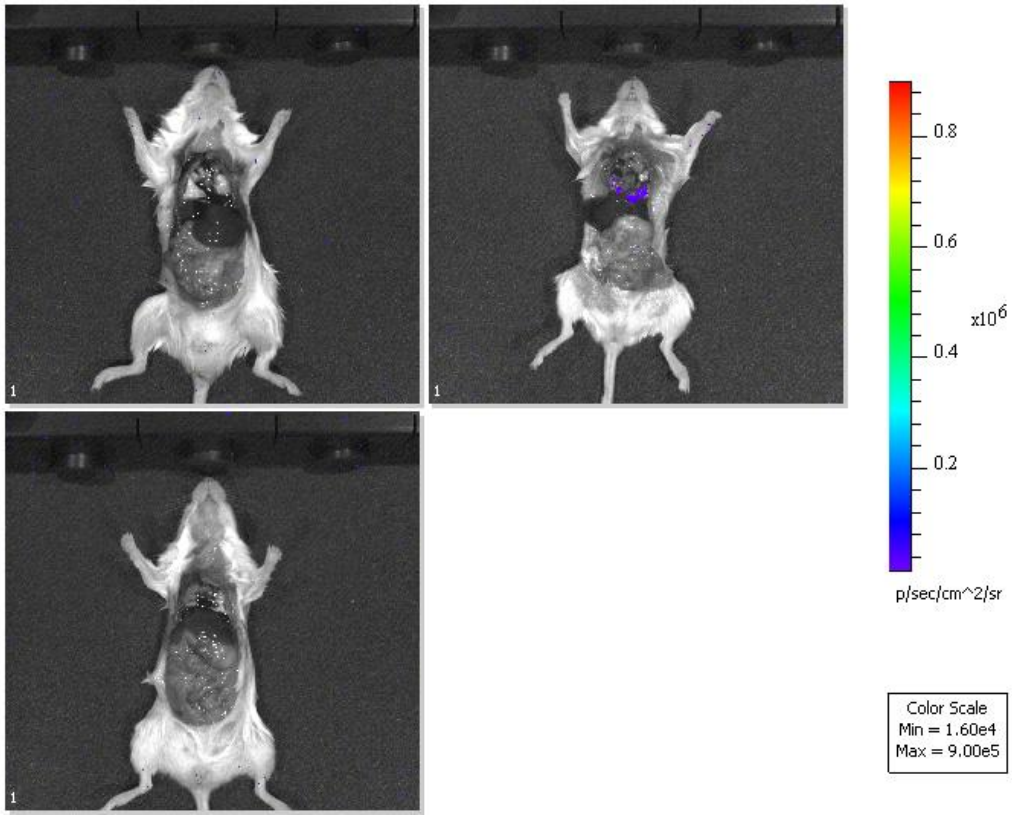

Figure 6.10: Bioluminescence images of group 2 (EBV-TCR T cells only) at sacrifice (day 23). Bioluminescent signal can only be seen in the lung fields of one mouse.

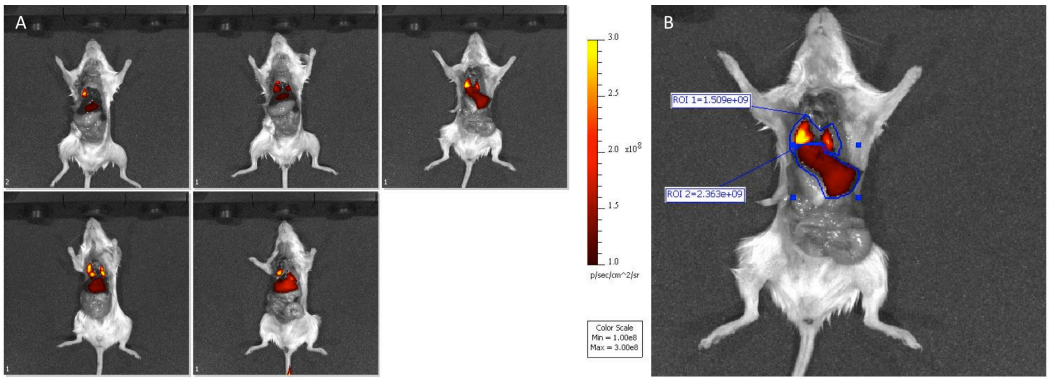

Figure 6.11: A- Example of DiR fluorescence imaging of the mice after sacrifice and removal of the chest wall and heart. B- This allowed accurate regions of interest (ROI) to be drawn around the lungs and liver for comparison of average DiR photon count between groups.

Fluorescence imaging of the liver and lungs was also completed at sacrifice, after the removal of the chest wall and heart for better visualization of the lungs (Figure 6.11). After DiR imaging at sacrifice, accurate ROIs were drawn around the lungs and liver, allowing comparison of DiR fluorescence signal between groups (Figure 6.11-B). This analysis revealed no significant difference in average DiR photon count in the liver or lungs between the groups (Figure 6.12). However, this may be due to the long half-life of DiR within biological tissue, rather than a failure of treatment.

Lung and liver weights were taken at sacrifice and showed no significant difference between the control group and any treatment group (Figure 6.13).

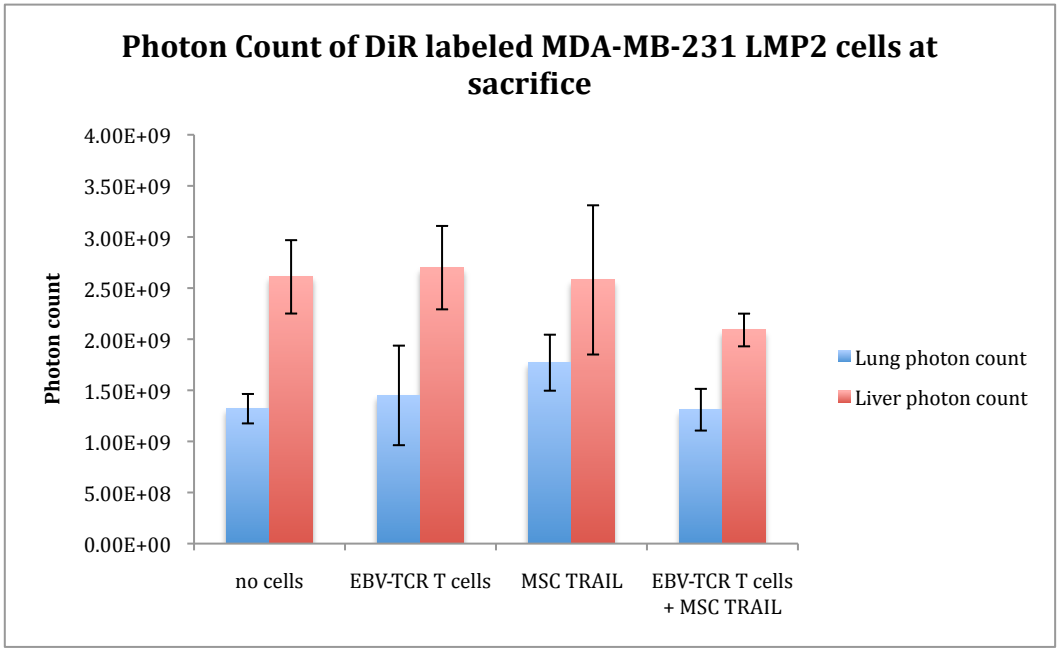

Figure 6.12: Average DiR photon count in the livers and lungs of each group after sacrifice and ROI analysis. There is no significant difference in photon counts between groups.

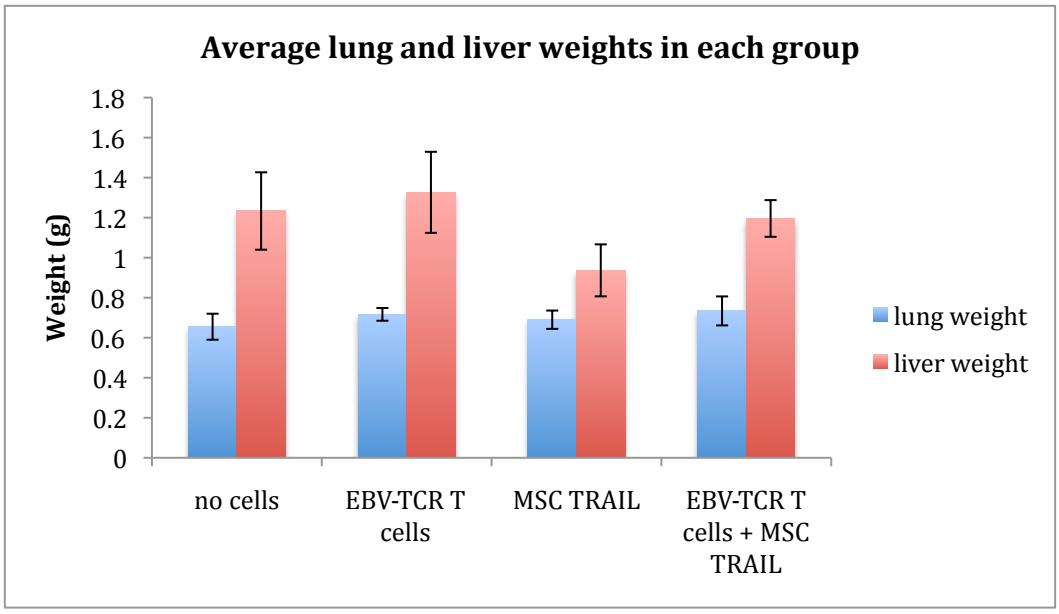

Figure 6.13: Average lung and liver weights in each group at sacrifice. There is no significant difference in lung or liver weight between the control group and any treatment group.

At sacrifice the spleens of all the mice were taken out, put into RPMI media, mashed and then stained with the appropriate antibodies for human T cells. The samples were run on a BD™ LSR II flow cytometer, using FACSDiva™ software, followed by analysis using FlowJo software. T cells and MSCs could be gated out separately on forward scatter and side scatter plots using their relative difference in sizes. Cells in the T cell size range were examined for human CD4 and CD8 (Figure 6.14), as well as for the murine cβ chain (data not shown). In all cases, there was no positive staining for these markers, demonstrating that there were no human EBV-TCR T cells in the spleen of any of the treatment groups. This result corresponds to the findings on bioluminescence imaging, where no signal was seen in the spleens, and signal was seen only in the lungs of one mouse in the T cell only treatment group.

Cells in the MSC size range were examined for DiI fluorescence. This was negative in all cases (Figure 6.15), indicating that there were no MSC TRAIL in the spleens of any treated mouse. This result was expected, as work done by others suggests that MSC injected intravenously typically become trapped in the capillary bed of the lungs. [218, 219] Indeed, it was this effect that I hoped to exploit to treat lung metastases in this tumour model.

Unfortunately, in this experiment 2 mice died in groups A, B and C, while all 5 mice in group D survived to the end of the experiment. This could be a result of the irradiation performed at the beginning of the experiment, uncontrolled tumour growth, or cell therapy delivery. However, two mice in the control group (group A) died, so it is unlikely that the cell therapies were a cause of death. Histology performed on the mice in these groups will confirm if uncontrolled tumour growth is a cause of death in groups A-C.

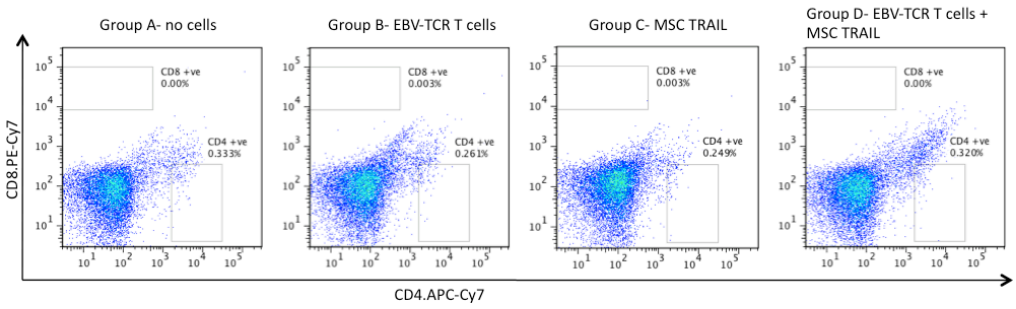

Figure 6.14: Representative flow cytometry plots of cells from the spleens of mice in each experimental group. Antibody staining to human CD4 and CD8 was negative in each case, indicating that there were no human EBV-TCR T cells in the spleens at the time of sacrifice.

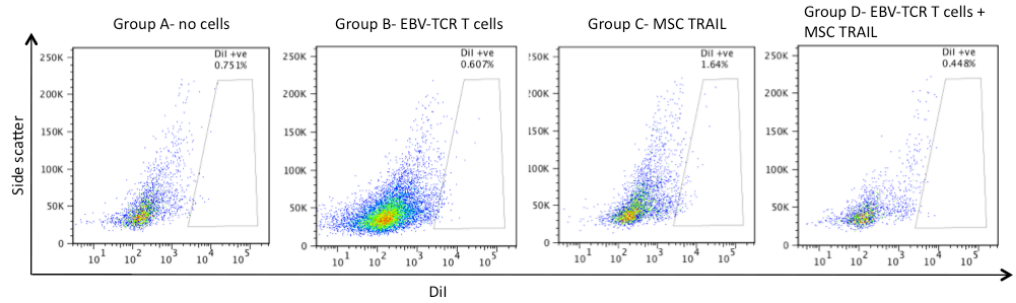

Figure 6.15: Representative flow cytometry plots of cells from the spleens of mice in each experimental group. All the cells were negative for DiI fluorescence in each mouse that received MSC TRAIL, indicating that there was also no MSC TRAIL in the spleen at the time of sacrifice.

The last analysis performed on this experiment used histology to look for differences between different treatment groups. After sacrifice the lungs and livers were processed and H&E staining was performed on 3 μm sections of tissue. Lung metastases were easily visualized by their increased haematoxylin staining compared to normal lung parenchyma (Figure 6.16).

In contrast, despite the DiR signal seen in the livers of the mice, there were no liver metastases in any sections of any mice (Figure 6.17). Hence the DiR signal seen may correspond to DiR that is trapped in liver macrophages after the breakdown of dead tumour cells.

In order to assess the effects of cell treatment, an analysis of the average diameter of lung metastases per group was performed. Using Leica SlidePath 2.0 software, the longest diameter of each lung metastasis was measured for each lung lobe in every mouse (Figure 6.18). The results were collated by group and a student's t test was performed to look for significant differences between groups. A significant difference ($p<0.01$) was seen between the control group and the EBV-TCR T cells treatment group, and the combined EBV-TCR T cell and MSC TRAIL group (Figure 6.19). This is an important positive result that indicates EBV-TCR T cells are highly active against LMP2-expressing MDA-MB-231 tumours *in vivo*, and that corroborates the *in vitro* findings from chromium-51 and co-culture experiments.

This data reveals that tumour burden is unlikely to be the cause of premature death before day 23 in groups A-C. Therefore, it is possible that the irradiation of the mice with 2.5 Gy before the experiment started was the cause of death, even though this was delayed until day 11.

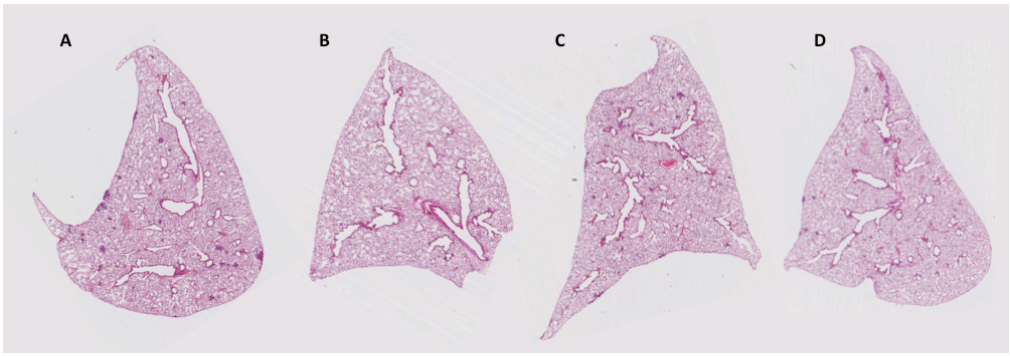

Figure 6.16: Representative H&E lung lobe sections from each treatment group, A- control group, B- EBV-TCR T cells only, C- MSC TRAIL only, D- EBV-TCR T cells and MSC TRAIL.

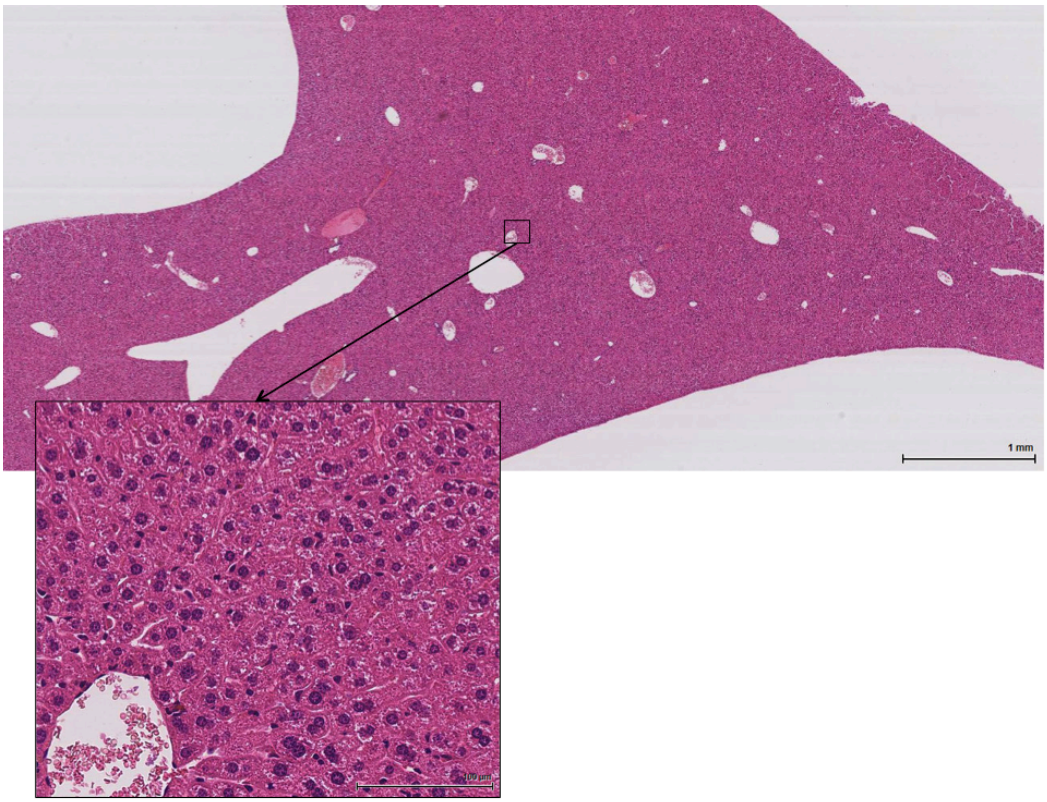

Figure 6.17: Representative H&E section of liver, showing no metastases and a homogenous liver parenchyma.

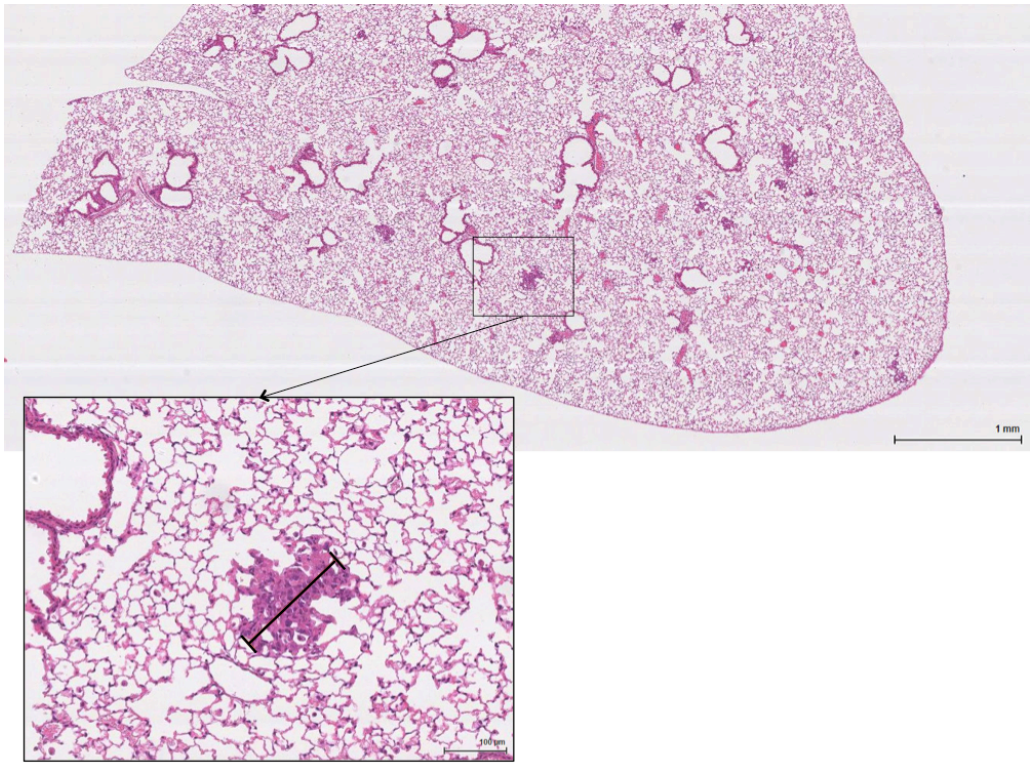

Figure 6.18: Representative H&E section of a lung lobe showing how the diameter of a lung metastasis was measured using the Leica SlidePath programme.

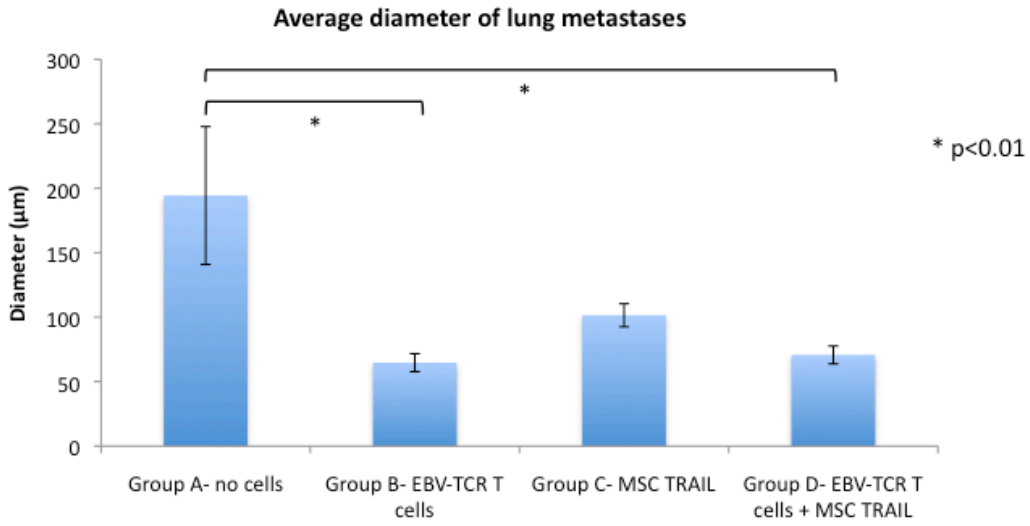

Figure 6.19: Bar chart showing the average diameter of lung metastases in each treatment group.

To further assess the difference in size of lung metastases between treatment groups I used a MATLAB® tool developed by UCL's Centre for Medical Image Computing, which automatically segmented the lung metastases and counted the area of pixels within each metastasis and the total area of the lung lobe. The percentage area of lung taken up by metastases could then be calculated for each lobe of the lung in every mouse (Figure 6.20). This analysis revealed significant differences in the area of lung metastases between the control group and the treated groups (Student's t test, $p<0.05$). This automated analysis provides more robust evidence of a significant reduction in tumour burden from cell therapy treatment with MSC TRAIL and/or EBV-TCR T cells.

It is important to note that this analysis is more robust that the method used by Loebinger et al. in their paper demonstrating a significant reduction of lung metastases with MSC TRAIL treatment, which relied on lung weights and an operator dependent use of Spot Advanced Imaging Software (Diagnostic Instruments Inc., Sterling Heights, MI) to measure the difference lung tumour burden. This may explain their confusing observation of a significant decrease in the number of lung metastases per unit area with inactivated TRAIL MSC treatment, which appears to contradict their *in vitro* co-culture experiments where inactivated MSC TRAIL seems to produce close to background levels of cell death and apoptosis.

Despite these experimental differences, the work in this thesis contributes to the growing body of evidence that MSC TRAIL treatment is effective against a variety of tumour lines including cervix adenocarcinoma and breast adenocarcinoma, [104], rhabdomysosarcoma, [220] and multiple mesothelioma cell lines. [221]

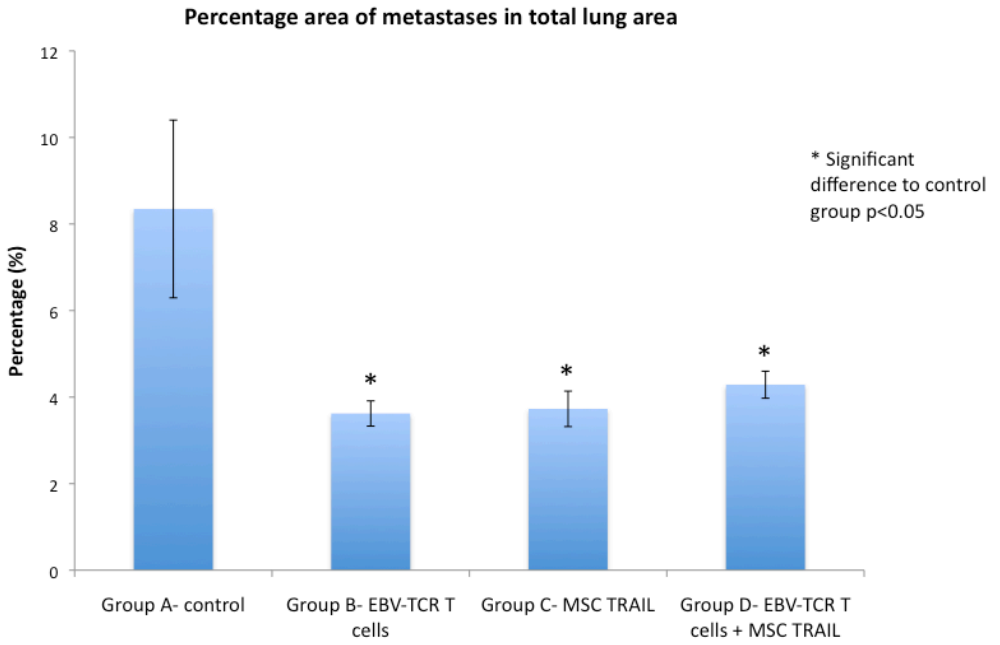

Figure 6.20: Bar chart showing the average percentage area of lung metastases in each group. There is a significant difference from the control group in each treatment group ($p<0.05$).

Finally, to prove that MSC TRAIL home to and incorporate within lung metastases, the immunostained sections were imaged using a standard upright Zeiss fluorescent microscope and a Leica TCS SPE confocal microscope. MSC TRAIL could be identified by their DiI fluorescence (excitation 555 nm), while EBV-TCR T cells were stained with a primary anti-Luciferase antibody and an Alexa Fluor® 647 secondary antibody (excitation 647 nm). Cell nuclei were counterstained with DAPI (excitation 350 nm) to show the underlying structure of the lung and the location of the cells. As expected from the previous bioluminescence imaging data, anti-luciferase staining was negative for EBV-TCR T cells present in the lung metastases. However, MSC TRAIL could be seen in multiple lung metastases in the MSC TRAIL treatment groups (Figure 6.21, Figure 6.22).

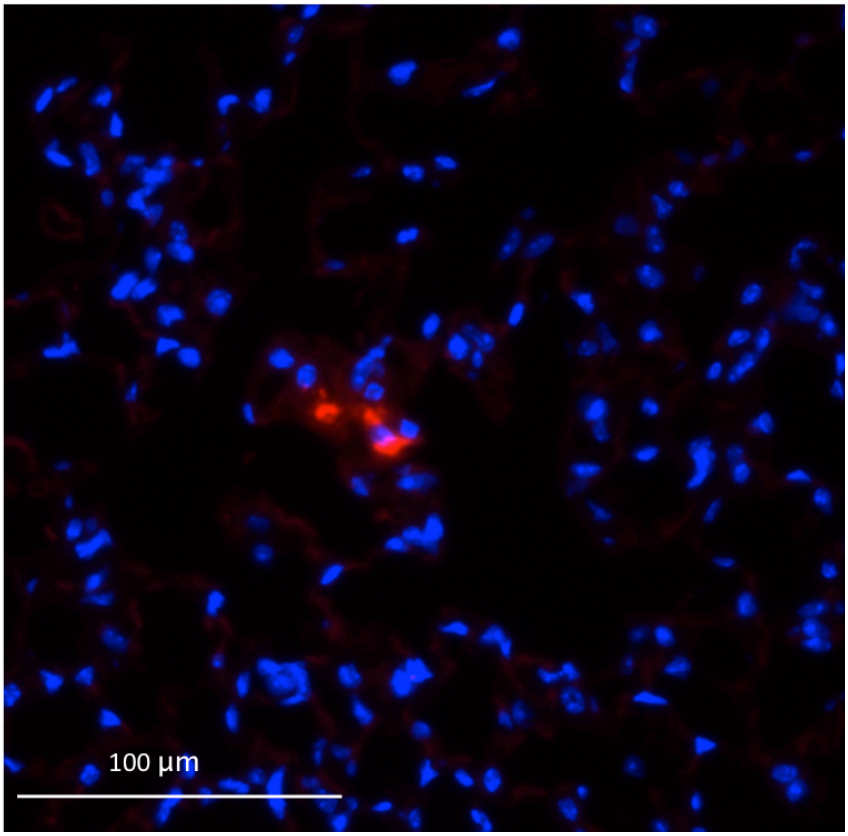

Figure 6.21: Immunofluorescence image of DiI labelled MSC TRAIL within a small lung metastasis.

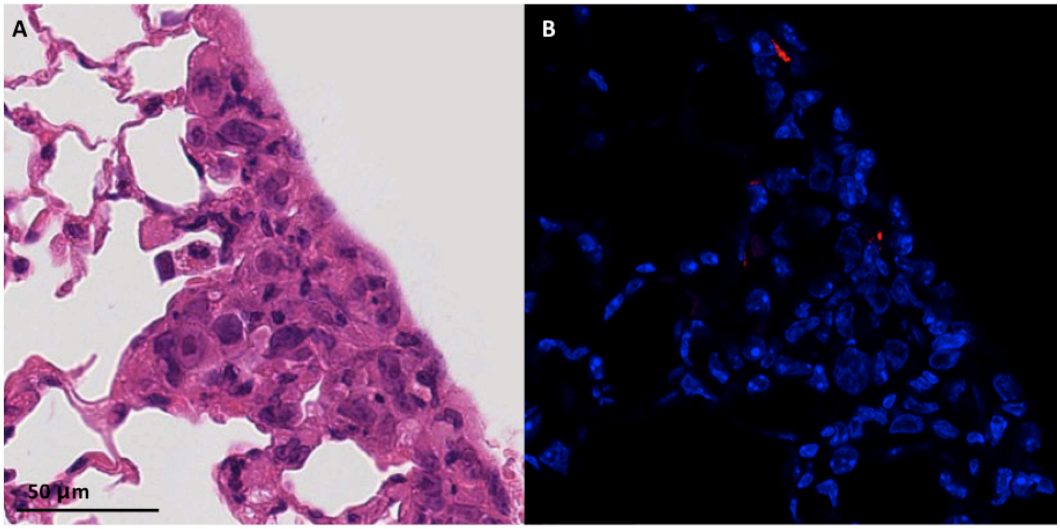

Figure 6.22: A- H&E stained section of a lung metastasis (x20), B- confocal image of the same metastasis (x20) showing DiI labelled MSC TRAIL within the metastasis.

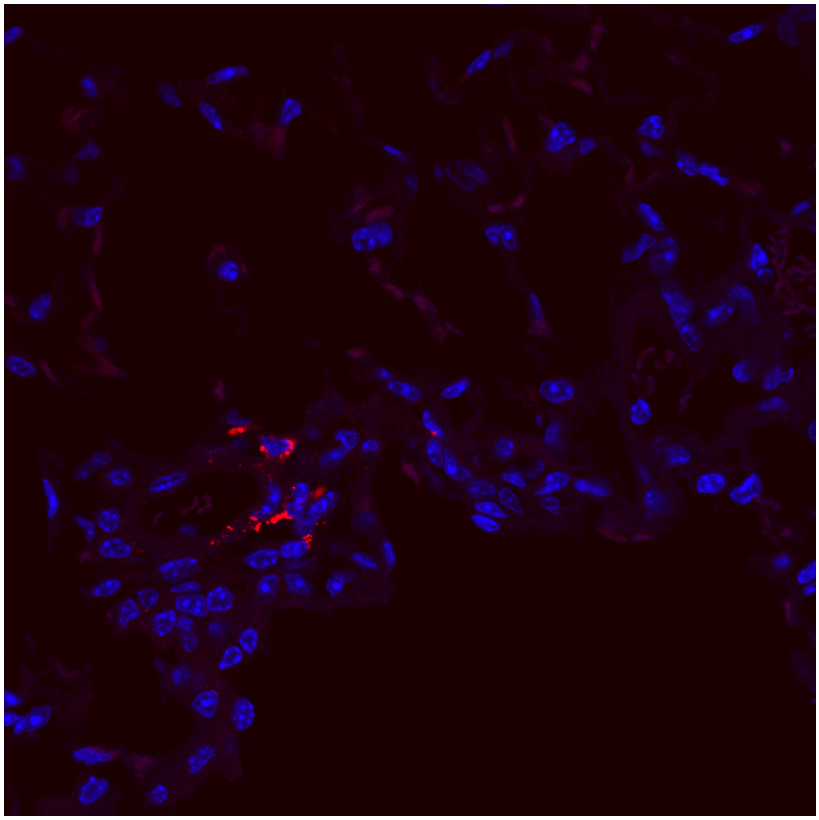

Figure 6.23: Confocal image (x20) of DiI labelled MSC TRAIL exiting a blood vessel and homing towards lung metastases.

DiI labelled MSC TRAIL were also seen extravasating from blood vessels within the lungs, and homing towards lung metastases (Figure 6.23). This provides further strong evidence that intravenously delivered MSC TRAIL are capable of trafficking towards lung metastases in this *in vivo* model.

6.3. Summary

In this chapter I have demonstrated that:

- Intravenously injected MDA-MB-231 LMP2 cells will form multiple small lung metastases within 20 days.
- Fluorescence imaging of DiR labelled tumour cells is not an accurate method to track tumour distribution or size.
- Injected EBV-TCR luciferase T cells are trapped in the lungs immediately after intravenous injection and still persist in the lungs 2 days post-injection where they provide anti-tumour effects.
- After day 6, bioluminescence signal returns close to baseline, indicating the T cells do not persist *in vivo*. This is confirmed by the absence of luciferase positive cells in immunostained lung sections.
- MSC TRAIL can be seen engrafted within lung metastases in immunostained lung sections.
- There is a significant difference in the diameter of lung metastases between the control group and both groups treated with EBV-TCR T cells.
- There is a significant difference in the percentage area of lung taken up by metastases between the control group and each treatment group.
- Similar to the *in vitro* data, there is no benefit to combining EBV-TCR T cells with MSC TRAIL as a dual cell therapy, thus disproving my hypothesis.

6.4. Discussion

Lung cancer is the second most common cancer in the UK, and the majority of these patients present at later stages of the disease. Unfortunately these patients have very poor survival rates, which have not shown much improvement since the 1970s. This is undoubtedly due to late presentation of the disease, as well as a paucity of targeted chemotherapy agents. Cell therapies that can home to lung tumours have the potential to improve survival compared with conventional anti-cancer treatments.

Adoptive transfer of tumour antigen specific T cells is a promising cancer therapy that redirects the specificity of TCRs on cytotoxic T cells so they target malignant cells. This approach has never been tested in models of lung cancer. Separately, MSC TRAIL have been shown to eliminate metastatic lung cancer in human xenograft models in NOD/SCID mice.

In this chapter I have demonstrated that both EBV-TCR T cells and MSC TRAIL are highly effective in a murine model of lung metastases. Significant differences were found between the size of lung metastases in the control group and mice that received either cell therapy, and the area of lung taken up by tumour between the control group and the groups that received a cell therapy. Tumour sections from the group that received MSC TRAIL show DiI labeled MSC TRAIL homing to and incorporating within lung metastases. For the group that received T cells, luciferase expressing EBV-TCR T cells could be seen in the lung fields using bioluminescence imaging for 6 days after injection, after which the signal returned close to background levels. Consequently, no anti-luciferase antibody staining was noted in lung sections, indicating that no luciferase expressing cells were present.

This is the first time EBV-TCR T cells have been used in an *in vivo* cancer model. It is also, to my knowledge, the first time T cells with high affinity TCRs for tumour associated antigen have been used to target lung cancer. Further experiments could examine the protocol for adoptive transfer of T cells to maximize tumour destruction *in vivo*. Several doses of T cells may improve the response to treatment, and this is the protocol used in several clinical trials. [195-197]

However, when EBV-TCR T cells and MSC TRAIL are combined as a dual cell therapy there is no benefit compared with a single cell therapy. Although this was also noted in *in vitro* experiments, this result was unexpected for the *in vivo* model, where cytokines produced by T cells could aid the homing and engraftment of MSCs.

Bartholomew et al. first described the immunomodulatory properties of MSCs in 2002, [222] when they discovered that MSCs cultured with unstimulated lymphocytes resulted in a 50% reduction in lymphocyte proliferation, and subsequently that administration of MSCs resulted in prolonged skin graft survival in baboons.

MSCs are now known to modulate the functions of cells of both the innate and adaptive immune system *in vitro*. However, the exact nature and mechanisms of this modulation still remain unclear with some *in vitro* studies claiming that MSC-T cell interaction is required, [108] and others pointing to soluble factors such as TGF-β and hepatocyte growth factor, [107] metabolites of tryptophan, [110] or IL-2 and IL-10, [223] all of which are now thought to suppress T cells.

Another avenue of research is the action of MSCs on regulatory T cells (Treg) as a mechanism of immunosuppression, particularly since MSCs have been shown to recruit, modulate and maintain Treg function *in vitro*. Naturally occurring Treg cells are characterized by their expression of CD4, CD25 and Foxp3, and inducible Treg cells can be generated from CD4+ T cells in co-cultures of MSCs and PBMCs with allogeneic stimulus. [224]

Interestingly, Prevosto et al. have hypothesized that two different mechanisms could be responsible for MSC-induced immunomodulation, dependant on the cell ratio. They propose that at high ratios, soluble factors secreted by MSCs are predominantly responsible, whereas at low cell ratios this is dependent on the generation of Treg cells by interaction with MSCs. [225] This hypothesis leads from their observation that in co-culture experiments, very low ratios of FACS sorted Treg cells (1:2,000) are able to suppress lymphocyte proliferation. Furthermore, the generation and action of these cells was not inhibited by the addition of soluble factor blocking antibodies to IL-10, TGF-β or prostaglandin

E2 into the culture media, suggesting an independent mechanism of action from soluble factors secreted by MSCs.

In co-culture experiments with MSCs and different T cell populations, Di Ianni et al. show that inducible Tregs are mainly recruited and upregulated from peripheral naïve Treg cells. [226] This group has also recently confirmed that Notch1 signaling is essential for MSC-induction of Tregs, by showing that MSCs predominantly express the Notch1 ligand Jagged1, and after co-culture with CD4+ T cells there was significant over-expression of Notch1 intracellular domain and its transmembrane/cytoplasmic portion in inducible Treg cells. [227] This effect was specific to Treg cells and not observed in other subtypes of T cells.

In addition to their other immunomodulatory effects, MSCs are now also known to suppress T helper 17 (Th17) cells, which are characterized by their secretion of IL-17A, and are highly immunogenic, linked to autoimmune and inflammatory diseases. This suppression appears to be mediated by prostaglandin E2 [228] and results in the inhibition of cytokine secretion by fully differentiated Th17 cells, and inhibition of differentiation of naïve T cells into Th17 cells. [229]

However, there is also evidence to suggest MSC-mediated immunomodulation is ineffective for activated cytotoxic T cells. Karlsson et al. have shown that MSCs are unable to affect the proliferation or function of activated established cytotoxic EBV T cells *in vitro*, [230] although they did suppress proliferation of naïve and memory T cells. Rasmusson et al. also showed MSC were unable to affect the cytotoxic function of activated CD8+ T cells. [231] This topic remains controversial, but it is possible that using activated T cells in my cell therapy model avoids MSC immunomodulation, particularly since EBV-TCR T cells were used after 3 rounds of restimulation, when cytotoxic CD8+ T cells were predominant.

It is important to note that the immunosuppressive role of MSCs is still unproven in large, randomized, controlled clinical trails. Despite some early success in a phase II clinical trial involving 55 patients with steroid-resistant, acute GVHD, where 30 patients had a complete response, and 9 showed improvement, [105] in

two large, multi-centre, phase III clinical trials there was no significant difference between MSC therapy and placebo. [106] Furthermore, donor MSCs have not been identified in the bone marrow aspirates of any patients weeks after MSC transfusion, although they have been identified in other areas of inflammation days after transfusion, suggesting successful cell delivery and homing, but no long-term MSC engraftment. Therefore, current evidence suggests that MSCs do not cause significant immunosuppressive effects *in vivo*.

In a recent attempt to overcome these problems, Kimbrel et al. have isolated a precursor MSC cell-type from human embryonic stem cells. [232]These cells were immunosuppressive in two mouse models of immune disease, lupus and autoimmune uveitis, as well as suppressing T cell proliferation *in vitro* and stimulating regulatory T cells. It is possible that these precursor cells may eventually prove more potent than mesenchymal stem cells, and their further work will assess the mechanism of immunosuppression and the use of these cells in other autoimmune disease models.

In the context of this work, MSC TRAIL could possibly cause immunosuppression due to the secretion of soluble factors such as TGF-β or IL-2. Cell ratios of MSC:T cell of between 1:1 to 1:10 have been found to produce this effect *in vitro* [225] and this ratio is probably achieved *in vivo* with the initial injection of $6x10^6$ EBV TCR T cells and $1x10^6$ MSC TRAIL. This may explain the lack of a significant benefit to combined cell therapy, since although the MSC TRAIL would suppress T cell function they would still be capable of triggering TRAIL-mediated tumour cell apoptosis, leading to no overall benefit to a dual-cell therapy, but a similar benefit to MSC TRAIL alone.

It is also possible that the lack of benefit to a combined therapy could be due to the generation of inducible Treg cells by cell contact-dependent action of MSC TRAIL on the EBV-TCR T cells. There is strong evidence to suggest that this effect occurs *in vitro*, and in this cancer model with tail vein delivery of the mixed EBV-TCR T cell and MSC TRAIL it is likely that the cells have come into close contact during the experiment, either in the eppendorf prior to cell injection, or *in vivo* in the lung parenchyma where they are delivered due to the first pass effect. This effect could also explain the lack of benefit of a dual cell

therapy as again the MSC TRAIL can continue to cause TRAIL-mediated tumour apoptosis, whilst the EBV-TCR T cells would have been rendered anergic.

Lastly it is important to note that the experiment was carried out with only a small number of mice per group (n=5). Perhaps with a larger cohort of animals, a significant difference could be demonstrated between the single cell and dual cell therapies.

7. Discussion

7.1. Overview

Lung cancer is the second most common cancer in the UK, and the majority of patients present at advanced stages of the disease. This late diagnosis has lead to very low 5-year survival rates of 7.8% for males and 9.3% for females. [1]

Chemotherapy, radiotherapy and surgery are currently the most effective and widely used treatments for lung cancer, and are usually combined for maximum anti-tumour effect. However, chemotherapy and radiotherapy both result in unpleasant side effects such as tiredness, nausea and vomiting, hair loss, immunosuppression and in some cases severe infections leading to death. This is a result of the poor selectivity of radiotherapy and chemotherapy, which often results in the death of rapidly dividing healthy cells as well as cancerous cells, and causes bone marrow suppression.

The use of a cell therapy to specifically target cancer cells would revolutionize cancer treatment, as well as dramatically reducing the side effects associated with cancer treatment. Both adoptive T cell immunotherapy, which harnesses the potential of T cells to specifically kill cancer cells, and MSC TRAIL, which uses a death ligand to target TRAIL receptors expressed by cancer cells, have resulted in promising anti-cancer effects *in vitro* and *in vivo*. Both cell types have been shown to home to tumour sites within the body, and specifically kill cancer cells. This thesis has combined these two separate fields of research into a dual pronged anti-cancer therapy, using both adoptive T cell immunotherapy and MSC TRAIL.

In addition to this dual cell therapy approach, my project has explored conventional and novel cell radiolabeling probes for imaging the cell therapies, eventually selecting bioluminescence imaging to track the engineered T cells homing to tumours. This part of the project aimed to answer questions about the location and persistence of transferred cells *in vivo*.

7.2. Engineering EBV-TCR T cells and their use *in vitro*

Adoptive transfer of tumour antigen specific cytotoxic T cells is a promising anti-cancer therapy that redirects the host's immune system against cancer cells. Modified TCRs with a high specificity for a tumour antigen of interest can be inserted into T cells using a retrovirus. These genetically engineered T cells can then be transfused into the patient.

The Epstein-Barr virus is ubiquitous, with established latency in 90% of adults, and is associated with certain malignancies, such as Hodgkin's lymphoma. The latent membrane protein 2 is expressed by some EBV infected cells and promotes a malignant phenotype, with many EBV-related cancers, for example nasopharyngeal carcinoma, expressing the LMP2 antigen. LMP2 is poorly immunogenic, eliciting only weak T cell responses, so a molecular biology approach has been used to generate TCRs with high specificity for adoptive immunotherapy.

In this thesis, I have used an engineered chimeric TCR that targets the EBV-associated LMP2 antigen in tumour cells. A retroviral vector was used to incorporate the EBV-TCR and luciferase into human donor PBMCs. T cells could be successfully and reproducibly transduced, as shown by the expression of a murine cβ chain and binding of the EBV-TCR to CLG peptide, as well as the production of light after administering D-luciferin, which could be imaged in an IVIS Lumina system. Transduced EBV-TCR T cells could produce cytokines and specifically lyse tumour cells expressing the LMP2 antigen after peptide activation.

Previously, LMP2 antigen specific T cells have failed to produce reliable clearance of tumour burden in clinical trials, [233, 234] possibly due to the immunosuppressive tumour environment, poor T cell survival *in vivo*, or the weak specificity of endogenous LMP2 targeting cytotoxic T cells. Therefore, a new approach was required, using an engineered TCR with a high affinity for LMP2. Using the chimeric EBV-TCR I have shown 60-100% death of peptide-coated target cells at T cell to target cell ratios of 0.75:1 and above. This is similar to the target cell cytotoxicity demonstrated in the original paper by Hart et al. describing the chimeric EBV-TCR, which shows target cell lysis of

between 30-90% at similar ratios. [64] A minor difference in my results is that the EBV-TCR T cells in my experiment are more functionally active at lower T cell to target cell ratios, for example at a ratio of 0.75:1 my results show 60% cell lysis, whereas at a ratio of 0.625:1 Hart et al. show target cell lysis of just 30%. This discrepancy can be accounted for by the observation that Hart et al. did not use peptide stimulation to increase the percentage of EBV-TCR positive cells prior to the chromium-51 cytotoxicity assay, they performed assays using 39% EBV-TCR positive T cells, whereas I used peptide stimulation to increase the population of EBV-TCR positive cells to 50% or greater before performing *in vitro* assays.

It may also be possible to increase the therapeutic effect of EBV-TCR T cells by combining them with another targeted anti-cancer therapy. This hypothesis was tested in this work by using a dual cell therapy of EBV-TCR T cells and MSC TRAIL in a murine lung metastasis model.

Mesenchymal stem cells are characterized by their ability to self-renew and to differentiate into osteoblasts, chondrocytes and adipocytes. [235] They can be easily acquired with a bone marrow biopsy and can be isolated from other cells by their ability to adhere onto tissue culture plastic. MSCs are immunoprivileged and exhibit a natural tropism towards tumours and metastases, which can be exploited to deliver anti-cancer therapies. MSCs expressing TRAIL can kill a variety of tumour cells, both *in vitro* and *in vivo*. [104]

Co-culture cytotoxicity assays using MSC TRAIL show apoptosis of 50% and death of 12% at a 1:1 MSC TRAIL to tumour cell ratio. This is superior to the death rate seen by Loebinger et al. in MDA-MB-231 cells, of 15.4% death after co-culture with MSC TRAIL. [104] However, in this study TRAIL expression by MSCs was inducible with doxycycline treatment, and 82% of MSCs were successfully transduced. The MSC TRAIL used in these experiments constitutively expressed TRAIL and were FACS sorted for 100% TRAIL expression. This may account for the differences in tumour cell death.

When MSC TRAIL were used in combination with EBV-TCR T cells, up to 95% of tumour cells were dead or apoptotic. However, tumour cell death was not increased by the dual EBV-TCR T cell and MSC TRAIL treatment, compared

with EBV-TCR T cells alone. This could be a failure of the *in vitro* assay to accurately stimulate the *in vivo* environment, or a direct result of competition between the two cell types to come into contact with tumour cells, although cell densities were kept deliberately low in an attempt to avoid physical competition. In combined co-culture experiments, at the maximum ratio (1:1) of effector cells to cancer cells, there was a total of 1.5×10^5 cells per well in a 6-well plate, well below the recommended seeding density of 3×10^5 cells per well.

Another possibility is that the MSC TRAIL cause immunosuppressive effects that reduce the function of EBV-TCR T cells. Prevosto et al. hypothesize that MSCs can cause immunosuppression by two mechanisms dependent on MSC, T cell ratios. They propose that at low MSC to T cell ratios, immunosuppression is mediated by the generation of inducible Treg cells, and at high ratios of 1:10 and above, it is a result of the secretion of soluble factors known to suppress T cells, such as hepatocyte growth factor. [225] This theory is attractive since it neatly ties together observations by many different labs that propose various soluble factors, enzymes or the induction of regulatory T cells to explain the inhibition of T cell function.

Di Nicola et al. show that transforming growth factor β1 and hepatocyte growth factor mediate the suppression of T cell proliferation by using neutralizing monoclonal antibodies to block their suppressive effect. [107] Transwell experiments were used to prove that this effect was not dependant on cell contact, but on soluble factors. Following this work, Meisel et al. published data showing that IFN-γ mediated IDO production in MSCs reduced tryptophan concentration in culture media and suppressed T cell allogeneic responses, as well as proliferation. [110] Either of these pathways could be responsible for the lack of a significant benefit to combined MSC TRAIL and EBV-TCR T cells in co-culture experiments.

Cell-contact dependent inhibition may also be responsible for a lack of benefit in combined cell therapy. MSC TRAIL and EBV-TCR T cells were mixed in an eppendorf and kept on ice for storage down to the Biological Sciences Unit, where they were then injected. It is also likely that these cells came into contact *in vivo* after injection, as they would have been trapped in the lung capillary bed

through the first pass effect. Soon after the work on soluble factors from MSCs inhibiting T cell proliferation and activation, Krampera et al. demonstrated that MSCs reduce the response of naïve and memory T cells to their cognate antigen by a cell contact dependent effect. [108] Other papers followed that also showed a cell contact dependent inhibition. [236]

Either the cell-contact dependent mechanism of inhibition, the secretion of soluble factors or perhaps both of these mechanisms may be responsible for the failure of a dual cell therapy to provide a significant increase in tumour cell death. These results are therefore in keeping with the work of others, which in general shows loss of T cell activity against their cognate antigen after exposure to MSCs or their supernatant.

Recent evidence suggests that MSCs can either suppress or promote immune responses depending on their environment. [237] It is likely that the *in vivo* environment differs in many significant respects to the *in vitro* testing of a dual cell therapy using co-cultures and flow cytometry analysis. Cancer cells adherent to tissue culture plastic represent a very different environment to a 3-dimensional lung tumour, with cancer cells packed tightly together and consequently difficult to access. Secondly, in the lung metastases model, cells must first home to the metastases before they can exert their effects, hence, cells are likely to arrive in significantly less numbers relative to cancer cells than the ratios used for co-culture experiments. It is possible that *in vitro* co-culture experiments significantly overestimate the true *in vivo* cancer cell death with these cell therapies. In this case, it may be easier to elucidate differences in cancer cell death *in vivo* between a single cell therapy with EBV-TCR T cells and a dual cell therapy combining them with MSC TRAIL.

7.3. Conventional cell radiolabeling methods

Indium-111 has been used since 1976 [148] to radiolabel leucocytes for clinical applications, such as imaging infection, fever of unknown origin and osteomyelitis. In the past 10 years indium-111 labeling has also been applied to tracking mesenchymal stem cells, with *in vitro* testing of cell viability revealing no effect on proliferation or differentiation at 30 Bq/cell [188], and *in vivo* imaging after intra-osseous delivery of labeled MSCs in a rat model showing detection of 3 x 10^5 cells. [156] In my pilot study I labeled 5 x 10^6 MSCs at 1 Bq/cell, and was able to confirm MSC retention in the lungs shortly after intravenous delivery using a nanoSPECT/CT system.

However, despite the availability and ease of use of indium-111, its main disadvantage is the high radiation dose of 3.5 mGy/decay, given to cells over its 67-hour half-life. [151] This is especially problematic for imaging T cells, which are more radiosensitive, with several studies recommending extremely low radiolabeling activities to conserve cell viability and homing. For example, Botti et al. recommend 0.04 Bq/cell, [193] and Kelson et al. use 0.15 Bq/cell and show 97-100% viability. [238] In a clinical protocol published by the European Journal of Nuclear Medicine & Molecular Imaging, 0.1 Bq/cell is recommended for leucocyte labeling, however no mention of viability is made. [178]

In my pilot study using Indium-111 to label EBV-TCR T cells at an activity of 1.67 Bq/cell, almost 100% of the administered T cells were dead after 24 hours. While decreasing the activity to 0.04 Bq/cell would have conserved lymphocyte viability, this very low total activity would have necessitated extremely long scan times to acquire a decent image using the SPECT/CT system. This would have been time-consuming and impractical for cell tracking, which is a dynamic process. Scan times also had to be kept less than three hours to conform to the project license. With such low initial activity, long-term tracking would be virtually impossible. Therefore, I searched for another method of direct radiolabeling that could minimize toxicity to the cell, allowing higher activities to be used in cell tracking experiments.

7.4. A novel tri-functional probe for T cell radiolabeling

In chapter 5, I explored the use of a tri-functional probe targeting cell membrane thiols. This probe had a fluorescent reporter, an iodine-125 reporter and a maleimide group for cell membrane thiol conjugation. Lymphocytes have been shown to express a large number of cell surface thiols, with thiol binding saturation occurring at 5 μM of maleimide probe concentration, [167] hence thiol labeling seemed like a good strategy. The purpose of using thiol labeling was to keep the iodine-125 reporter away from the radiosensitive cell nucleus by binding it to the cell surface membrane instead, unlike conventional cell radiolabeling techniques where the radiolabel diffuses inside the cell cytoplasm.

Two probes with different fluorescent reporters were tested, but both were extremely cytotoxic and were found to bind intracellular structures, as well as the cell surface membrane, using confocal microscopy. However, the radiolabeling characteristics were extremely good, with approximately 65% of the labeled activity on the cells after 24 hours. This is dramatically improved compared to the retention of conventional radiolabels.

Cell labeling experiments performed with an Alexa Fluor maleimide probe also showed close to 100% cell death after 24 hours. This experiment demonstrated that the maleimide group was implicated in the toxicity of the tri-functional probe. To assess this further, HPLC analysis was performed on the cell supernatant after labeling and this showed an interesting result, a large amount of a ^{125}I-DM-glutathione complex. This indicates that as well as entering the cell and binding to organelles, the probe is also binding to intracellular glutathione and then exiting the cell.

Glutathione plays a central role in cell redox homeostasis by acting as a thiol-disulphide redox buffer. [210] Redox homeostasis is essential for many intracellular processes, including gene transcription, DNA synthesis and enzyme activation. The cell must also counteract the large number of reactive oxygen species that are generated during normal biological reactions, such as oxidative phosphorylation in mitochondria. As a result, the intracellular redox status is tightly regulated, and the most important component of this system is glutathione which can be either oxidized or reduced by reactions of its thiol group. [211] The

average concentration of glutathione in the cytosol is 1-11 mM, and glutathione-disulphide, its oxidized form, is excreted from cells as a mechanism of protection from oxidative stress. [239] Therefore, binding of the maleimide probe to glutathione and a large efflux of ^{125}I-DM-glutathione from the cell could rapidly produce cell apoptosis and death by interfering with the cell's redox control.

The multi-drug resistance protein-1 pump (MRP1) is a member of the ATP-binding cassette superfamily of transport proteins, and exports glutathione compounds formed during oxidative reactions to maintain cell redox homeostasis. [212] Therefore, it is likely that the MRP1 pump is responsible for the export of the ^{125}I-DM-glutathione complex, in an attempt to regulate the redox environment in the cell after labeling. This hypothesis could be tested by inhibiting MRP1 function using verapamil added to cell culture media and repeating the HPLC analysis on the supernatant of ^{125}I-DM labeled cells.

Redox homeostasis is especially important for T cells, because their function can be influenced by changes in their redox status. [240] The reverse is also true, since during T cell activation there is an increase in intracellular reactive oxygen species, with a corresponding increase in the transcription of anti-oxidant molecules and enzymes. [241] Gringhuis et al. demonstrated that reduced intracellular glutathione in T cells resulted in impairment of TCR function and T cell hyporesponsiveness. [242] Hence, labeling T cells with this probe would impair their effector function, as well as their viability. Therefore, the tri-functional probe is not a good choice for direct labeling of a T cell therapy.

It is interesting to note that the paper by Digilio et al. describing labeling of cell surface thiols by gadolinium complexes, shows 90% viability immediately after labeling, however, longer-term viability measurements were not reported. [169] The authors also describe internalization of their probe resulting in good labeling. This work has not been translated into preclinical models, so it is possible that these complexes also caused significant cell toxicity that was not reported in the paper.

Another paper by Amartey et al. investigating radiolabeled maleimide derivatives for cell labeling also demonstrated good *in vitro* labeling but failed to assess cell viability after a final time-point of 180 minutes, when cell viability

was 95% or greater. [171] These cells were injected into a nude mouse to assess the initial biodistribution of labeled cells. Similar to my data showing cells trapped in the lungs after 1 hour and then predominantly in the liver at 24 hours indicating cell death, the authors state that at 1 hour the labeled cells were predominantly in the lungs and then in the liver after 24 hours. They argue that this distribution could indicate that the labeled cells were still viable. However, this may not be accurate since my data showed that luciferase expressing T cells trapped in the liver at 24 hours post-injection were not viable on bioluminescence imaging. The authors conclude that further viability testing is needed to assess this labeling strategy for *in vivo* applications. There have been no further publications from this group applying these iodinated maleimide derivatives in preclinical models, suggesting that after further evaluation of cell viability these probes were discovered to be unsuitable for cell tracking.

Therefore, the work presented in chapter 5 complements the work of others since I show good cell labeling of cell surface thiol groups at similar or lower concentrations of tri-functional probe to the agents they developed. The high toxicity I observe at 24 hours is not seen in other authors's work because they do not track cell survival beyond 3 hours. However, the biodistribution data from Amartey et al. suggests that cell viability is problematic with the radiolabeled maleimide derivatives because at 24 hours a high proportion of radiolabel resides in the liver.

Following these results, the development of the tri-functional probe was halted because modifications proposed to reduce to cell toxicity would also reduce the labeling efficiency, as a smaller proportion of the probe would enter the cytoplasm. Fortunately, the EBV-TCR plasmid used in these experiments also contained the luciferase gene; hence long-term T cell monitoring *in vivo* could still be achieved using bioluminescence imaging, despite the negative results from direct cell radiolabeling.

7.5. A combined MSC TRAIL and EBV-TCR T cell cancer therapy

Chapter 6 explored the use of MSC TRAIL and EBV-TCR T cells as a dual cell therapy against lung cancer. In order to test this therapy, a lung metastases model using intravenously injected MDA-MB-231 human breast cancer cells in a NOD/SCID mouse was developed. MSC TRAIL and EBV-TCR T cells were both shown to kill cancer cells *in vivo*, resulting in a significantly reduced tumour burden compared with controls. Using MSC TRAIL and EBV-TCR T cells as a dual cell therapy also resulted in cancer cell death, however, there was no significant improvement compared with using a single cell therapy.

To confirm delivery of the T cells, bioluminescence imaging was used to track EBV-TCR T cells homing to lung metastases. In fact, due to the first-pass effect the majority of injected T cells were delivered first to the lung capillary bed. Encouragingly, the EBV-TCR T cells then resided in the lungs until they died 6 days later, without moving to the spleen or other organs. This is an encouraging demonstration of tumour site specificity since a biodistribution study by Pittet et al. reports that 24 hours after systemic injection of adoptively transferred T cells, there are few cells remaining in the lungs and the majority reside in the liver and spleen. [243] Following sacrifice, anti-luciferase immunostaining was negative in lung sections, confirming that all the luciferase-expressing EBV-TCR T cells had died. Flow cytometry on cells derived from the spleens of each mouse also confirmed that no EBV-TCR T cells persisted *in vivo* at sacrifice.

Despite the death of the transfused cells after 6 days and the presumed exponential growth of any remaining cancer cells, at sacrifice on day 23 there was still a significant decrease in lung metastases diameter and percentage area of metastases, compared with control mice. This difference was very similar to that observed using MSC TRAIL, which did not die *in vivo* and could be seen within lung metastases using confocal imaging. This is the first *in vivo* demonstration of the efficacy of the engineered chimeric EBV TCR, since the previously published data only reported cytotoxicity assays using T2 target cells coated with LMP2 peptide. Furthermore, these T cells were shown to be as effective as divided doses of MSC TRAIL, which has a proven track record of activity against MDA-MB-231 lung metastases. [104] Due to the different MSC

TRAIL used (doxycycline induced TRAIL expression versus constitutive expression in my model) and methodology for assessing tumour burden, it is difficult to make a direct comparison between my MSC TRAIL only cell therapy results and the results from Loebinger et al using MSC TRAIL in a similar model. However, both data sets show a significant decrease in lung metastases.

It is possible that repeated doses of EBV-TCR T cells spaced 7 days apart could provide further benefit in this lung metastases model. A preclinical study by Kircher et al. suggests that multiple doses of adoptively transferred T cells result in better intra-tumoral distribution and engraftment, corresponding to a more effective treatment compared with a single dose. [244] In fact, several clinical trials have favoured this approach, administering T cells in divided doses spaced 2 days [196] or 2-4 weeks apart [197]. Future mouse studies could assess the optimum dose of EBV-TCR T cells and dosing schedule. Repeated doses of EBV-TCR T cells similar to the protocol used for MSC TRAIL therapy, would overcome the poor *in vivo* persistence of transferred T cells and potentially provide greater anti-tumour efficacy.

It is interesting that the dual cell therapy resulted in no additional benefit compared with a single cell therapy. The initial hypothesis was that cytokines released by activated cytotoxic T cells would aid the homing and engraftment of MSC TRAIL to tumour sites. Inflammatory mediators secreted by tumours are known to recruit macrophages and lymphocytes, as well as MSCs. The receptors involved in homing of MSCs to tumours are numerous, with ligands including growth hormones, cytokines, adhesion molecules and immune surveillance molecules, and there is also some overlap with T cell homing in cytokine receptors CCR1-CCR10 and CXCR3-CXCR6. [175] In addition, Hemeda et al. have shown that MSCs are highly responsive to TNF-α and IFN-γ, both of which are secreted by activated cytotoxic T cells. In particular, they showed that TNF-α increased the cytokine response of MSCs and induced migration. [245] Data by Croitoru-Lamoury et al. suggests that both TNF-α and IFN-γ are major regulators of the expression of chemokines and their receptors in MSCs. [246] However, to my knowledge there have been no studies specifically examining the role of activated T cells in MSC migration, and the literature is primarily concerned with examining the effect of MSCs on T cell function.

Unfortunately, confocal microscopy imaging of DiI fluorescent MSC TRAIL in lung metastases could not be used as accurate measure of MSC cell numbers in order to compare homing efficiency between the MSC TRAIL only group and the MSC TRAIL combined with EBV-TCR T cells group. This would have required imaging of serial sections throughout the entire lung volume to get an accurate picture of MSC distribution, since overall MSC numbers were extremely low. It would also not examine the distribution and number of MSC TRAIL throughout the time-course of the experiment. Further experiments using MSC TRAIL transduced with another, complementary bioluminescent reporter gene could allow more accurate quantification of cell numbers and behaviour. Differences could then be sought in MSC migration with or without the presence of EBV-TCR T cells.

It is possible that the lack of benefit of a combined cell therapy can be explained by the immunosuppressive effect of MSCs on T cells. However, there are conflicting studies about the effect of MSCs on T cells. Krampera et al. showed MSC inhibition of cytotoxicity, proliferation and IFN-γ production in naïve, memory and antigen-reactive T cells. [108] Others have reported that the immunosuppressive effects of MSCs on T cells could be discounted if the T cells had been previously activated, [230, 231] as was the case in this work, during peptide stimulation and expansion. Furthermore, data from Polchert et al. suggests that MSCs of a low passage are required for the suppression of T cells in acute GVHD. [247] Clinically, low passage MSCs (passage 1-3) are commonly used to treat acute GVHD after allogeneic hematopoietic stem cell transplantation. [248] The MSC TRAIL used in this thesis were all passage 9 or 10, therefore, according to these studies they are unlikely to have strong immunosuppressive effects, especially since the EBV-TCR T cells had been previously expanded and activated *in vitro*.

Co-culture experiments in chapter 3 revealed MSC TRAIL had no effect on T cell survival. In fact, activated cytotoxic T cells also express TRAIL, hence it seems unlikely that TRAIL expression by the MSCs could have deleterious effects on the EBV-TCR T cells.

During the *in vivo* experiment using bioluminescent imaging, EBV-TCR T cells that were co-injected with MSC TRAIL behaved similarly in their location and persistence to EBV-TCR T cells alone, lending further weight to the argument that the immunosuppressive effects of MSC TRAIL on EBV-TCR T cells can be discounted. To determine if this is the case, co-culture experiments with tumour cells, MSC TRAIL and EBV-TCR T cells could be repeated and the supernatant could be taken for IL-2 and IFN-γ ELISA, to measure if co-culture with MSC TRAIL reduces cytokine secretion by EBV-TCR T cells. However, although these factors are not secreted by MSCs in culture, Schinköthe et al. found that they were consumed by MSCs, making interpretation of the results from this assay difficult. [249] Real-time confocal imaging of the interaction between fluorescently labeled tumour cells, MSC TRAIL and EBV-TCR T cells may shed light on the interaction between these cells. The data from these experiments cannot elucidate if the killing effect of MSC TRAIL or EBV-TCR T cells predominates *in vitro* or *in vivo*.

The work presented in this thesis advances the field of cell therapies for cancer by demonstrating two important findings. The first is that MSC TRAIL treatment *in vivo* is similar to the EBV-TCR T cell anti-tumour effect. In fact, there was no significant difference between these groups in the average diameter of lung metastases after treatment, or the percentage area of metastases in total lung area, however both showed a significant difference compared to the control group.

There have been no previous reports in the literature comparing the efficacy of adoptive T cell therapy versus MSC TRAIL, hence these results are interesting to those who are developing clinical cell therapy treatments. Cost-benefit analysis may favour the development of MSC TRAIL therapy since their immunoprivileged status allows them to be an 'off-the-shelf' treatment, without the need to isolate and expand cells on an individual patient basis, and the consequent costs involved in such an individually tailored approach.

The second important finding is that the use of a combined MSC TRAIL and EBV-TCR T cell therapy does not result in a significant treatment benefit in this model. This finding must be put into context with the emerging body of evidence suggesting that in certain environments MSCs can modulate the immune

response. As described above, they have been shown by many groups to reduce the activation and effector function of cytotoxic T cells. The soluble factors implicated in this immunomodulation are inducible by inflammatory cytokines involved in the immune response, and are minimally expressed in inactivated MSCs. This immunomodulation effect of MSCs may explain the lack of benefit to combined cell therapy. Antibody blockage of the inflammatory cytokines involved, such as TNF-α and IFN-γ, might reduce the immunosuppressive effect of MSCs, but this would be at the expense of the T cell therapy and is unlikely to result in better tumour cell death. Therefore, further work in developing this combined cell therapy is unlikely to yield promising results.

As demonstrated in this thesis, individually, both cell therapies show promise for the treatment of lung cancer and should be developed further. Many questions still remain about adoptive T cell therapy, in particular, the dose and timing of T cell delivery, and the need to establish T cell persistence and memory. Along with these scientific challenges there are also commercial problems that need solving, such as cell expansion protocols, GMP cell culture facilities, product quality and safety. These concerns also apply to the development of MSC TRAIL as a cell therapy for lung cancer.

8. Summary and Future Directions

This thesis has demonstrated that both LMP2-specific EBV-TCR T cells and MSC TRAIL are highly effective cell therapies for lung cancer in a NOD/SCID mouse model. However, as a combination therapy, there is no additional benefit in reduction of lung metastases diameter or the total percentage area of metastases in the lung. Many basic science questions about the interaction between MSC TRAIL and EBV-TCR T cells *in vivo* remain unanswered. Whilst the cells did not appear to hinder one another in cancer cell killing, the lack of any benefit to combined treatment is surprising.

Future *in vitro* studies could look at the effect of cytokines secreted by activated T cells on MSC TRAIL homing. Quantification of MSC TRAIL in lung metastases using histology sections is unreliable and difficult, so I could not draw any conclusions about differences in MSC TRAIL numbers between the MSC TRAIL only group and the dual cell therapy group. Further *in vivo* experiments could use Renilla luciferase-expressing MSC TRAIL and bioluminescence imaging to quantify photon flux as a surrogate marker for cell numbers. The use of Renilla luciferase in MSC TRAIL would provide a dual-reporter system with Firefly luciferase in EBV-TCR T cells, allowing imaging of both cell therapies. [250]

The timing and dose of EBV-TCR T cells also needs study. It is possible that divided doses could result in improved metastases clearance, thus negating the need for another cell therapy.

The data presented in this thesis has shown that tumour antigen specific T cells can provide significant benefit in treating lung metastases. Consequently, it will be important to identify common tumour associated antigens expressed by non-small cell lung carcinoma, and engineer corresponding TCR candidates that are highly active against these antigens. These tumour assocated antigen targets and engineered TCR T cells will need to be tested first *in vitro* and then in mouse models to verify their efficacy, before they can be used in patients. Lung cancer

is the second most common cancer in the UK; therefore any increase in lung cancer survival has the potential to benefit a large number of patients.

References

1. Cancer Registration Statistics 2009. UK Office for National Statistics, 20th July 2011.

2. Youlden DR, Cramb SM, Baade PD. The international epidemiology of lung cancer: geographical distribution and secular trends. J Thorac Oncol 2008;3(8):819-831.

3. Rollins KD, Lindley C. Pemetrexed: a multitargeted antifolate. Clin Ther 2005;27(9):1343-1382.

4. Ciuleanu T, Brodowicz T, Zielinski C, Kim JH, Krzakowski M. Maintenance pemetrexed plus best supportive care versus placebo plus best supportive care for non-small-cell lung cancer: a randomised, double-blind phase III study. The Lancet 2009;374(9699):1432-1440.

5. Cagle PT, Chirieac LR. Advances in treatment of lung cancer with targeted therapy. Arch Pathol Lab Med 2012;136(5):504-509.

6. Horn L, Pao W. EML4-ALK: Homing in on a new target in non-small cell lung cancer. JCO 2009;27(26):4232-4235.

7. Soda M, Choi YL, Enomoto M, Takada S, Yamashita Y, Ishikawa S. Identification of the transforming EML4-ALK fusion gene in non-small-cell lung cancer. Nature 2007;448:561-566.

8. Shaw AT, Yeap BY, Solomon BJ, Riely GJ, Gainor J. Effect of crizotinib on overall survival in patients with advanced non-small cell lung cancer harbouring ALK gene rearrangement: a retrospective analysis. Lancet Oncol 2011;12(11):1004-1012.

9. Aberle DR, Adams AM, Berg CD, Black WC, Clapp JD. Reduced lung cancer mortality with low-dose computed tomographic screening. New Engl J Med 2011;365(5):395-409.

10. Baldwin DR, Hansell DM, Duffy SW, Field JK. Lung cancer screening with low dose computed tomography. BMJ 2014;348:1970-1971.

11. Rosell R, Bivona TG, Karachaliou N. Genetics and biomarkers in personalisation of lung cancer treatment. Lancet 2013;382:720-731.

12. Rosenberg SA, Yang JC, Topalian SL, Schwartzentruber DJ, Weber JS, Parkinson DR. Treatment of 283 consecutive patients with metastatic melanoma

or renal cell cancer using high-dose bolus interleukin 2. JAMA 1994;271(12):907-913.

13. Lynch TJ, I B, Luft A. Ipilimumab in combination with paclitaxel and carboplatin as first-line treatment in stage IIIB/IV non-small cell lung cancer: results from a randomized, double-blinded, multicenter phase II study. J Clin Oncol 2012;30(17):2046-2054.

14. Ramlau R, Quoix E, Rolski J. A pahse II study of TG4010 (Mva-Muc1-IL2) in association with chemotherapy in patients with stage III/IV non-small cell lung cancer. J Thorac Oncol 2008;3(7):735-744.

15. Neninger Vinageras E, de la Torre A, Rodriguez M. Phase II randomized controlled trial of an epidermal growth factor vaccine in advanced non-small cell lung cancer. J Clin Oncol 208;26(9):1452-1458.

16. Vansteenkiste J, Zielinski M, Linder A. Final results of a multi-center, double-blind, randomized, placebo-controlled phase II study to assess the efficacy of MAGE-A3 immunotherapeutic as adjuvant therapy in stage IB/II non-small cell lung cancer (NSCLC). ASCO Meeting Abstracts 2007;25(18 supplu):7554.

17. Quoix E, Ramlau R, Westeel V. Therapeutic vaccination with TG4010 and first-line chemotherapy in advanced non-small cell lung cancer: a controlled phase 2B trial. Lancet Oncol 2011;12(12):1125-1133.

18. Lydyard PM, Whelan A, Fanger MW. Immunology: BIOS Scientific Publishers Limited, 2001.

19. Davis MM, Bjorkman PJ. T-cell antigen receptor genes and T-cell recognition. Nature 1988;334:395-402.

20. Germain RN. T-cell development and the CD4-CD8 lineage decision. Nat Rev Immunol 2002;2:309-322.

21. Kisielow P, Hung ST, Bluthmann H, Von Boehmer H. Positive selection of antigen-specific T cells in thymus by restricting MHC molecules. Nature 1988;335:730-733.

22. Surh CD, Sprent J. T-cell apoptosis detected in situ during positive and negative selection in the thymus. Nature 1994;372:100-103.

23. Starr TK, Jameson C, Hogquist KA. Positive and negative selection of T cells. Annu Rev Immunol 2003;21:139-176.

24. Saito H, Kranz DM, Takagaki Y, Hayday AC, Eisen H, Tonegawa S. Complete primary structure of a heterodimeric T-cell receptor deduced from cDNA sequences. Nature 1984;309:757-762.

25. Alarcon B, Berkhout B, Breitmeyer J, Terhorst C. Assembly of the human T cell receptor-CD3 complex takes place in the endoplasmic reticulum and involves intermediary complexes between the CD3-Y-d-E core and single T cell receptor a and b chains. J Biol Chem 1988;263(6):2953-2961.

26. Zhu J, Paul WE. CD4 T cells: fates, functions, and faults. Blood 2008;112(5):1557-1569.

27. Paul WE, Seder RA. Lymphocyte responses and cytokines. Cell 1994;76:241-251.

28. Mosmann TR, Coffman RL. TH1 and TH2 cells: different patterns of lymphokine secretion lead to different functional properties. Annu Rev Immunol 1989;7:145-173.

29. Weaver CT, Harrington LE, Mangan PR, Gavrieli M, Murphy KM. Th17: an effector CD4 T cell lineage with regulatory T cell ties. Immunity 2006;24:677-688.

30. Sakaguchi S. Naturally arising CD4+ regulatory T cells for immunologic self-tolerance and negative control of immune responses. Annu Rev Immunol 2004;22:531-562.

31. Zinkernagel RM. Cellular immune recognition and the biological role of major transplantation antigens. Scandinavian Journal of Immunology 1997;46:423-436.

32. Kloetzel P-M, Ossendorp F. Proteasome and peptidase function in MHC-class-I-mediated antigen presentation. Curr Opin Immunol 2004;16(1):76-81.

33. Andersen MH, Schrama D, thor Straten P, Becker JC. Cytotoxic T cells. J Invest Dermatol 2006;126:32-41.

34. Castelli C, Rivoltini L, Andreola G, Carrabba M, Renkvist N, Parmiani G. T-cell recognition of melanoma-associated antigens. J Cell Physiol 2000;182:323-331.

35. Shresta S, Pham CTN, Thomas DA, Graubert TA, Ley TJ. How do cytotoxic lymphocytes kill their targets? Curr Opin Immunol 1998;10(5):581-587.

36. Morris E, Hart D, Gao L, Tsallios A, Xue S, Stauss H. Generation of tumour-specific T-cell therapies. Blood Reviews 2006;20(61-69).

37. Igney FH, Krammer PH. Immune escape of tumors: apoptosis resistance and tumor counterattack. J Leuko Biol 2002;71(6):907-920.

38. Shankaran V, Ikeda H, Bruce AT, White JM, Swanson PE, Old LJ, et al. IFN(gamma) and lymphocytes prevent primary tumour development and shape tumour immunogenicity. Nature 2001;410:1107-1111.

39. Ho WY, Blattman JN, Dossett ML, Yee C, Greenberg PD. Adoptive immunotherapy: Engineering T cell responses as biologic weapons for tumor mass destruction. Cancer Cell 2003;3(5):431-437.

40. Dawson CW, Port RJ, Young LS. The role of the EBV-encoded latent membrane proteins LMP1 and LMP2 in the pathogenesis of nasopharyngeal carcinoma (NPC). Semin Cancer Biol 2012;22(2):144-153.

41. Sharkey MS, Lizee G, Gonzales MI, Patel S, Topalian SL. CD4(+) T-cell recognition of mutated B-RAF in melanoma patients harboring the V599E mutation. Cancer Res 2004;64(5):1595-1599.

42. Robbins PF, El-Gamil M, Li YF, Kawakami Y, Loftus D, Appelia E, et al. A mutated beta-catenin gene encodes a melanoma-specific antigen recognized by tumor infiltrating lymphocytes. J Exp Med 1996;183(3):1185-1192.

43. Sierra JR, Tsao M-S. c-MET as a potential therapeutic target and biomarker in cancer. Ther Adv Med Oncol 2011;3((1 Suppl)):S21-S35.

44. Gattinoni L, Powell DJ, Rosenberg SA, Restifo NP. Adoptive immunotherapy for cancer: building on success. Nat Rev Immunol 2006;6(5):383-393.

45. Yee C, Thompson JA, Byrd D, Riddell SR, Roche P, Celis E, et al. Adoptive T cell therapy using antigen-specific CD8+ T cell clones for the treatment of patients with metastatic melanoma: In vivo persistance, migration and antitumour effect of transferred T cells. Proc Natl Acad Sci 2002;99(25):16168-16173.

46. Dudley ME, Wunderlich JR, Robbins PF, Yang JC, Hwu P, Schwartzentruber DJ, et al. Cancer regression and autoimmunity in patients after clonal repopulation with antitumour lymphocytes. Science 2008;298:850-854.

47. Dudley ME, Wunderlich JR, Yang JC, Sherry RM, Topalian SL, Restifo NP, et al. Adoptive cell transfer therapy following non-myeloablative but

lymphodepleting chemotherapy for the treatment of patients with refractory metastatic melanoma. J Clin Oncol 2005;23(10):2346-2357.

48. Rosenberg SA, Dudley ME. Cancer regression in patients with metastatic melanoma after the transfer of autologous antitumour lymphocytes. PNAS 2004;101(5):14639-14645.

49. Roszkowski JJ, Lyons GE, Kast WM, Yee C, Van Besien K, Nishimura MI. Simultaneous generation of CD8+ and CD4+ melanoma-reactive T cells by retroviral-mediated transfer of a single T-cell receptor. Cancer Res 2005;65(4):1570-1576.

50. Zhao Y, Zheng Z, Robbins PF, Khong HT, Rosenberg SA, Morgan RA. Primary human lymphocytes tansduced with NY-ESO-1 antigen-specific TCR genes recognize and kill diverse human tumour cell lines. J Immunol 2005;174(7):4415-4423.

51. Morgan RA, Dudley ME, Wunderlich JR, Hughes MS, Yang JC, Sherry RM. Cancer regression in patients after transfer of genetically engineered lymphocytes. Science 2006;314(5796):126-129.

52. Cooper LJ, Kalos M, Lewinsohn DA, Riddell SR, Greenberg PD. Transfer of specificity for human immunodeficiency virus type 1 into primary human T lymphocytes by introduction of T-cell receptor genes. Virol 2000;74:8207-8212.

53. Hu HM, Winter H, Urba WJ, Fox BA. Divergent roles for CD4+ T cells in the priming and effector/memory phases of adoptive immunotherapy. J Immunol 2000;165(8):4246-4253.

54. Dossett ML, Teague RM, Schmitt TM, Tan X, Cooper LJN, Pinzon C, et al. Adoptive immunotherapy of disseminated leukemia with TCR-transduced CD8+ T cells expressing a known endogenous TCR. Mol Ther 2009;17(4):742-749.

55. Xue S, Gao L, Hart D, Gillmore R, Qasim W, Thrasher A, et al. Elimination of human leukemia cells in NOD/SCID mice by WT1-TCR gene-transduced human T cells. Immunobiology 2005;106(9):3062-3067.

56. Xue S, Gao L, Thomas S, Hart DP, Xue JZ, Gillmore R, et al. Development of a Wilm's tumour antigen-specific T-cell receptor for clinical trials: engineered patient's T cells can eliminate autologous leukemia blasts in NOD/SCID mice. Haematologica 2010;95(1):126-134.

57. Junker AK. Epstein-Barr Virus. Pediatr Rev 2005;26(3):79-85.

58. Murray RJ, Kurilla MG, Brooks JM, Thomas WA, Rowe M, Kieff E. Identification of target antigens for the human cytotoxic T cell response to Epstein–Barr virus (EBV): implications for the immune control of EBV-positive malignancies. J Exp Med 1992(176):157-168.

59. Heslop HE, Rooney CM. Adoptive cellular immunotherapy for EBV lymphoproliferative diseases. Immunol Rev 1997;157(1):217-222.

60. Lucas KG, Salzman D, Garcia A, Sun Q. Adoptive immunotherapy with allogeneic Epstein–Barr virus (EBV)-specific cytotoxic T-lymphocytes for recurrent, EBV-positive Hodgkin disease. Cancer 2004;100(9):1892-1901.

61. Comoli P, Pedrazzoli P, Maccario R, Basso S, Carmnati O, Labirio M, et al. Cell Therapy of Stage IV Nasopharyngeal Carcinoma With Autologous Epstein-Barr Virus–Targeted Cytotoxic T Lymphocytes. JCO 2005;23(35):8942-8949.

62. Bollard CM, Straathof KCM, Huls MH, Leen A, Lacuesta K, Davis A, et al. The generation and characterization of LMP2-specific CTLs for use as adoptive transfer from patients with relapsed EBV-positive Hodgkin Disease. Journal of Immunotherapy 2004;27(4):317-327.

63. Bollard CM, Gottschalk S, Leen AM, Weiss H, Straathof KC, Carrum G, et al. Complete responses of relapsed lymphoma following genetic modification of tumor-antigen presenting cells and T-lymphocyte transfer. Blood 2007;110:2838-2845.

64. Hart DP, Xue S, Thomas S, Cesco-Gaspere M, Tranter A, Willcox B, et al. Retorviral transfer of a dominant TCR prevents surface expression of a large proportion of the endogenous TCR repertoire in human T cells. Gene Therapy 2008;15:625-631.

65. Kradin RL, Boyle LA, Preffer FI, Callahan RJ, Barlai-Kovach M, Strauss HW, et al. Tumor-derived interleukin-2-depedent lymphocytes in adoptive immunotherapy of lung cancer. Cancer Immunol Immunother 1987;24:76-85.

66. Kimura H, Yamaguchi Y. Adjuvant immunotherapy with interleukin 2 and lymphokine-activated killer cells after noncurative resection of primary lung cancer. Lung Cancer 1995;13:31-44.

67. Ratto GB, Melioli G, Zino P, Mereu C, Mirabelli S, Fantino G, et al. Immunotherapy with the use of tumour-infiltrating lymphocytes and interleukin-

2 as adjuvant treatment in stage III non-small-cell lung cancer: A pilot study. J Thorac Cardiovasc Surg 1995;109:1212-1217.

68. Ratto GB, Zino P, Mirabelli S, Minuti P, Aquilina R, Fantino G, et al. A randomized trial of adoptive immunotherapy with tumor-infiltrating lymphocytes and interleukin-2 versus standard therapy in the postoperative treatment of resected nonsmall cell lung carcinoma. Cancer 1995;78(2):244-251.

69. Ratto GB, Cafferata MA, Scolaro T, Bruzzi P, Alloisio A, Costa R, et al. Phase II study of combined immunotherapy, chemotherapy and radiotherapy in the postoperative treatment of advanced non-small-cell lung cancer. J Immunother 2000;23(1):161-167.

70. Ratto GB, Costa R, Maineri P, Alloisio A, Piras MT, D'Agostino A, et al. Neo-adjuvant chemo/immunotherapy in the treatment of stage III (N2) non-small cell lung cancer: a phase I/II pilot study. Int J Immunopathol Pharmacol 2011;24(4):1005-1016.

71. Murala S, Alli V, Kreisel D, Gelman AE, Krupnick AS. Current status of immunotherapy for the treatment of lung cancer. J Thorac Dis 2010;2(4):237-244.

72. Babiak A, Steinhauser M, Gotz M, Herbst C, Dohner H, Greiner J. Frequent T cell responses against immunogenic targets in lung cancer patients for targeted immunotherapy. Oncol Rep 2014;31(1):384-390.

73. Dudley ME, Wunderlich JR, Robbins PF, Yang JC, Hwu P, Schwartzentruber DJ. Cancer regression and autoimmunity in patients after clonal repopulation with antitumour lymphocytes. Science 2002;298(5594):850-854.

74. Yee C, Thompson JA, Roche P, Byrd DR, Lee PP, Piepkorn M. Melanocyte destruction after antigen-specific immunotherapy of melanoma. J Exp Med 2000;192(11):1637-1644.

75. Pankhurst MR, Yang JC, Langan RC, Dudley ME, A ND, A FS. T cells targeting carcinoembryonic antigen can mediate regression of metastatic colorectal cancer but induce severe transient colitis. Mol Ther 2011;19:620-626.

76. Stauss HJ, Morris EC. Immunotherapy with gene-modified T cells: limiting side effects provides new challenges. Gene Ther 2013;20:1029-1032.

77. Di Stasi A, Tey SK, Dotti G, Fujita Y, Kennedy-Nasser A, Martinez C. Inducible apoptosis as a safety switch for adoptive cell therapy. N Engl J Med 2011;365:1673-1683.

78. Khong HT, Restifo NP. Natural selection of tumor variants in the generation of "tumour escape" phenotypes. Nat Immunol 2002;3(11):999-1005.

79. Hofbauer GF, Kamarashev J, Geertsen R, Boni R, Dummer R. Melan A/MART-1 immunoreactivity in formalin-fixed paraffin-embedded primary and metastatic melanoma: frequency and distribution. Melanoma Res 1998;8(4):337-343.

80. Restifo NP, Marincola FM, Kawakami Y, Taubenberger J, Yannelli JR, Rosenberg SA. Loss of functional B2-microglobulin in metastatic melanomas from five patients receiving immunotherapy. J Natl Cancer Inst 1996;88(2):100-108.

81. Pittenger MF, Mackay AM, Beck SC, Jaiswal RK, Douglas R, Mosca JD, et al. Multilineage Potential of Adult Human Mesenchymal Stem Cells. Science 1999;284(5411):143-147.

82. Karp JM, Leng Teo GS. Mesenchymal Stem Cell Homing: The Devil is in the Details. Cell Stem Cell 2009;4:206-216.

83. Feng B, Chen L. Review of Mesenchymal Stem Cells and Tumors: Executioner or Coconspirator? Cancer Biother Radiopharm 2009;24(6):717-721.

84. Mohr A, Lyons M, Deedigan L, Harte T, Shaw G, Howard L, et al. Mesenchymal stem cells expressing TRAIL lead to tumour growth inhibation in an experimental lung cancer model. J Cell Mol Med 2008;12(6b):2628-2643.

85. Loebinger MR, Kyrtatos PG, Turmaine M, Price AN, Pankhurst Q, Lythgoe MF, et al. Magnetic resonance imaging of mesenchymal stem cells homing to pulmonary metastases using biocompatible magnetic nanoparticles. Cancer Res 2009;69(23):8862-8867.

86. Reagan MR, Kaplan DL. Concise review: Mesenchymal stem cell tumor-homing: Detection methods in disease model systems. Stem Cells 2011;29(6):920-927.

87. Wang H, Cao F, De A, Cao Y, Contag C, Gambhir SS, et al. Trafficking mesenchymal stem cell engraftment and differentiation in tumor-bearing mice by bioluminescence imaging. Stem Cells 2009;27(7):1548-1558.

88. Anderson SA, Glod J, Arbab AS, Noel S, Ashari P, Fine HA, et al. Noninvasive MR imaging of magnetically labeled stem cells to directly identify neovasculature in a glioma model. Blood 2005;105(1):420-425.

89. Hung S-C, Deng W-P, Yang WK, Liu R-S, Lee C-C, Su T-C, et al. Mesenchymal stem cell targeting of microscopic tumors and tumor stroma development monitored by noninvasive in vivo positron emission tomography imaging. Clin Cancer Res 2005;11:7749-7756.

90. Loebinger MR, Janes SM. Stem cells as vectors for antitumour therapy. Thorax 2010;65:362-369.

91. Levine AJ. p53, the cellular gatekeeper for growth and division. Cell 1997;88(3):323-331.

92. Chang F, Syrjanen S, Kurvinen K, Syrjanen K. The p53 tumor suppressor gene as a common cellular target in human carcinogenesis. Am J Gastroenterol 1993;88(2):174-186.

93. Wiley SR, Schooley K, Smolak PJ, Din WS, Huang C-P, Nicholl JK. Identification and characterisation of a new member of the TNF family that induced apoptosis. Immunity 1995;3:673-682.

94. Pitti RM, Marsters SA, Ruppert S, Donahue CJ, Moore A, Ashkenazi A. Induction of apoptosis by Apo-2 ligand, a new member of the tumour necrosis factor cytokine family. J Biol Chem 1996;271:12687-12690.

95. MacFarlane M. TRAIL-induced signalling and apoptosis. Toxicol Lett 2003;139:89-97.

96. Pan G, O'Rourke K, Chinnaiyan AM, Ebner R, Ni J, Dixit VM. The receptor for the cytotoxic ligand TRAIL. Science 1997;276:111-113.

97. Sherian JP, Marsters SA, Pitti RM, Gurney A, Skubatch M, Baldwin D, et al. Control of TRAIL-induced apoptosis by a family of signaling and decoy receptors. Science 1997;277(5327):818-821.

98. Ashkenazi A, Dixit VM. Apoptosis control by death and decoy receptors. Curr Opin Cell Biol 1999;11:255-260.

99. Kimberley FC, Screaton GR. Following a TRAIL: Update on a ligand and its five receptors. Cell Res 2004;14(5):359-372.

100. Emery JG, McDonnell P, Burke MB, Deen KC, Lyn S, Silverman C, et al. Osteoprotegerin is a receptor for the cytotoxic ligand TRAIL. J Biol Chem 1998;273(14363-14367).

101. C S Mitsiades SPT, N Mitsiades, Y Shima, P Richardson. TRAIL/Apo2L ligand selectively induces apoptosis and overcomes drug resistance in mulitple myeloma: therapeutic applications. Blood 2001;98(3):795-804.

102. Ashkenazi A, Pai RC, Fong S, Leung S, Lawrence DA, Marsters SA, et al. Safety and antitumor activity of recombinant soluble Apo2 ligand. J Clin Invest 1999;104(2):155-162.

103. Herbst RS, Eckhardt SG, Kurzrock R, Ebbinghaus S, O'Dwyer PJ, Gordon MS, et al. Phase I dose-escalation study of recombinant human Apo2L/TRAIL, a dual proapoptotic receptor agonist, in patients with advanced cancer. JCO 2010;28(17):2839-2846.

104. Loebinger ML, Eddaoudi A, Davies D, Janes SM. Mesenchymal stem cell delivery of TRAIL can eliminate metastatic cancer. Cancer Res 2009 May 15;69(10):4134-4142.

105. Le Blanc K, Frassoni F, Ball L, Locatelli F, Roelofs H. Mesenchymal stem cells for treatment of steroid-resistant, severe, acute graft-versus-host disease: a phase II study. Lancet 2008;371(9624):1579-1586.

106. Lin Y, Hogan WJ. Clinical Application of Mesenchymal Stem Cells in the Treatment and Prevention of Graft-versus-Host Disease. Advances in Hematology 2011;2011:17.

107. Di Nicola M, Carlo-Stella C, Magni M, Milanesi M, Longoni PD, Matteucci P, et al. Human bone marrow stromal cells suppress T-lymphocyte proliferation induced by cellular or non-specific mitogenic stimuli. Blood 2002;99(3838-3843).

108. Krampera M, Glennie S, Dyson J, Scott D, Laylor R, Simpson E, et al. Bone marrow mesenchymal stem cells inhibit the response of naive and memory antigen-specific T cells to their cognate peptide. Blood 2003(101):3722-3729.

109. Mellor A, Munn DH. IDO expression by dendritic cells: tolerance and tryptophan catabolism. Nat Rev Immunol 2004;4:762-774.

110. Meisel R, Zibert A, Laryea M, Gobel U, Daubener W, Dilloo D. Human bone maarrow stromal cells inhibit allogeneic T-cell responses by indoleamine 2,3-dioxygenase-mediated typtophan degradation. Blood 2004;103(12):4619-4621.

111. Glennie S, Soeiro I, Dyson PJ, Lam EW, Dazzi F. Bone marrow mesenchymal stem cells induce division arrest anergy of activated T cells. Blood 2004;105(7):2821-2827.

112. Rasmusson I, Ringden O, Sundberg B, Le Blanc K. Mesenchymal stem cells inhibit the formation of cytotoxic T cells, but not activated cytotoxic T lymphocytes or natural killer cells. Transplantation 2003;76(8):1208-1213.

113. Srinivas M, Aarntzen EHJG, Bulte JWM, Oyen WJ, Heerschap A, de Vries IJM, et al. Imaging of cellular therapies. Adv Drug Deliv Rev 2010;62:1080-1093.

114. Kircher MF, Gambhir SS, Grimm J. Noninvasive cell-tracking methods. Nat Rev Clin Oncol 2011;8:677-688.

115. Pittet MJ, Grimm J, Berger CR, Tamura T, Wojtkiewiz G, Nahrendorf M, et al. In vivo imaging of T cell delivery to tumors after adoptive transfer therapy. Proc Natl Acad Sci 2007;104(30):12457-12461.

116. Zhou R, Thomas DH, Qiao H, Bal HS, Choi S, Alavi A, et al. In vivo detection of stem cells grafted in infarcted rat myocardium. J Nucl Med 2005;46(5):816-822.

117. Blasberg RG, Gelovani J. Molecular-genetic imaging: a nuclear medicine-based perspective. Mol Imaging 2002;1(3):280-300.

118. Kang JH, Chung J-K. Molecular-genetic imaging based on reporter gene expression. J Nucl Med 2008;49:164S-179S.

119. Tannous BA, Grimm J, Perry KF, Chen JW, Weissleder R, Breakefield XO. Metabolic biotinylation of cell surface receptors for in vivo imaging. Nat Methods 2006;3:391-396.

120. DeMarco U, Xu H, Goins WF, Ahrens ET. A new transgene reporter for in vivo magnetic resonance imaging. Nat Methods 2005;11(4):450-454.

121. Gilad AA, McMahon MT, Walczak P, Winnard PT. Artificial reporter gene providing MRI contrast based on proton exchange. Nat Biotechnol 2007;25:217-219.

122. Welsh DK, Kay SA. Bioluminescent imaging in living organisms. Curr Opin Biotechnol 2005;16:73-78.

123. Gomi K, Kajiyama N. Oxyluciferin, a luminescence product of firefly luciferase, is enzymatically regenerated into luciferin. J Biol Chem 2001;276:36508-36513.

124. De Wet JR, Wood KV, DeLuca M, Helinski DR, Subramani S. Firefly luciferase gene: structure and expression in mammalian cells. Mol Cell Biol 1987;7(2):725-737.

125. Luker KE, Luker GD. Applications of Bioluminescence Imaging to Antiviral Research and Therapy: Multiple Luciferase Enzymes and Quantitation. Antiviral Res 2008;78(3):179-187.

126. Rice BW, Cable MD, Nelson MB. In vivo imaging of light-emitting probes. J Biomed Opt 2001;6(4):432-440.

127. Chudakov DM, Lukyanov S, Lukyanov KA. Fluorescent proteins as a toolkit for in vivo imaging. Trends Biotecnol 2005;23(12):605-613.

128. Troy T, Jekic-McMullen D, Sambucetti L, Rice B. Quantitative comparison of the sensitivity of detection of fluorescent and bioluminescent reporters in animal models. Mol Imaging 2004;3(1):9-23.

129. Weissleder R. Scaling down imaging: molecular mapping of cancer in mice. Nat Rev Cancer 2002;2:11-18.

130. Lin MZ, McKeown MR, Ng H-L, Aguilera TA, Shaner NC, Campbell RE, et al. Autofluorescent proteins with excitation in the optical window for intravital imaging in mammals. Chem Biol 2009;16(11):1169.

131. Smith AM, Mancini MC, Nie S. Second window for in vivo imaging. Nat Nanotechnol 2009;4(11):710-711.

132. Adonai N, Nguyen KN, Walsh J, Iyer M, Toyokuni T, Phelps ME, et al. Ex vivo cell labeling with 64Cu-pyruvaldehyde-bis(N4-methylthiosemicarbazone) for imaging cell trafficking in mice with positron-emission tomography. Proc Natl Acad Sci 2002;99(5):3030-3035.

133. Gambhir SS. Molecular imaging of cancer with positron emission tomography. Nat Rev Cancer 2002;2:683-693.

134. Ametamey SM, Honer M, Schubiger PA. Molecular imaging with PET. Chem Rev 2008;108:1501-1516.

135. Rahmim A, Zaidi H. PET versus SPECT: strengths, limitations and challenges. Nucl Med Comm 2008;29:193-207.

136. Sanchez-Crespo A, Andreo P, Larssan SA. Positron flight in human tissues and its influence on PET image spatial resolution. Eur J Nucl Med Mol Imaging 2004;31(1):44-51.

137. Franc BL, Acton PD, Mari C, Hasegawa BH. Small-animal SPECT and SPECT/CT: Important tools for preclinical investigation. J Nucl Med 2008;49(10):1651-1663.

138. Bailey DL, Willowson KP. An evidence-based review of quantitative SPECT imaging and potential clinical applications. J Nucl Med 2013;54:83-89.

139. Ishizu K, Mukai T, Yonekura Y, Pagani M, Fujita T, Magata Y, et al. Ultra-high resolution SPECT system using four pinhole collimators for small animal studies. J Nucl Med 1995;36:2282-2287.

140. Lyra M, Ploussi A. Filtering in SPECT image reconstruction. Int J Biomed Imaging 2011;2011:693795.

141. Tjuvajev JG, Finn R, Watanabe K, Joshi R, Oku T, Kennedy J, et al. Noninvasive imaging of herpes virus thymidine kinase gene transfer and expression: a potential method for monitoring clinical gene therapy. Cancer Res 1996;56(18):4087-4095.

142. Iyer M, Barrio JR, Namavari M, Bauer E, Satyamurthy N, Nguyen K, et al. 8-[18F]-Fluoropenciclovir: an improved reporter probe for imaging HSV1-tk reporter gene expression in vivo using PET. J Nucl Med 2001;42(1):96-105.

143. Acton PD, Zhou R. Imaging reporter genes for cell tracking with PET and SPECT. Q J Nucl Med Mol Imaging 2005;49(4):349-360.

144. Riddell SR, Elliott M, Lewinsohn DA, Gilbert MJ, Wilson L, Manely SA, et al. T-cell mediated rejection of gene-modified HIV-specific cytotoxic T lymphocytes in HIV-infected patients. Nat Med 1996;2:216-223.

145. Moroz MA, Serganova I, Zanzonico P, Ageyeva L, Beresten T, Dyomina E, et al. Imaging hNET reporter gene expression with (124)I-MIBG. J Nucl Med 2007;48(5):827-836.

146. Miyagawa M, Beyer M, Wagner B, Anton M, Spitzweg C, Gansbacher B, et al. Cardiac reporter gene imaging using the human sodium/iodide symporter gene. Cardiovasc Res 2005;65(1):195-202.

147. Jacobs A, Voges J, Reszka R, Lercher M, Gossmann A, Kracht L, et al. Positron-emission tomography of vector-mediated gene expression in gene therapy for gliomas. Lancet 2001;358(9283):727-729.

148. Segal AW, Arnot RN, Thakur ML, Lavender JP. Indium-111-labelled leucocytes for localisation of abscesses. Lancet 1976;308(7994):1056-1058.

149. Datz FL. Indium-111-labeled leukocytes for the detection of infection: current status. Semin Nucl Med 1994;24(2):92-109.

150. Peters AM, Saverymuttu SH, Reavy HJ, Danpure HJ, Osman S, Lavender JP. Imaging of inflammation with indium-111 tropolonate labeled leukocytes. J Nucl Med 1982;24(1):39-44.

151. McLean JR, Wilkinson D. The radiation dose to cells in vitro from intracellular indium-111. Biochem Cell Biol 1989;67(9):661-665.

152. Peters AM, Danpure HJ, Osman S, Hawker RJ, Henderson BL, Hodgson HJ, et al. Clinical experience with 99mTc-Hexamethylpropylene-amineoxime for labeling leucocytes and imaging inflammation. Lancet 1986;328(8513):946-949.

153. Uno K, Yoshikawa K, Imazeki K, Minoshima S, Arimizy N. Technetium-99m HMPAO labeled leukocytes in inflammation imaging. Ann Nucl Med 1991;5(2):77-81.

154. Cox PH, Buscombe JR. The Imaging of Infection and Inflammation (Developments in Nuclear Medicine): Springer, 1998.

155. de Vries EFJ, Roca M, Jamar F, Israel O, Signore A. Guidelines for the labelling of leucocytes with (99m)Tc-HMPAO. Eur J Nucl Med Mol Imaging 2010;37:842-848.

156. Gildehaus FJ, Haasters F, Drosse I, Wagner E, Zach C, Mutschler W, et al. Impact of indium-111 oxine labelling on viability of human mesenchymal stem cells in vitro, and in 3D cell-tracking using SPECT/CT in vivo. Mol Imaging Biol 2011;13(6):1204-1214.

157. Bulte JW. In vivo MRI cell tracking: clinical studies. AJR Am J Roentgenol 2009;193(2):314-325.

158. Sun C, Lee JS, Zhang M. Magnetic nanoparticles in MR imaging and drug delivery. Adv Drug Deliv Rev 2008;60(11):1252-1265.

159. Ordidge KL, Duffy BA, Wells JA, Kalber TL, Lythgoe ML. Imaging the paediatric lung: what does nanotechnology have to offer? Paediatr Respir Rev 2012;13(2):84-88.

160. Yaghoubi SS, Jensen MC, Satyamurthy N, Budhiraja S, Paik D, Czernin J, et al. Noninvasive detection of therapeutic cytolytic T cells with 18F-FHBG PET in a patient with glioma. Nat Clin Pract Oncol 2009;6(1):53-58.

161. Kraitchman DL, Bulte JWM. In vivo imaging of stem cells and beta cells using direct cell labeling and reporter gene methods. Arterioscler Thromb Vasc Biol 2009;29:1025-1030.

162. Lukawska JJ, Livieratos L, Sawyer BM, Lee T, O'Doherty M, Blower PJ, et al. Real-time differential tracking of human neutrophil and eosinophil migration in vivo. J Allergy Clin Immunol 2014;133(1):233-239.

163. Blocket D, Toungouz M, Kiss R, Lambermont M, Velu T, Duriau D, et al. 111In-oxine and 99m-Tc-HMPAO labelling of antigen-loaded dendritic cells: in vivo imaging and influence on motility and actin content. Eur J Nucl Med Mol Imaging 2003;30(3):440-447.

164. de Vries IJM, Lesterhuis WJ, Barentsz JO, Verdijk P, van Krieken JH, Boerman OC, et al. Magnetic resonance tracking of dendritic cells in melanoma patients for monitoring of cellular therapy. Nature Biotechnol 2005;23(11):1407-1413.

165. Champe PC, Harvey RA. Biochemistry. 2 ed: Lippincott Williams & Wilkins, 1987.

166. Winterbourn CC, Hampton MB. Thiol chemistry and specificity in redox signaling. Free Radic Biol Med 2008;45(5):549-561.

167. Sahaf B, Heydari K, Herzenberg LA, Herzenberg LA. Lymphocyte surface thiol levels. Proc Natl Acad Sci 2003;100(7):4001-4005.

168. Laragione T, Bonetto V, Casoni F, Massignan T, Bianchi G, Gianazza E, et al. Redox regulation of surface protein thiols: Identification of integrin alpha-4 as a molecular target by using redox proteomics. Proc Natl Acad Sci 2003;100(25):14737-14741.

169. Digilio G, Catanzaro V, Fedeli F, Gianolio E, Menchise V, Napolitano R, et al. Targeting exofacial protein thiols with Gd(III) complexes. An efficient procedure for MRI cell labelling. Chem Commun 2009:893-895.

170. Stephan MT, Moon JJ, Um SH, Bershteyn A, Irvine DJ. Therapeutic cell engineering with surface-conjugated synthetic nanoparticles. Nat Med 2010;16(9):1035-1042.

171. Amartey JK, Parhar RS, Shi Y, Al-Mohanna F. Preliminary evaluation of two radioiodinated maleimide derivatives targeting peripheral and membrane sulfhydryl groups for in vitro cell labeling. Appl Radiat Isotopes 2011;69:163-170.

172. Kosower NS, Kosower EM. Thiol labeling with bromobimanes. Methods Enzymol 1987;143:76-84.
173. Sippel TO. New fluorochromes for thiols: maleimide and iodoacetamide derivatives of a 3-phenylcoumarin fluorophore. J Histochem Cytochem 1981;29(2):314-316.
174. Yan R, El-Emir E, Rajkumar V, Robson M, Jathoul AP, Pedley B, et al. One-pot synthesis of an I(125)-labled trifunctional reagent for multiscale imaging with optical and nuclear techniques. Angew Chem Int Edit 2011;123(30):6925-6927.
175. Spaeth E, Klopp A, Dembinski J, Andreeff M, Marini F. Inflammation and tumor microenvironments: defining the migratory itinerary of mesenchymal stem cells. Gene Ther 2008;15:730-738.
176. Shapiro HM. Multistation multiparameter flow cytometry: a critical review and rationale. Cytometry 1983;3(4):227-243.
177. Boniface JJ, Rabinowitz JD, Wulfing C, Hampl J, Reich Z, Altman JD, et al. Initiation of signal transduction throught the T cell receptor requires the multivalent engagement of peptide/MHC ligands. Immunity 1998;9(4):459-466.
178. Roca M, de Vries EFJ, Jamar F, Israel O, Signore A. Guidelines for the labelling of leucocytes with 111-In-oxine. Eur J Nucl Med Mol Imaging 2010;37:835-841.
179. Sahaf B, Heydari K, Herzenberg LA, Herzenberg LA. The extracellular microenvironment plays a key role in regulating the redox status of cell surface proteins in HIV-infected subjects. Arch Biochem Biophys 2005;434(1):26-32.
180. Ellman GL. Tissue sulfhydryl groups. Arch Biochem Biophys 1959;82:70-77.
181. Falschlehner C, Schaefer U, Walczak H. Following TRAIL's path in the immune system. Immunol 2009;127(2):145-154.
182. Kayagaki N, Yamaguchi N, Nakayama M, Eto H, Okumura K. Type I interferons (IFNs) regulate tumour necrosis factor-related apoptosis-inducing ligand (TRAIL) expression on human T cells: A novel mechanism for the antitumour effects of type I IFNs. J Exp Med 1999;189(9):1451-1460.
183. Mirandola P, Ponti C, Gobbi G, Sponzilli I, Vaccarezza M. Activated human NK and CD8+ T cells express both TNF-related apoptosis-inducing

ligand (TRAIL) and TRAIL receptors but are resistant to TRAIL-mediated cytotoxicity. Blood 2004;104(8):2418-2424.

184. Jeremias I, Herr I, Boehler T, Debatin KM. TRAIL/Apo-2-ligand-induced apoptosis in human T cells. Eur J Immunol 1998;28(1):143-152.

185. Barry M, Bleackley RC. Cytotoxic T lymphocytes: all roads lead to death. Nat Rev Immunol 2002;2:401-409.

186. Peters AM, Osman S, Reavy HJ, Chambers B, Deenmamode M, Lewis SM. Erythrocyte radiolabelling: in vitro comparison of chromium, technetium, and indium in undamaged and heat damaged cells. J Clin Pathol 1986;39:717-721.

187. Swirski FK, Pittet MJ, Kircher MF, Aikawa E, Jaffer FA, Libby P, et al. Monocyte accumulation in mouse atherogenesis is progressive and proportional to extent of disease. Proc Natl Acad Sci 2006;103(27):10340-10345.

188. Bindslev L, Haack-Sorensen M, Bisgaard K, Kragh L, Mortensen S, Hesse B, et al. Labelling of human mesenchymal stem cells with indium-111 for SPECT imaging: effect on cell proliferation and differentiation. Eur J Nucl Med Mol Imaging 2006;33(10):1171-1177.

189. Kidd S, Spaeth E, Dembinski JL, Dietrich M, Watson K, Klopp A, et al. Direct evidence of mesenchymal stem cell tropism for tumor and wounding microenvironments using in vivo bioluminescent imaging. Stem Cells 2009;27(10):2614-2623.

190. Santos EB, Yeh R, Lee J, Nikhamin Y, Punzalan B, Punzalan B, et al. Sensitive in vivo imaging of T cells utilizing a membrane bound Gaussia princeps luciferase enzyme. Nat Med 2009;15(3):338-344.

191. Blizer M, Roggel F, Gerbes AL. Role of Kupffer cells in host defense and liver disease. Liver Int 2006;26(10):1175-1186.

192. Wagstaff J, Gibson C, Thatcher N, Ford WL, Sharma H, Benson W, et al. A method for following human lymphocyte traffic using indium-111 oxine labelling. Clin Exp Immunol 1981;43:435-442.

193. Botti C, Negri DR, Seregni E, Ramakrishna V, Arienti F, Maffioli L, et al. Comparison of three different methods for radiolabelling human activated T lymphocytes. Eur J Nucl Med 1997;24(5):497-504.

194. van Montfrans C, Bennink RJ, de Bruin K, de Jonge W, Verberne HJ, ten Kate FJW, et al. In vivo evaluation of (111)In-labeled T-lymphocyte homing in experimental colitis. J Nucl Med 2004;45:1759-1765.

195. Khanna R, Bell S, Sherritt M, Galbraith A, Burrows SR, Rafter L, et al. Activation and adoptive transfer of Epstein-Barr virus-specific cytotoxic T cells in solid organ transplant patients with posttransplant lymphoproliferative disorder. Proc Natl Acad Sci 1999;96(18):10391-10396.

196. Goedegebuure PS, Douville LM, Li H, Richmond GC, Schoof DD, Scavone M, et al. Adoptive immunotherapy with tumor-infiltrating lymphocytes and interleukin-2 in patients with metastatic malignant melanoma and renal cell carcinoma: a pilot study. JCO 1995;13(8):1939-1949.

197. Dudley ME, Wunderlich JR, Yang JC, Hwu P, Schwartzentruber, Topalian SL, et al. A phase I study of nonmyeloablative chemotherapy and adoptive transfer of autologous tumour antigen-specific T lymphocytes in patients with metastatic melanoma. J Immunother 2002;25(3):243-251.

198. Merz T, Tatum J, Hirsch J. Technetium-99m-labeled lymphocytes: a radiotoxicity study. J Nucl Med 1986;27:105-110.

199. Segal AW, Deteix P, Garcia R, Tooth P, Zonelli GD. Indium-111 labeling of leukocytes: a detrimental effect on neutrophil and lymphocyte function and an improved method of cell labeling. J Nucl Med 1978;19(11):1238-1244.

200. Laragione T, Bonetto V, asoni F, Massignan T, Bianchi G, Gianazza E, et al. Redox regulation of surface protein thiols: Identification of integrin alpha-4 as a molecular target by using redox proteomics. Proc Natl Acad Sci 2003;100(25):14737-14741.

201. Reiners JJ, Mathieu P, Okafor C, Putt DA, Lash LH. Depletion of cellular glutathione by conditions used for the passaging of adherent cultured cells. Toxicol Lett 2000;115(2):153-163.

202. Moran LK, Gutteridge JM, Qunilan GJ. Thiols in cellular redox signalling and control. Curr Med Chem 2001;8(7):763-772.

203. Johnson LV, Walsh ML, Bockus BJ, Chen LB. Monitoring of relative mitochondrial membrane potential in living cells by fluorescence microscopy. J Cell Biol 1981;88(3):526-535.

204. Nestmann ER, Douglas GR, Matula TI, Grant CE, Kowbel DJ. Mutagenic activity of rhodamine dyes and their impurities as detected by mutation induction in Salmonella and DNA damage in Chinese Hamster Ovary cells. Cancer Res 1979;39:4412-4417.

205. Torres AG, Gait MJ. Exploiting cell surface thiols to enhance cellular uptake. Trends Biotechnol 2012;30(4):185-190.

206. Aubrey S, Burlina F, Dupont E, Delaroche D, Joliot A, Lavielle S. Cell-surface thiols affect cell netry of disulfide-conjugated peptides. FASEB J 2009;23(9):2956-2967.

207. Alford R, Simpson H, Duberman J, Hill GC, Ogawa M, Regino C. Toxicity of organic fluorophores used in molecular imaging: literature review. Mol Imaging 2009;8(6):341-354.

208. Kruh GD, Belinsky MG. The MRP family of drug efflux pumps. Oncogene 2003;22:7537-7552.

209. Hammond CL, Marchan R, Krance SM, Ballatori N. Glutathione export during apoptosis requires functional multidrug resistance-associated proteins. J Biol Chem 2007;282(19):14337-14347.

210. Schafer FQ, Buettner GR. Redox environment of the cell as viewed through the redox state of the glutathione disulfide/glutathione couple. Free Radical Bio Med 2001;30(11):1191-1212.

211. Arrigo A-P. Gene expression and the thiol redox state. Free Rad Biol Med 1999;27(9/10):936-944.

212. Hipfner DR, Deeley RG, Cole SPC. Structural, mechanistic and clinical aspects of MRP1. Biomembranes BBA 1999;1461(2):359-376.

213. Zinn KR, Chaudhuri TR, Szafan AA, O'Quinn D, Weaver C, Dugger K, et al. Noninvasive bioluminescence imaging in small animals. ILAR J 2008;49(1):103-115.

214. Bosma MJ, Carroll AM. The SCID mouse mutant: definition, characterization, and potential uses. Annu Rev Immunol 1991;9:323-350.

215. Frangioni JV. In vivo near-infrared fluorescence imaging. Curr Opin Chem Biol 2003;7(5):626-634.

216. Ruan J, Song H, Li C, Bao C, Fu H, Wang K, et al. DiR-labeled embryonic cells for targeted imaging of in vivo gastric cancer cells. Theranostics 2012;2(6):618-628.

217. Fischer UM, Harting MT, Jimenez F, Monzon-Posadas WO, Xue H, Savitz SI, et al. Pulmonary passage is a major obstacle for intravenous stem cell delivery: the pulmonary first-pass effect. Stem Cells Dev 2009;18(5):683-691.

218. Schrepfer S. Stem cell transplantation: the lung barrier. Transplant Proc 2007;39(573-576).

219. Gao J. The dynamic in vivo distribution of bone marrow-derived mesenchymal stem cells to the infarcted myocardium: feasibility, cell migration and body distribution. Circulation 2001;2003(108):863-868.

220. Barti-Juhasz H, Mihalik R, Nagy K, Grisendi G. Bone marrow derived mesenchymal stem/stromal cells transduced with full length human TRAIL repress the growth of rhabdomyosarcome cells in vitro. Haematologica 2011;96(3):e21-e22.

221. Sage EK, Kolluri KK, McKnulty K, Lourenco S, Kalber T. Systemic but not topical TRAIL-expressing mesenchymal stem cells reduce tumour growth in malignant mesothelioma. Thorax 2014;69(7):638-647.

222. Bartholomew A, Sturgeon C, Siatskas M, Ferrer K, McIntosh K. Mesenchymal stem cells suppress lymphocyte proliferation in vitro and prolong skin graft survival in vivo. Exp Hematol 2002;30(1):42-48.

223. Rasmusson I, Ringden O, Sundberg B, Le Blanc K. Mesenchymal stem cells inhibit lymphocyte proliferation by mitogens and alloantigens by different mechanisms. Blood 2005;305(1):33-41.

224. Maccario R, Podesta M, Moretta A, Cometa A. Interaction of human mesenchymal stem cells with cells involved in alloantigen-specific immune response favors the differentiation of CD4+ T-cell subsets expressing a regulatory/suppressive T cell phenotype. Hematol 2007;90:516-525.

225. Prevosto C, Zancolli M, Canevali P, Zocchi MR. Generation of CD4+ or CD8+ regulatory T cells upon mesenchymal stem cell-lymphocyte interaction. hematol 2007;92(7):881-888.

226. Di Ianni M, Del Papa B, De Ioanni M, Moretti L. Mesenchymal stem cells recruit and regulate T regulatory cells. Exp Hematol 2008;36:309-318.

227. Del Papa B, Sportoletti P, Cecchini D, Rosati E, Balucani C, Baldoni S. Notch1 modulates mesenchymal stem cells mediated regulatory T-cell induction. Eur J Immunol 2013;43(1):182-187.

228. Duffy MM, Pindjakova J, Hanley SA, McCarthy C, Weidhofer GA. Mesenchymal stem cell inhibition of T-helper 17 cell-differentiation is triggered by cell-cell contact and mediated by prostaglandin E2 via the EP4 receptor. Eur J Immunol 2011;41(10):2840-2851.

229. Ghannam S, Pene J, Torcy-Moquet G, Jorgensen C, Yssel H. Mesenchymal stem cells inhibit human Th17 cell differentiation and function and induce a T regulatory cell phenotype. J |mmunol 2010;185(1):302-312.

230. Karlsson H, Samarasinghe S, Ball LM, Sundberg B, Lankester AC, Dazzi F, et al. Mesenchymal stem cells exert differential effects on alloantigen and virus-specific T-cell responses. Blood 2008;112(3):532-541.

231. Rasmusson I, Ringden O, Sundberg B, Le Blanc K. Mesenchymal stem cells inhibit the formation of cytotoxic T lymphocytes, but not activated cytotoxic T lymphocytes or natural killer cells. Transplant 2003;76:1208-1213.

232. Kimbrel EA, Kouris NA, Yavanian GJ, Chu J, Qin Y. Mesenchymal stem cell population derived from human pluripotent stem cells displays potent immunomodulatory and therapeutic properties. Stem Cells Dev 2014;Epub ahead of print.

233. Bollard CM, Aguilar L, Straathof KC, Gahn B, Huls MH, Rousseau A, et al. Cytotoxic T lymphocyte therapy for Epstein-Barr virus+ Hodgkin's disease. JEM 2004;200(12):1623-1633.

234. Rooney CM, Roskrow MA, Suzuki N, Ng CYC, Brenner MK, Heslop H. Treatment of relapsed Hodgkin's disease using EBV-specific cytotoxic T cells. Ann Oncol 1998;9(Suppl. 5):S129-S132.

235. Dwyer RM, Khan S, Barry FP, O'Brien T, Kerin MJ. Advances in mesenchymal stem cell-mediated gene therapy for cancer. Stem Cell Red Ther 2010;1(3):25.

236. Tse W, Pendleton JD, Beyer WM, Egalka MC, Guinan EC. Suppression of allogeneic T-cell proliferation by human bone marrow stromal cells: implications in transplantation. Transplant 2003;75(3):389-397.

237. Ma S, Xie N, Li W, Yuan B, Shi Y. Immunobiology of mesenchymal stem cells. Cell Death Differ 2014;21:216-225.

238. Kelsen J, Agnholt J, Falborg L, Nielsen JT, Romer JL. 111Indium-labelled human gut-derived T cells from healthy subjects with strong in vitro

adhesion to MAdCAM-1 show no detectable homing to the gut in vivo. Clin Exp Immunol 2004;138(1):66-74.

239. Smith CV, Jones DP, Guenther TM, Lash LH, Lauterburg BH. Contemporary issues in toxicology. Compartmentation of glutathione: implications for the study of toxicity and disease. Toxicol Appl Pharmacol 1996;140:1-12.

240. Gelderman KA, Hultqvist M, Holmberg J, Olofsson P, Holmdahl R. T cell surface redox levels determine T cell reactivity and arthritis susceptibility. Proc Natl Acad Sci 2006;103(34):12831-12836.

241. Griffiths HR, Dunston CR, Bennett SJ, Grant MM, Phillips DC. Free radicals and redox signalling in T-cells during chronic inflammation and ageing. Biochem Soc Trans 2011;39(5):1273-1278.

242. Gringhuis SI, Papendreht-van der Voort EAM, Leow A, Levarht EWN, Breedveld FC, Verweij CL. Effect of redox balance alterations on cellular localization of LAT and downstream T-cell receptor signaling pathways. Mol Cell Biol 2002;22(2):400-411.

243. Pittet MJ, Grimm J, Berger CR, Tamura T, Wojtkiewicz G. In vivo imaging of T cell delivery to tumors after adoptive transfer therapy. Proc Natl Acad Sci 2007;104(30):12457-12461.

244. Kircher MF, Allport JR, Graves EE, Love V, Josephson L, Lichtman AH, et al. In vivo high resolution three-dimensional imaging of antigen-specific cytotoxic T-lymphocyte trafficking to tumors. Cancer Res 2003;63:6838.

245. Hemeda H, Jakob M, Ludwig AK, Giebel B, Lang S, Brandau S. Interferon-gamma and tumor necrosis factor-alpha differentially affect cytokine expression and migration properties of mesenchymal stem cells. Stem Cells Dev 2010;19(5):693-706.

246. Croitoru-Lamoury J, Lamoury FM, Zaunders JJ, Veas LA, Brew BJ. Human mesenchymal stem cells constitutively express chemokines and chemokine receptors that can be upregulated by cytokines, IFN-beta, and Copaxone. J Interferon Cytokine Res 2007;27(1):53-64.

247. Polchert D, Sobinsky J, Douglas GW, Kidd M, Moadsiri A, Reina E, et al. IFN-gamma activation of mesenchymal stem cells for treatment and prevention of graft versus host disease. Eur J Immunol 2008;38(6):1745-1755.

248. Resnick IB, Barkats C, Shapira K, Stepensky P, Bloom AI, Shimoni A, et al. Treatment of severe steroid resistant acute GVHD with mesenchymal stromal cells (MSC). Am J Blood Res 2013;3(3):225-238.

249. Schinkothe T, Bloch W, Schmidt A. In vitro secreting profile of human mesenchymal stem cells. Stem Cells Dev 2008;17:199-205.

250. Bhaumik S, Gambhir SS. Optical imaging of Renilla luciferase reporter gene expression in living mice. Proc Natl Acad Sci 2002;99(1):377-382.